Charles University
Faculty of Science

Study program: Cell biology

Bc. Kateryna Turchyna

The identification of novel MT1-MMP interaction partners
Identifikace nových interakčních partnerů proteinu MT1-MMP

Diploma thesis

Supervisors: prof. RNDr. Jan Brábek, Ph.D.
doc. RNDr. Daniel Rösel, Ph.D.
Advisors: RNDr. Ondřej Tolde, Ph.D.
Kateřina Strouhalová, MSc.

Prague, 2024

Prohlášení

Prohlašuji, že jsem závěrečnou práci zpracovala samostatně a že jsem uvedla všechny použité informační zdroje a literaturu. Tato práce ani její podstatná část nebyla předložena k získání jiného nebo stejného akademického titulu.

V Praze, 12. 12. 2024 Bc. Kateryna Turchyna

Acknowledgements

I would like to express my heartfelt gratitude to my supervisors, Prof. RNDr. Jan Brábek, Ph.D., and Doc. RNDr. Daniel Rösel, Ph.D., for their guidance throughout this project. I also deeply appreciate the assistance provided by my colleague, RNDr. Ondřej Tolde, Ph.D., and all the members of our laboratory team.

Special thanks belong to my former colleague, Kateřina Strouhalová, MSc., who introduced me to the world of scientific research. Her patience, expertise, and mentorship were instrumental during the early stages of this project, which began as part of her PhD work.

Finally, I am profoundly grateful to my partner, family, and friends for their unwavering support throughout my studies in the Czech Republic. Their encouragement has been a constant source of strength and inspiration.

The project National Institute for Cancer Research (Programme EXCELES, ID Project No. LX22NPO5102) - Funded by the European Union – Next Generation EU.

Abstract

Membrane Type 1 Matrix Metalloproteinase (MT1-MMP) is an enzyme with critical role in cancer cells invasiveness. In this work we aimed to investigate interaction partners of MT1-MMP to broaden our understanding of the processes the enzyme takes an active part in. We have modified sequences of the metalloproteinase and its mutant variants with Strep/FLAG-tags insertion to allow for affinity purification and subsequent analysis of isolated potential interactors via mass spectrometry. Our preliminary data suggest that desmoglein-2 (DSG2) potentially binds MT1-MMP in human cells. Here we tried to verify the supposed interaction using coimunoprecipitation assays.

Key words:

Cancer invasiveness, metalloproteinases, MT1-MMP, interaction partners, desmoglein-2, coimmunoprecipitation.

Abstrakt

Membránová matrixová metaloproteáza typu 1 (MT1-MMP) je enzym, který se zásadně podílí na invazivitě nádorových buněk. V této práci jsme se zaměřili na zkoumání interakčních partnerů MT1-MMP, abychom rozšířili naše porozumění buněčným procesům, kterých se tento enzym aktivně účastní. Abychom mohli MT1-MMP purifikovat a následně analyzovat její interaktory hmotnostní spektrometrií, fúzovali jsme WT a mutantní varianty tohoto enzymu se Strep/FLAG značkou. Naše předběžné výsledky naznačují, že v lidských buňkách MT1-MMP zřejmě interaguje s proteinem desmoglein-2. Tuto potenciální interakci jsme se zde snažili ověřit pomocí imunoprecipitačních experimentů.

Klíčová slova:

Invazivita nádorových buněk, metaloproteázy, MT1-MMP, interakční partneři, desmoglein-2, koimunoprecipitace.

Table of contents

Abbreviations list

AHNAK	Neuroblast differentiation-associated protein
AHNAK2	AHNAK Nucleoprotein 2
AP-2	Clathrin adaptor complex
APS	Ammonium persulfate
BSA	Bovine serum albumin
dCAT	MT1-MMP catalytic domain deletion mutant
CAT	MT1-MMP's catalytic domain
CCP	Clathrin-coated pit
CD44	Cell surface adhesion receptor
CMV	Cytomegalovirus
dCP	MT1-MMP cytoplasmic domain deletion mutant
CRISPR	Clustered Regularly Interspaced Short Palindromic Repeats
CT	Cytoplasmic tail
DAPI	4',6-diamidino-2-phenylindole
DH5alpha	Echerichia coli strain (TOP10)
DMEM	Dulbecco´s Modified Eagle´s Medium
DMP	Dimethyl pimelimidate
DMSO	Dimethyl sulfoxide
DSG2	Desmoglein-2
DTT	DL-dithiothreitol
ECM	Extracellular matrix
EDTA	Ethylenediaminetetraacetic acid
EGFP	Enhanced Green Fluorescent Protein
EMT	Epithelial-to-mesenchymal transition
EPHA2	Ephrin type-A receptor 2
ERK	Extracellular signal-regulated kinase
ERM proteins	Ezrin, radixin, moesin
FAK	Focal adhesion kinase
FBS	Fetal bovine serum
FFSS	Strep/FLAG-tag
FT	Flow through
GAPDH	Glyceraldehyde 3-phosphate dehydrogenase
GFP	Green fluorescent protein
HA-tag	Hemagglutinin-derived tag
HEK293	Human embryonic kidney cell line
HPX	MT1-MMP's hemopexin domain
HRP	Horseradish peroxidase
HT1080	Human fibrosarcoma cell line
HT1080 MMP14 KO (F3), HT1080 MT1-MMP KO (F3)	Human fibrosarcoma cells with CRISPR/Cas knockout of MT1-MMP gene, clone F3
IP	Immunoprecipitation

KO	(Gene) Knockout
LIMK	LIM domain kinase
LLY	MT1-MMP C-terminal amino acid replacement mutant with LLY^{573} substituted for AAA
LMW PEI	Polyethylenimine of low molecular weight
MET	Mesenchymal-to-epithelial transition
MLC	Myosin light chain
MMP	Matrix metalloproteinase
MMP14	Matrix metalloproteinase 14
MMP2	Matrix metalloproteinase 2
MMP9	Matrix metalloproteinase 9
MTCBP-1	MT1-MMP cytoplasmic tail binding protein 1
dNTPs	Deoxynucleotide triphosphates
PAGE	Polyacrylamide gel electrophoresis
PBS	Phosphate buffered saline
PC	Protein convertase
PCR	Polymerase chain reaction
PDB	Proximity-dependent biotinylation
PFA	Paraformaldehyde
PKC	Protein kinase C
RCF	Relative Centrifugal Force
ROCK	Rho kinase
RPM	Revolutions per minute
RT	Room temperature
SDS	Sodium dodecylsulfate
SV40	Simian virus 40
TBS	Tris-buffered saline
TEG	Tris-EDTA-glucose
TEMED	Tetramethylethylendiamin
TIMP	Tissue inhibitor of metalloproteinase
TJP2	Tight Junction Protein 2
TLL	Tolloid-like protein
TM	MT1-MMP's trans-membrane domain
TOP10	*Escherichia coli DH5alpha*
TTBS	Tween Tris-buffered saline
VEGF	Vascular endothelial growth factor
VEGFR-2	VEGF receptor 2
WASP	Wiskott-Aldrich syndrome proteins
WAVE	WASP-family verprolin-homologous proteins
WB	Western blot
WCL	Whole cell lysate
WT	Wild type
ZO-2	Zonula occludens 2, a tight junction protein

1. Literature review

1.1. Cancer, metastasis, and EMT-MET model

Nowadays, cancer is a leading cause of death worldwide, accounting for nearly 10 million deaths in 2020 (Ferlay et al., 2020). Metastasis, or spread of cancer cells from original (primary) tumour to different (secondary) sites within the body, is the main cause of cancer-related mortalities (Sleeman & Steeg, 2010). Metastasis is a multi-step process encompassing the (i) local infiltration of tumour cells into the adjacent tissue, (ii) entry of cancer cells into the vasculature termed intravasation, (iii) survival in the circulatory system, (iv) extravasation and (v) subsequent proliferation in competent organs leading to colonization (Eger & Mikulits, 2005). In tumours of epithelial origin, local invasion must happen for metastasis to begin, and to do so tumour cells undergo the so-called epithelial-to-mesenchymal transition (EMT), a vital process by which epithelial cells change biochemically to achieve mesenchymal phenotypes (Hay, 1995). EMT is quite rigid, since it involves relatively extensive alternations in gene transcription (for a review, see (Craene & Berx, 2013)), eventually leading to the disruption of cell–cell adhesion and cellular polarity, remodelling of the cytoskeleton, and changes in cell–matrix adhesion. A reverse process, mesenchymal-to-epithelial transition (MET), is believed to be realized by cancer cells when they reach a desirable metastatic niche to develop secondary tumours (Roche, 2018). The whole process including its particular steps and transitions is schematically summarized in Figure 1.

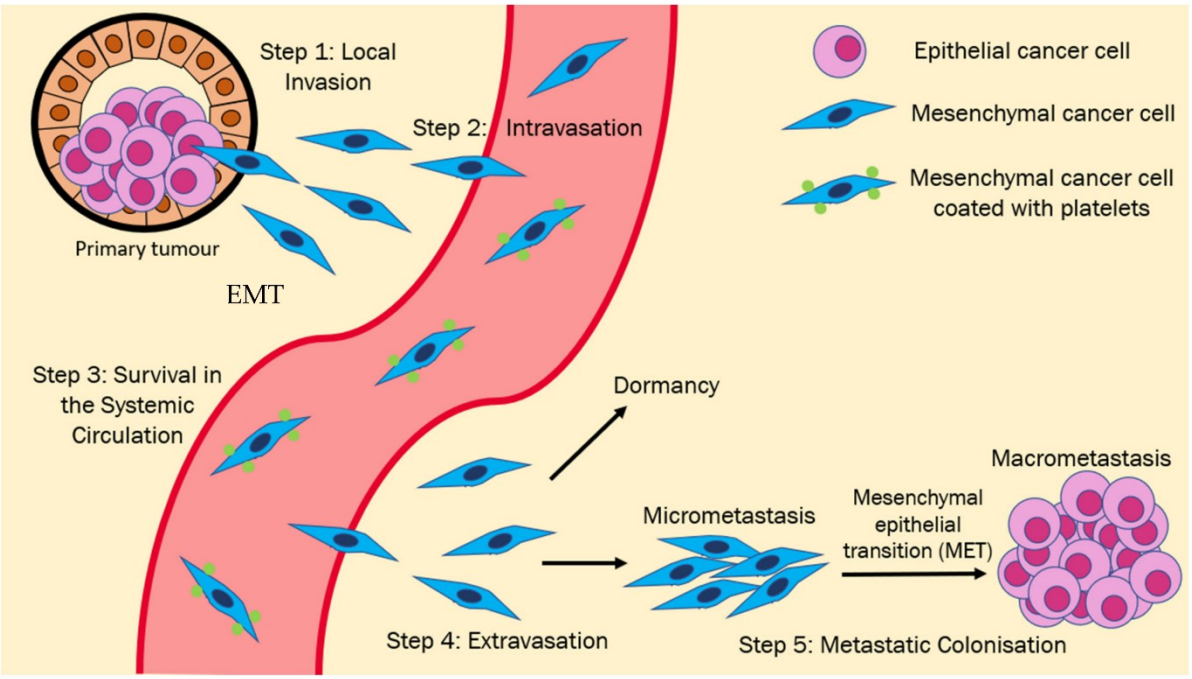

Figure 1. EMT-MET model for the metastatic cascade: Epithelial cancer cells undergo EMT, which causes them to lose their cell-cell junctions and gain the ability to invade the surrounding tissue parenchyma (Step 1). These EMT-induced cells may then intravasate into the systemic circulation (Step 2) and must survive in the circulation (Step 3) before reaching the target organ site. Upon reaching the target organ site, the cells must then extravasate into the tissue parenchyma (Step 4), following which they may either enter a state of dormancy or form micro metastases. Subsequent development into clinically detectable and potentially life-threatening macro metastases requires MET activation (Step 5) (Datta et al., 2021).

1.2. Modes of invasion

The process of metastasizing is enabled by invasiveness of cancer cells – their ability to infiltrate surrounding healthy tissue. Generally, in order to overcome barriers of extracellular matrix (ECM), tumour cells develop different strategies and migrate either collectively, or individually. Single cells utilize two main modes of migration: mesenchymal and amoeboid. Mesenchymal invasiveness operates through invadopodia and is protease-dependent, which allows tumour cells to migrate using proteolytic enzymes to degrade ECM on their path. Amoeboid-like invasiveness, on the contrary, relies on Rho/ROCK signaling pathway and actomyosin contractility, and is thus protease-independent since such cells translocate via squeezing through ECM gaps or deforming of ECM fibers using force generation for invasion into the surrounding tissue.

1.3. Amoeboid invasiveness

In amoeboid mode of migration, cortically localized actin and myosin play a key role. They mediate cycles of expansion and contraction of the cell body typical for this migration type (Yumura et al., 1984). Enhanced contractility of such cells enables their squeezing through ECM gaps and adapting their bodies to the pre-existing spaces (Friedl et al., 2001; Mandeville et al., 1997; Wolf et al., 2003), or generating sufficient force to deform collagen fibers and push through the ECM (Provenzano et al., 2008; Rösel et al., 2008; Wyckoff et al., 2006). Besides, in metastatic cells, myosin light chain (MLC) phosphorylation allows the cells to elevate force generation and thus increase invasion (Wyckoff et al., 2006). The phosphorylation is regulated by Rho/ROCK signaling pathway (Wyckoff et al., 2006), which promotes a rounded bleb-associated mode of amoeboid motility because of the tension maintained by cortical actomyosin (Keller & Eggli, 1998) (summarized in Figure 2), independently of pericellular proteolysis (Sahai & Marshall, 2003). The low-adhesion attachment to the substrate enables

cells with amoeboid mode of invasion to translocate at velocities 4 to 50 times higher than those of the mesenchymal type of invasiveness (Friedl et al., 1994, 1998; Sahai & Marshall, 2003).

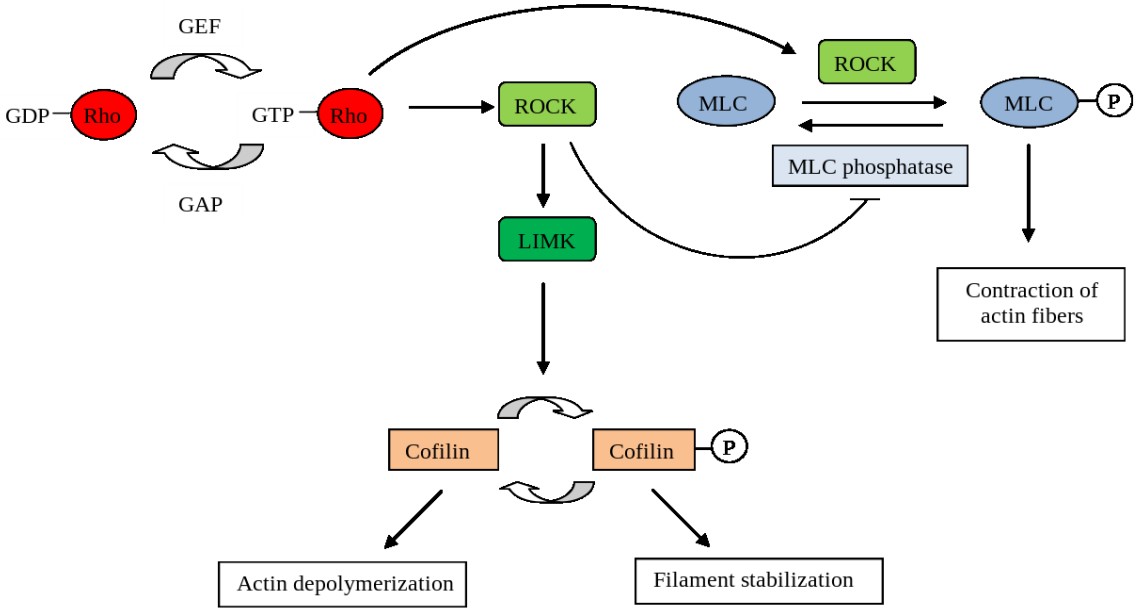

Figure 2. The Rho/ROCK signaling pathway regulates fundamental cytoskeleton activities. MLC phosphorylation by ROCK allows for the contraction of actin fibers, whereas LIMK phosphorylation leads to phosphorylation of cofilin thus regulating the stability of actin filaments. ROCK = Rho kinase; MLC = myosin light chain; LIMK = LIM domain kinase; GEF = Guanine nucleotide exchange factor; GAP = GTPase-activating protein (Adapted from Wang & Chang, 2014).

1.4. Mesenchymal invasiveness

Mesenchymal cell migration is characterized by cell polarization to form a leading edge that extends actin-rich protrusions, such as lamellipodia and filopodia. On a molecular level, this process is driven by small Rho GTPases, mainly Rac and Cdc42 (Cell division control protein 42 homolog) (Nobes & Hall, 1995). These GTPases regulate WASP/WAVE proteins (i.e., Wiskott-Aldrich syndrome proteins/WASP-family verprolin-homologous proteins) (Miki et al., 1998), which in turn interact with Arp2/3 (actin-related protein 2/3 complex) (Rohatgi et al., 1999), leading to nucleation of the polymerization and branching of actin, forming the actin network at the leading edge (Suetsugu et al., 2001). Summary of these signal-induced changes in the actin cytoskeleton is depicted in Figure 3.

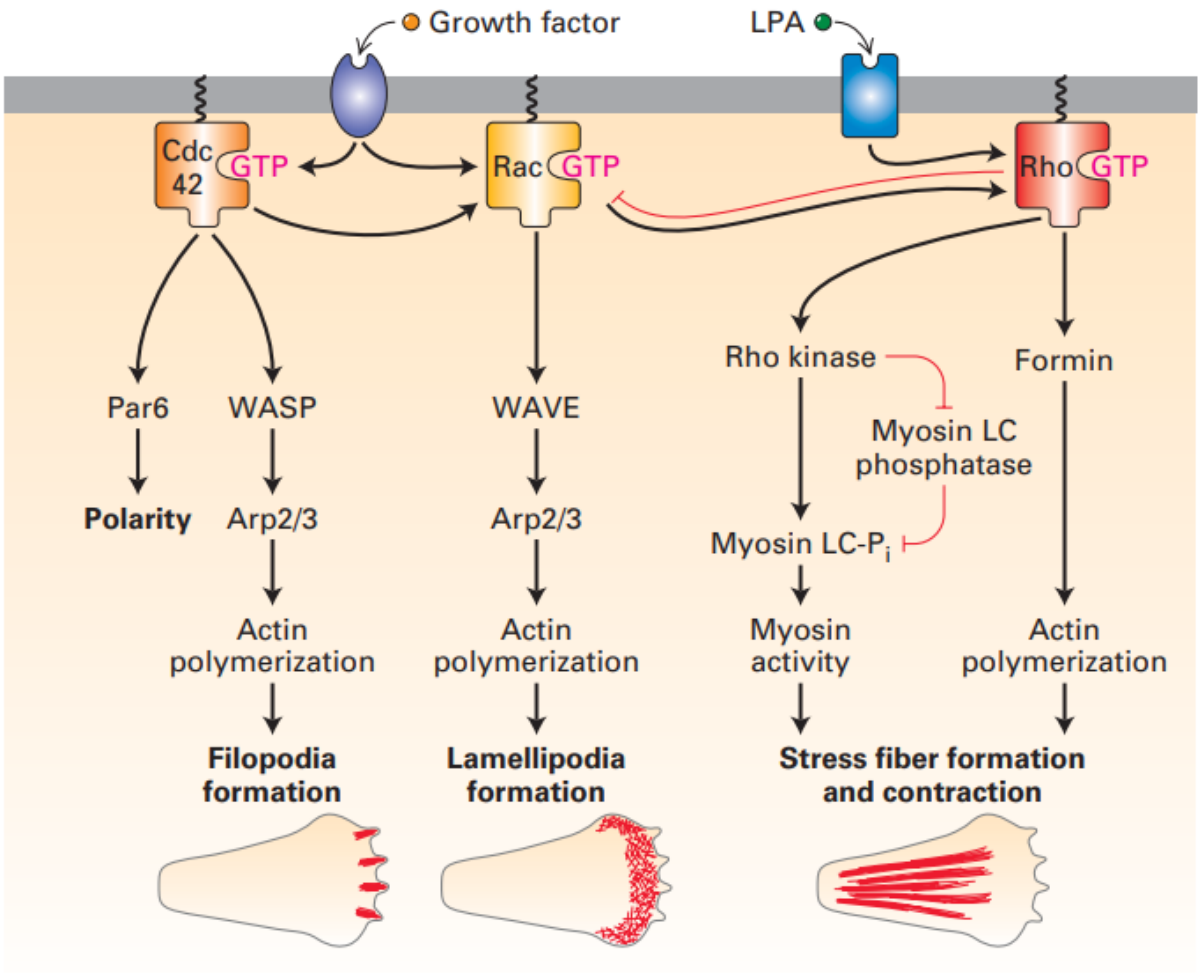

Figure 3. Summary of signal-induced changes in the actin cytoskeleton. Specific signals, such as growth factors and lysophosphatidic acid (LPA), are detected by cell-surface receptors. Detection leads to the activation of the small GTP-binding proteins, which then interact with effectors to bring about cytoskeletal changes as indicated (Lodish et al., 2016).

1.4.1. Integrins and invadopodia

Both cell poles adhere to ECM via integrins – transmembrane receptors that mechanically link ECM and actin cytoskeleton at focal contacts in the front of lamellipodia. Actin stress fibers attached to the poles then generate traction forces between the anterior and posterior cell edges, thereby driving the contraction (Sheetz et al., 1998). On the cell surface within cell-ECM contacts arise invadopodia – actin-rich protrusions of the plasma membrane associated with degradation of the ECM (Eddy et al., 2017; Murphy & Courtneidge, 2011). Formation of invadopodia is a complex process involving substantial reorganization in cytoskeleton dynamics and membrane transport and encompassing three main stages: initiation, stabilization, and maturation. The initiation phase includes activation of the Arp2/3 complex in response to extracellular stimuli. Arp2/3 initiates actin nucleation to assemble actin-

based precursor complexes and start cortactin-dependent actin polymerization that extends plasma membrane and drives elongation of cellular protrusions (Augoff et al., 2020). Then comes stabilization phase, where newly formed actin filaments are crosslinked into tightly packed bundles and anchored to plasma membrane by various proteins, so that a stable, three-dimensional structure is formed (Li et al., 2010; Schoumacher et al., 2010). The maturation phase involves targeted delivery and exocytosis of proteins with proteolytic activity, such as MMP2, MMP9, and MMP14, to invadopodia, making them able to promote focal ECM degradation (Jacob & Prekeris, 2015). It has been shown that integrins clustered on invadopodia play a significant role in recruiting these proteolytic enzymes on the surface of invasive cells, thus facilitating pericellular ECM remodelling and generating the path for migrating cells (Brooks et al., 1996; Wei et al., 1996).

1.4.2. Matrix metalloproteinases

Matrix metalloproteinases (MMPs) are multidomain zinc-dependent endopeptidases that play a fundamental role in ECM remodelling (Page-McCaw et al., 2007) owing to their ability to degrade a broad spectrum of extracellular matrix components including collagens, elastins, gelatine, matrix glycoproteins, and proteoglycan (for a review, see Nagase & Woessner, 1999). Although the structure of individual metalloproteinases differs, they all share a catalytic domain with the HEXGH motif responsible for ligating zinc, which is essential for catalytic function (Chambers & Matrisian, 1997). The MMPs are also known as matrixins, which together with astacins, adamalysins, and serralysins, belong to a larger family of proteases known as the metzincin superfamily (Figure 4).

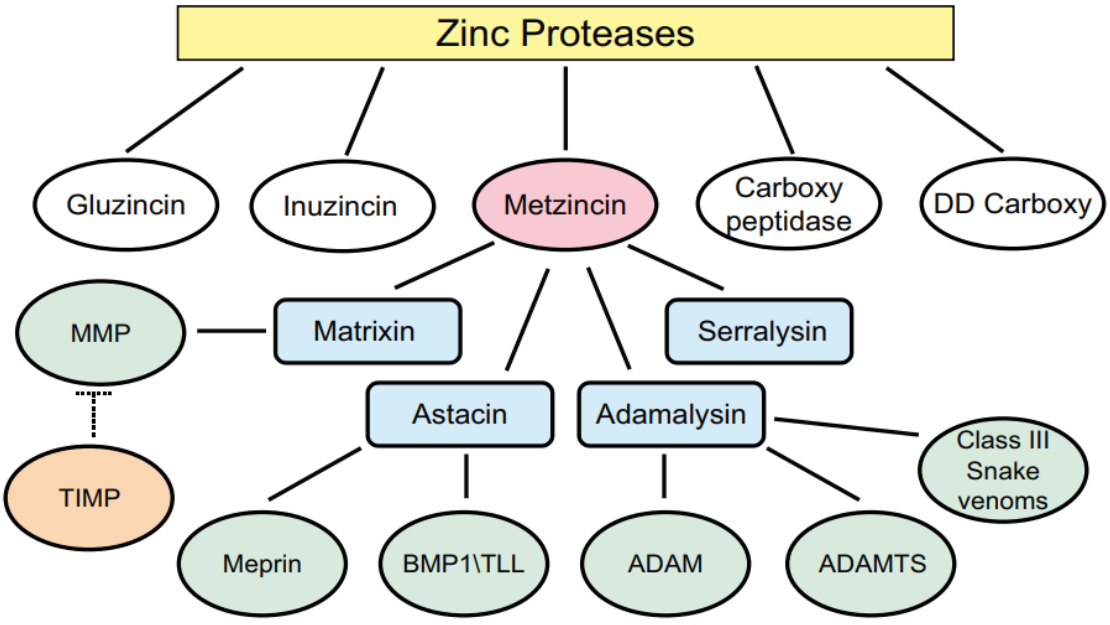

Figure 4. Schematic representation of subdivisions within the Metzincin superfamily. MMP = matrix metalloproteinase; TIMP = tissue inhibitor of metalloproteinase; BMP1 = bone morphogenetic protein 1; TLL = Tolloid-like protein; ADAM = a disintegrin and metalloproteinase; ADAMTS = a disintegrin and metalloproteinase with thrombospondin motifs (Adapted from Huxley-Jones et al., 2007).

Apart from degrading all kinds of extracellular molecules, MMPs are also known to be involved in the cleavage of cell surface receptors, the release of apoptotic ligands (such as the Fas ligand), and chemokine/cytokine inactivation (Van Lint & Libert, 2007). MMPs also play a major role in wide range of cell behaviours, such as cell proliferation, migration, differentiation, angiogenesis, apoptosis, and host defence. Depending on the form of enzyme, MMPs can be categorized into two subgroups: soluble and membrane-anchored MMPs. The membrane-type subgroup comprises MMPs that either contain a transmembrane domain (MT1-, MT2-, MT3-, MT5-MMP) or a glycosylphosphatidylinositol (GPI) anchor, which tethers them to the surface of the cell (MT4-, MT6-MMP) (Nagase et al., 2006).

1.5. Membrane Type 1 Matrix Metalloproteinase

MT1-MMP, also known as MMP14, is an integral type I transmembrane peptidase involved in the remodelling of the ECM in physiological (wound healing, bone growth and remodelling) as well as pathological processes (arthritis, tumour growth). MT1-MMP promotes cell migration and invasion by localizing to invadopodia and lamellipodia (Figure 5) – membrane structures where degradation of the ECM barrier takes place in order to make a path for migrating cells (Itoh, 2006). Functions of MT1-MMP extend from regulating the turnover of various ECM components, such as type I, II, III and IV collagens, fibronectin, vitronectin, laminin, fibrin and proteoglycan (d'Ortho et al., 1997; Ohuchi et al., 1997), to activation of secreted MMPs such as pro-MMP-2 (Sato et al., 1994) and pro-MMP-13 (Knäuper et al., 1996), which, in turn, will cleave multiple matrix substrates (for a review, see Seiki, 2002).

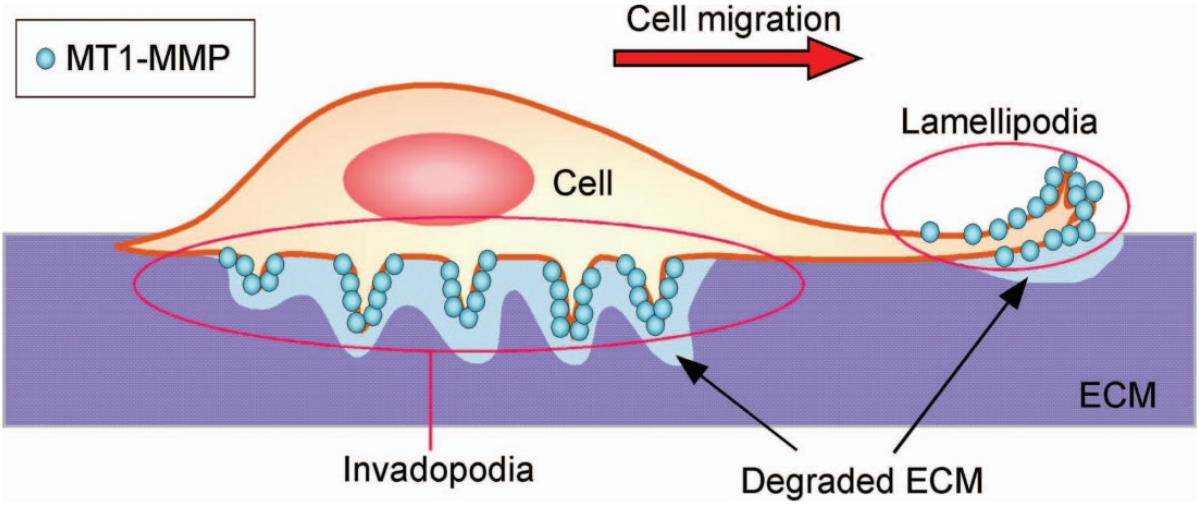

Figure 5. Localization of MT1-MMP dictates polarized pericellular ECM degradation. MT1-MMP localizes at membrane structures called lamellipodia and invadopodia. These are the areas in which ECM degradation takes place. Regulated positioning of MT1-MMP to these structures enables focal degradation of ECM during cell migration (Itoh, 2006).

1.5.1. MT1-MMP's role in cancer

MT1-MMP is an important mediator of cell migration and mesenchymal invasion (Hotary et al., 2000; Kajita et al., 2001), which contribute to metastasis, and thus, the malignancy of numerous tumour types (for a review, see Yana & Seiki, 2002). MT1-MMP has been shown to be expressed in invasive cancer cells (Sato et al., 1994) as well as many other cell types, such as mesenchymal stem cells (Ries et al., 2007), fibroblasts, osteoblasts (Hikita et al., 2006), osteoclasts (Sato et al., 1997), chondrocytes (Imai et al., 1997), epithelial cells (Kadono et al., 1998), endothelial cells (Hiraoka et al., 1998), adipocytes (Chun et al., 2006), myeloid cells (Gonzalo et al., 2010), neuronal cells (Beliën et al., 1999), T-cells (Esparza et al., 1999), and B-cells (G. Jin et al., 2011).

1.5.2. Structure and forms of the enzyme

As to the structure of MT1-MMP, the protein is synthesized as a pre-pro-MT1-MMP zymogen consisting of five main domains (Figure 6, bottom): an inhibitory pro-peptide, a catalytic domain (CAT), a hemopexin-like domain (HPX), a trans-membrane domain (TM), and a short cytoplasmic tail (CT). MT1-MMP also contains two flexible regions – hinge and linker – that link the catalytic domain to hemopexin-like domain, and hemopexin-like domain to the transmembrane domain. A signal peptide located at the N-terminus is removed by signal peptidase in rough endoplasmic reticulum (Gifford & Itoh, 2019). For activation of MT1-MMP, it is required that protein convertases (PCs), such as furin, remove the pro-peptide in the

trans-Golgi during the secretory process (Sato et al., 1994). PCs remove the pro-peptide directly by recognizing a ^{108}RRKR motif at the C-terminus of the pro-domain (Sato et al., 1994).

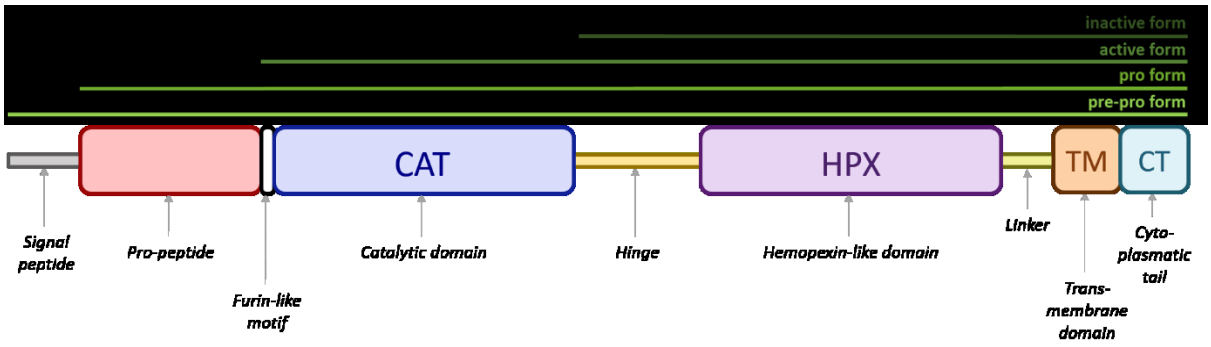

Figure 6. A schematic representation of MT1-MMP structure and forms. CAT = catalytic domain; HPX = hemopexin-like domain; TM = transmembrane domain; CT = cytoplasmic tail.

Consequently, several MT1-MMP forms can be found in a cell (Figure 6, top): pre-pro-MT1-MMP (unprocessed form after translation), pro-MT1-MMP (signal peptide cleaved, N terminus starts at Ser^{24}), active MT1-MMP (pro-peptide cleaved, N terminus starting at Tyr^{112} (Hernandez-Barrantes et al., 2000)), and inactive (membrane-tethered form lacking the catalytic domain due to autocatalytic processing (Cho et al., 2008)) forms.

1.6. Cytoplasmic tail of MT1-MMP

Cytoplasmic tail (CT) is a small, but one of the most important, part of MT1-MMP. Since this 20 amino acids long region is the only part of the protein located inside the cell (Figure 7), it serves as a hub of incoming and outgoing signaling.

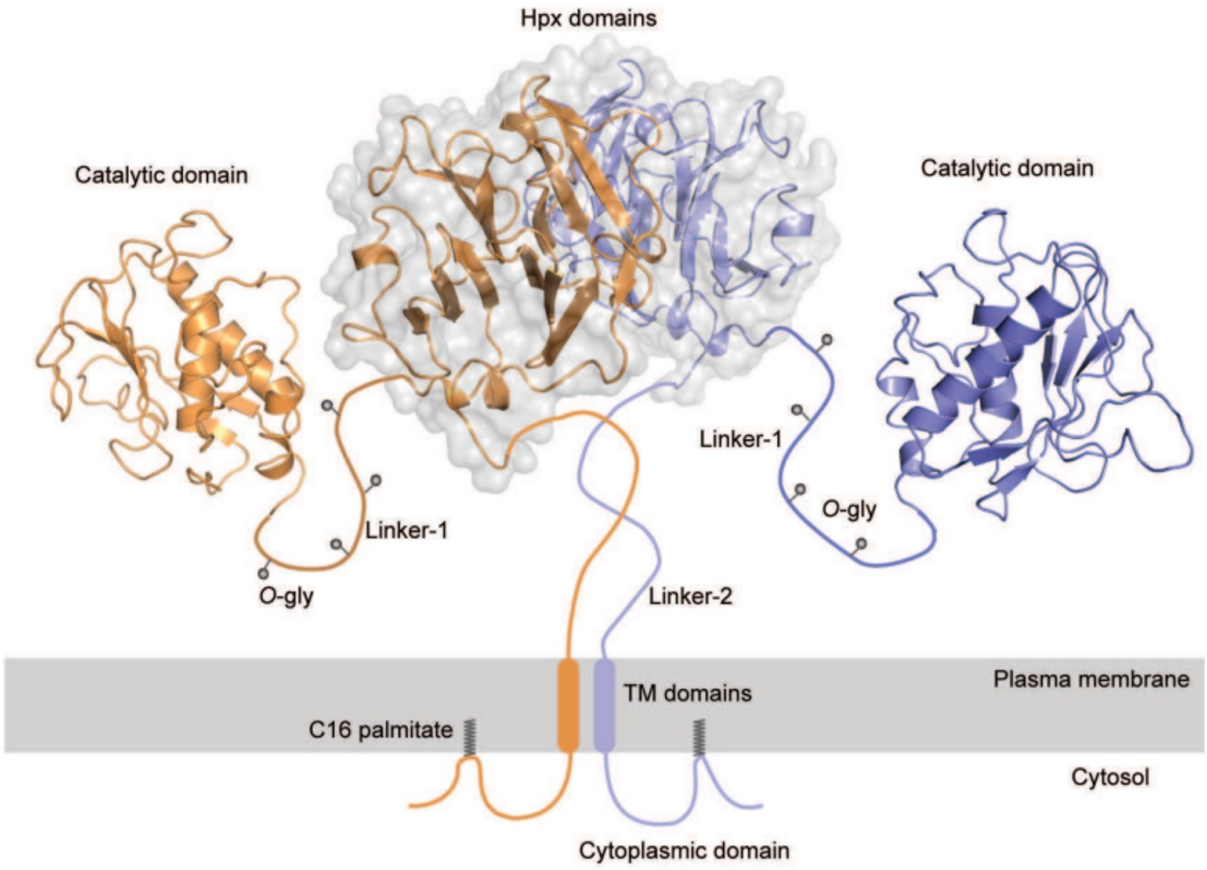

Figure 7. A tentative model of a full-length MT1-MMP dimer on the cell surface. Based on the symmetrical interaction, other domains of MT1-MMP molecules are put together to a full-length model. The regions of linker-1, linker-2, transmembrane (TM) domain, and cytoplasmic domain are illustrated schematically. The linker-1 has four O-glycosylation sites, which would extend the structure. Cys^{574} in the cytoplasmic domain is palmitoylated, which would create a loop structure. The relative positioning of the two catalytic domains could not be predicted at the time (Tochowicz et al., 2010).

1.6.1. Structure of the CT

In human MT1-MMP sequence (Attachment 1), the CT comprises residues 563–582 (UniProt ID P50281 (Kasurinen et al., 2018)), and contains multiple amino acids, which are post-translationally modified, as well as several binding sites for intracellular proteins. My colleagues from Laboratory of Cancer Cell Invasion have summarized MT1-MMP regulation and cell signaling modulation via CT in their recent review (Strouhalova et al., 2023). They distinguish four regions in the CT sequence (Figure 8, left side): a juxtamembrane basic cluster (^{563}RRH^{565}), an amphipathic region (^{566}GTPRR^{570}), a nonpolar region (^{571}LLYC^{574}), and a final

amphipathic region ([575]QRSLLDKV[582]), – and name particular CT interactors along with their binding sites (Figure 8, right side).

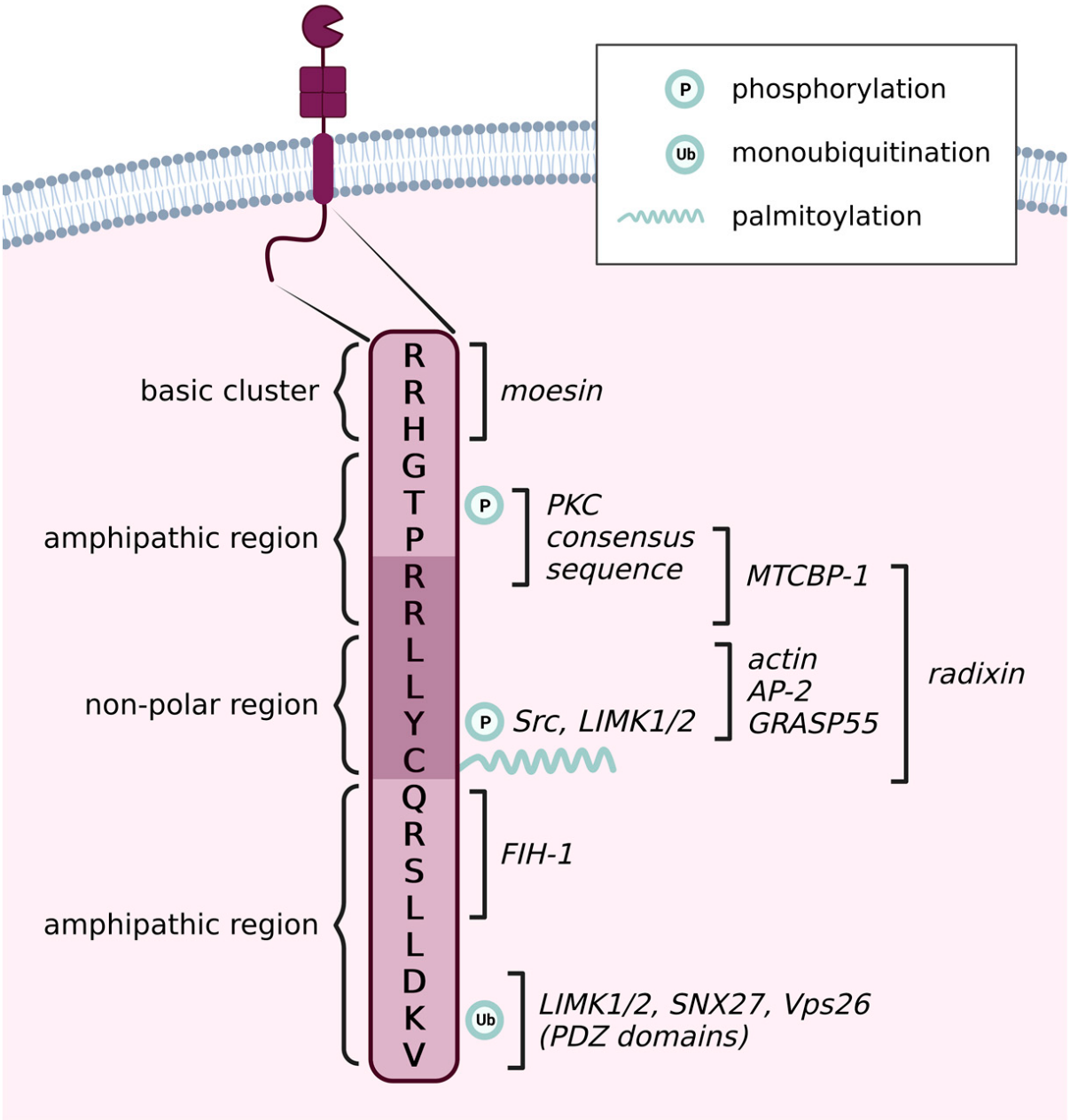

Figure 8. Overview of the cytoplasmic tail of MT1-MMP and its main interactors. The CT contains one basic cluster, one non-polar region, and two amphipathic regions. Residues Arg[569]-Cys[574] can form a β-sheet-like structure (dark purple background). Thr[567] and Tyr[573] can be phosphorylated, Lys[581] can be ubiquitinated, and Cys[574] can undergo palmitoylation. Interacting partners and known binding sites are depicted on the right side of the diagram (Strouhalova et al., 2023).

1.6.2. The role of amino acid modifications within the CT

As can be seen from Figure 8, the CT contains multiple amino acids that can be modified, thus influencing different processes inside the cell – from regulating MT1-MMP trafficking and cell invasion to affecting cellular metabolism. Namely Cys^{574} palmitoylation, Thr^{567} and Tyr^{573} phosphorylations, and Lys^{581} ubiquitination have been extensively studied in order to identify their particular roles.

In particular, Cys^{574} palmitoylation (Anilkumar et al., 2005) by ZDHHC13 (Zinc Finger DHHC-Type Palmitoyltransferase 13) (Song et al., 2014) causes the tethering of the CT to the plasma membrane (Anilkumar et al., 2005), and affects clathrin endocytosis and cell motility. Additionally, this site is also crucial for multimerization of the enzyme, as well as proper adhesion, migration, and invasion (Labrecque et al., 2004; Rozanov et al., 2001).

Phosphorylation of Thr^{567} is performed by PKC (protein kinase C) in response to β1 integrin activation in tetraspanin-enriched domains, the sites where tetraspanins cluster MT1-MMP, PKC, and β1 integrins together (Schröder et al., 2013; Suárez et al., 2020; X. A. Zhang et al., 2001). Thr^{567} phosphorylation has been shown to promote MT1-MMP internalization (Williams & Coppolino, 2011), and contribute to increased adhesion of cancer cells (J. Yang et al., 2017). In addition, cells carrying the phosphodeficient Thr^{567} mutant demonstrate lower migration and invasion rates than the WT despite the mutant being more abundant on the cell surface, and conversely, a phosphomimetic mutant or a high phosphorylation state increases migration and invasion (Grafinger et al., 2020; Williams & Coppolino, 2011; J. Yang et al., 2017).

Tyr^{573} phosphorylation happens either by means of Src kinase or one of its downstream effector kinases (Nyalendo et al., 2007), or LIMK1/2 (LIM domain containing kinase 1 and 2) (Lagoutte et al., 2016). This phosphorylation allows for MT1-MMP association with an adaptor protein p130Cas (CRK-associated substrate) (Gingras et al., 2008) – an important substrate of Src, dominantly localized at focal adhesions of adherent cells (Janoštiak et al., 2011), where MT1-MMP is targeted to via an interaction with FAK (focal adhesion kinase)-p130Cas complex (Wang & McNiven, 2012) – thus allowing for ECM degradation at focal adhesions. Apart from this, phosphorylation of Tyr^{573} is known to be a mechanism of ERK pathway downregulation (D'Alessio et al., 2008). As to the regulation of invasiveness, Tyr^{573} phosphorylation has been shown to promote migration, matrix degradation, and invasion while increasing MT1-MMP concentration on the surface (Lagoutte et al., 2016; Moss et al., 2009; Nyalendo et al., 2007).

Another modification of interest is the monoubiquitination of Lys^{581} by the E3 ubiquitin-protein ligase NEDD4 (neural precursor cell expressed developmentally down-regulated protein 4). It has been demonstrated to downregulate the uptake of MT1-MMP into cells (Eisenach et al., 2012) impacting trafficking and, therefore, function of MT1-MMP. Moreover, this modification is essential for invasion through type I collagen (Eisenach et al., 2012). Interestingly, ubiquitination of Lys^{581} is interconnected with the previously described phosphorylation of Tyr^{573}: in order to phosphorylate the Tyr, LIMK1/2 binds the C-terminal DKV^{582} motif, and, conversely, Tyr^{573} phosphorylation is indispensable for Lys^{581} ubiquitination (Eisenach et al., 2012; Lagoutte et al., 2016).

1.6.3. Known interaction partners of the MT1-MMP's CT

Apart from multiple modifications, the CT also contains numerous binding sites for MT1-MMP interactors, which affect the enzyme in one way or another regulating its processing or function. For instance, a dileucine motif LL^{572} is known to ensure proper glycosylation of MT1-MMP by a yet unknown mechanism (Ludwig et al., 2008), and to be necessary for the invadopodia formation (Ferrari et al., 2019). Moreover, LLY^{573} has been found to be a binding site for GRASP55 (Golgi reassembly-stacking protein of 55 kDa) (Roghi et al., 2010), a protein responsible for the morphology of the Golgi apparatus and regulation of proteins glycosylation (Pothukuchi et al., 2021; Xiang et al., 2013), as well as the interaction with furin, which potentially leads to MT1-MMP pro-domain cleavage and enzyme activation (Roghi et al., 2010). Furthermore, the LLY^{573} motif was found to be a site of direct F-actin binding, indispensable for invadopodia formation and invasion through ECM (Uekita et al., 2001; Yu et al., 2012). Besides, the LLY^{573} motif interacts with the μ2 subunit of AP-2, a clathrin-coated pit (CCP) cargo adaptor protein, leading to MT1-MMP endocytosis in CCPs (Uekita et al., 2001). Here, the already mentioned Cys^{574} palmitoylation facilitates the interaction by bringing LLY^{573} close to membrane (Anilkumar et al., 2005).

Another motif, RRH^{565}, is the binding site of moesin – one of ERM (ezrin, radixin, moesin) proteins, which link transmembrane proteins to the actin cytoskeleton and act as organizers of plasma membrane domains (Fehon et al., 2010). Interaction of RRH^{565} with moesin is necessary for MT1-MMP clustering in tetraspanin-enriched domains in cell protrusions, which likely mediates trans-autocatalytic removal of the CAT domain of MT1-MMP (Suárez et al., 2020), leading to the above-mentioned inactive form of the enzyme. Integrity of this juxtamembrane region is also crucial for endocytosis of MT1-MMP (Suárez et al., 2020).

The PRR^{570} motif is a known binding site of MTCBP-1 (MT1-MMP cytoplasmic tail binding protein 1) – a regulator of MT1-MMP activity which inhibits MT1-MMP-mediated migration, ECM degradation and invasion (Qiang et al., 2019; Uekita et al., 2004). As their binding sites are directly adjacent, MTCBP-1 prevents MT1-MMP from binding actin, and this disruption leads to the loss of MT1-MMP targeting to invadopodia, independently of invadopodia number reduction onto overexpression of MTCBP-1 (Qiang et al., 2019).

The RRLLYC^{574} sequence of MT1-MMP interacts with radixin, which simultaneously binds the CT of CD44 (T. Mori et al., 2008; Terawaki et al., 2015), therefore forming a stable ternary complex comprising MT1-MMP, ERM proteins, and CD44 at the invasive front (Terawaki et al., 2015).

The YCQR^{576} region is necessary for ERK (extracellular signal-regulated kinase) activation in the presence of TIMP2 (D'Alessio et al., 2008). This MT1-MMP-mediated activation of ERK results in survival and proliferation in 3D gels (Takino et al., 2010).

The QRSL^{578} sequence, especially Arg^{576}, is important for MT1-MMP's interaction with FIH-1 (factor inhibiting HIF1-α), which activates HIF-1α (subunit α of hypoxia-inducible factor 1) in normoxic conditions thus inducing Warburg metabolism (Sakamoto et al., 2011).

Additionally, MT1-MMP was found to form a complex with VEGFR-2 (VEGF receptor 2) and Src, leading to the activation of Akt and mTOR, ultimately stimulating VEGF-A expression, and thus, angiogenesis (Eisenach et al., 2010). It has been shown that this process requires the aforementioned Tyr^{573}, Cys^{574}, and DKV^{582} (Eisenach et al., 2010; Song et al., 2014; Sounni et al., 2004).

The terminal Val^{582}, along with the mentioned Cys^{574}, proved to be essential for forming a complex with phosphorylated caveolin-1 during caveolae-dependent endocytosis of MT1-MMP (Labrecque et al., 2004). C-terminal DKV^{582} motif was found to interact with sorting nexin 27 (SNX27) and the Vps26 subunit of the retromer – a protein complex responsible for sorting transmembrane proteins from the endosomes, – thus promoting MT1-MMP recycling (Seaman, 2021). This motif is necessary for the maturation and proteolytic function of invadopodia, and therefore invasion through ECM (Labrecque et al., 2004; Sharma et al., 2019).

1.7. Background summary

Taking into consideration all the examples listed above, it becomes obvious that the cytoplasmic tail is a pivotal region regulating not only MT1-MMP itself – its function, trafficking, and localization, – but also big cellular processes, such as migration, invasion,

ECM degradation, adhesion, angiogenesis, and metabolism. Therefore, the CT and its interactions turn to be an interesting subject of investigation, and so multiple binding partners have been identified in recent years. However, it should also be considered that other proteins, whose interactions have not been discovered yet, may bind the CT sequence as well, and either engage in these known interactions regulating them, or even impact other cell pathways, creating new, yet unknown, connections between different cellular processes. For these reasons, in our project we aim to identify potential novel binding partners of the CT of MT1-MMP, which would help us understand more accurately the processes in which the enzyme takes an active part, and the ways they might impact cancer cell phenotype and behaviour in general. Outcomes of this project may contribute to anti-metastatic drug development, as inhibitors against the CT or its interactors might impede cancer metastasis, as well as influence adhesive properties or metabolism of cancer cells.

2. Aims

In this work we aim to achieve the two major goals:

1. To investigate the pool of MT1-MMP's interactions and to identify potential novel MT1-MMP binding partners;
2. To verify the supposed interactions by coimmunoprecipitation and colocalization essays.

We strive to accomplish these goals through the following minor steps:

1. Investigation of MT1-MMP's interactions pool and identification of the potential novel MT1-MMP binding partners:
   I. DNA constructs preparation:
      a) Introducing AviTag into cytoplasmic tail of MT1-MMP;
      b) *E. coli* biotin ligase (BirA) cloning into IRES vector.
   II. Transient transfection of HT1080 cells with the prepared constructs.
   III. Isolation of MT1-MMP along with its interactors:
      a) Proximity-dependent biotinylation of MT1-MMP and its close surrounding;
      b) Affinity purification of the biotinylated proteins on streptavidin beads.
   IV. Identification of the isolated proteins by mass spectrometry.

2. Verification of the supposed interactions by coimmunoprecipitation and colocalization essays:
   I. Insertion of FLAG/Strep-tags into the available MT1-MMP DNA plasmids.
   II. Verification of MT1-MMP variants expression and enzyme functioning in mammalian cells:
      a) Transfection of the prepared constructs into HT1080 mammalian cell line;
      b) Assessing the MT1-MMP variants expression levels via lysates preparation, SDS-PAGE, Western blot and immunolabelling;
      c) Testing the MT1-MMP enzymatic activity with gelatine degradation assays.
   III. Transfection of the prepared constructs into HT1080 cells, lysates preparation.
   IV. Coimmunoprecipitation of MT1-MMP and its interactors, samples analysis with SDS-PAGE, Western blot and immunolabelling.
   V. Determination of the spatial localization of MT1-MMP and its binding partner in a cell using colocalization essay.

3. Material and methods

3.1. Material

3.1.1. Mammalian cell lines

HT1080	human fibrosarcoma cell line
HT1080 MT1-MMP KO (F3)	human fibrosarcoma cells with CRISPR/Cas knockout of MT1-MMP gene, clone F3
HEK293	human embryonic kidney cell line
HeLa	immortalized cell line derived from cervical cancer
U2OS	human osteosarcoma cell line

3.1.2. Bacterial cultures

Escherichia coli ***DH5α (Top10)***: *dlacZ Delta M15 Delta (lacZYA-argF) U169 recA1 endA1 hsdR17 (rK-mK+) supE44 thi-1 gyrA96 relA1*

3.1.3. Material used in methods

Table 1. Chemicals and media used in cell culture methods.

CELL CULTURE MATERIAL		
Chemicals	**Producer**	**Catalogue number**
4',6-diamidino-2-phenylindole (DAPI)	EMD Millipore	90229
Ciprofloxacin	Sigma	17850-25G-F
Dimethyl sulfoxide (DMSO)	Sigma	D4540
Dulbecco´s Modified Eagle´s Medium (DMEM)	Sigma	D6429
Dulbecco´s phosphate buffered saline (PBS)	Sigma	D1408
Fetal bovine serum (FBS)	Sigma	F7524
Ethyl alcohol 96% (EtOH)	Lach:ner	64-17-5
QCM™ Gelatin Invadopodia Assay (Red)	Millipore	ECM671
Glutaraldehyde 50% aq. soln.	Thermo Scientific	A10500
Mounting medium	Ibidi	50001
Paraformaldehyde (PFA)	Sigma	P-6148
Polyethylenimine of low molecular weight (LMW PEI)	Polysciences	24885-2
Poly-L-lysine 0.01% solution	Sigma	P4707
SiR-actin Kit	Tebubio	SC001
SPY650-FastAct™	Tebubio	SC505
10x Trypsin-EDTA solution	Sigma	T4049
Media	**Composition**	
culture medium	DMEM with 10% FBS and 1% ciprofloxacin	
freezing medium	FBS and DMSO in a 9:1 ratio	

Table 2. Chemicals and media used in protein methods.

PROTEIN METHODS MATERIAL		
Chemicals	**Producer**	**Catalogue number**
Acrylamide/bis-acrylamide, 30%	Sigma	A3699

Ammonium persulfate (APS)	Serva	7727-54-0
Anti-FLAG® M2 magnetic beads	Millipore	M8823
Biotin	Sigma	B4501
Bovine serum albumin (BSA)	Sigma	A7030
DC Protein Assay Reagent A	Bio-Rad	5000113
DC™ Protein Assay Reagent S	Bio-Rad	5000115
Dimethyl pimelimidate dihydrochloride (DMP)	Sigma	D8388
DL-dithiothreitol (DTT)	Sigma	D9779
Dry milk	-	-
Ethylenediaminetetraacetic acid (EDTA)	Sigma	EDS-500G
Glycine	Sigma	G8898
Hydrochloric acid (HCl)	Sigma	320331
Nonidet P-40 (Igepal CA 630)	Sigma	56741
nProtein A Sepharose™ 4 Fast Flow	Cytiva	17528001
Methanol	Lach:ner	67-56-1
PageRuler™ Plus Prestained Protein Ladder 10 to 250 kDa	Thermo Scientific	26619
Pierce™ 3X DYKDDDDK Peptide	Thermo Scientific	A36805
Protease inhibitor mix (mammalian)	Biomake	B14002
Protein Assay Reagent B	Bio-Rad	5000114
Sodium chloride (NaCl)	Sigma	71380
Sodium deoxycholate	Sigma	D6750
Sodium dodecylsulfate (SDS)	Sigma	L5750
Sodium fluoride (NaF)	Sigma	7681-49-4
Strep-Tactin® elution buffer 10x	Iba	2-1000-025
Strep-Tactin® Super Flow® 50% suspension	Iba	2-1206-010
Tetramethylethylendiamin (TEMED)	Serva	35925
Triton X-100	Sigma	T8787
Trizma®base (Tris)	Sigma	93352
Tween 20	Sigma	P1379
WesternBright™ ECL	Advansta	K-12045-D50

Buffers	**Composition**
0.2% SDS lysis buffer	50 mM Tris-Cl (pH 7.4), 0.5 M NaCl, 0.2% SDS, DTT (1000x), mammalian protease inhibitors (100x)
0.5% Triton X-100 lysis buffer	50 mM Tris, 150 mM NaCl, 0.5% Triton X-100, 1 mM EDTA (pH 7.4); autoclaved; mammalian protease inhibitors (200x)
20x (1 mM) biotin medium	4.88 mgbiotin, 20 ml serum-free DMEM; pass through 0.22 μm filter to sterilize
4x Tris/SDS stacking buffer	0.5M Tris, 0.4% SDS (pH 6.8)
4x Tris/SDS separation buffer	1.5M Tris, 0.4% SDS (pH 8.8)
5x SDS buffer	15.1g Tris, 72 g glycine, 5 g SDS in 1000 ml H_2O (pH 8.3-8.4)
5x Transfer Turbo buffer	1.5 M Tris, 1.5 M glycine, 0.125% SDS
Alternative lysis buffer 1	100 mM KCl, 2 mM NaCl, 1 mM Na2ATP, 3.5 mM MgCl2, 10 mM HEPES, 1% Triton X-100, mammalian protease inhibitors (200x)
Alternative lysis buffer 2	100 mM KCl, 2 mM NaCl, 1 mM Na2ATP, 3.5 mM MgCl2, 10 mM HEPES, 0.5% Nonidet P-40, mammalian protease inhibitors (200x)
Equilibration buffer	0.2% SDS lysis buffer with 0.1 volume of 20% Triton X-100 and 0.9 volume of Tris-Cl
Laemmli buffer 6x	3.8 g glycerol, 1g SDS, 1.2 g bromphenol blue, 10 ml Tris (pH 6.8)
RIPA lysis buffer	150 mM NaCl, 50 mM Tris-HCl, 1% Nonidet P-40, 0.1% sodium deoxycholate, 5 mM EDTA, 50 mM NaF in ddH_2O
Stripping buffer	25 mM glycine, 1% SDS (pH 2)
Transfer buffer	25 mM Tris, 192 mM glycine, 20% methanol
Tris-buffered saline (TBS)	150mM NaCl, 50mM Tris (pH 7.1); autoclaved
Tween Tris-buffered saline (TTBS)	1g Tween 20 in 2000 ml TBS

Table 3. List of antibodies.

ANTIBODIES			
Name	**Producer**	**Catalogue number**	**Dilution**
Primary			
Anti-DSG2 (Rb)	Abcam	ab150372	1:5000
Anti-FLAG (Ms)	Sigma	F1804	1:1000
Anti-FLAG (Rb)	Cell Signaling	14793	1:1000
Anti-GAPDH (Ms)	Invitrogen	MA5-15738	1:5000
Anti-GFP (Rb)	Abcam	ab290	1:5000
Anti-GFP, mAb 3E6 (Ms)	Invitrogen	A11120	1:1000
Anti-HA (Ms)	Abcam	ab24779	1:5000
Anti-MMP-2 (Ms)	Abcam	ab2462	1:200
Anti-TIMP2 (Rb)	Cell Signaling	D18B7	1:1000
Secondary			
Anti-mouse-HRP (goat)	Abcam	ab97023	1:15000
Anti-rabbit-HRP (goat)	Abcam	ab97051	1:15000
Anti-rabbit-HRP (goat)	Santa Cruz Biotechnology	sc-2030	1:15000
Chicken anti-Rabbit IgG (H+L), Alexa Fluor™ 488 (CAR)	Invitrogen	A21441	1:1000
Streptavidin-Peroxidase Polymer, Ultrasensitive	Supelco	S2438-250UG	1:5000

Table 4. Chemicals and media used in bacterial cultures methods.

BACTERIAL CULTURE MATERIAL		
Chemicals	**Producer**	**Catalogue number**
Agar	VWR	84609
Ammonium acetate (NH_4AC)	Penta	22570-31000
Ampicillin	Sigma	E5354
Calcium chloride dihydrate ($CaCl_2 \cdot 2H_2O$)	Sigma	C3306
Glucose 25%	BIOCEV media	-
Glycerol	Sigma	G6279
Isopropanol	Lach:ner	67-63-0
Kanamycin	Sigma	K1377
LB broth low salt	Duchefa Biochemie	L1703
Magnesium chloride hexahydrate ($MgCl_2 \cdot 6H_2O$)	Penta	16330-30500
Peptone	Sigma	1.07043
Phenol-chloroform	Roth	A156.2
Phosphates: Sodium phosphate dibasic dodecahydrate ($Na_2HPO_4 \cdot 12H_2O$),	Sigma	71649
Phosphates: Sodium phosphate dibasic dihydrate ($Na_2HPO_4 \cdot 2H_2O$)	Sigma	71643
Sodium hydroxide (NaOH)	Sigma	S5881
Super optimal medium with catabolic repressor (S.O.C. medium)	Thermo Scientific	15544034
Yeast extract	VWR	84601

Media and buffers	**Composition**
10M NaOH	16 g NaOH in 40 ml H_2O
Agar plates	20 g/l LB broth low salt, 20 g/l agar, kanamycin/ampicillin; on plates
KB medium (500 ml)	5 g peptone, 5 g yeast extract, 465 ml dH_2O; autoclave; then filter 10 ml 25% glucose (0.5% final conc.) and 25 ml 2M phosphates
LB medium	20g LB broth low salt in 1000 ml H_2O; autoclaved
Lysis solution	8.8 ml H_2O, 200 µl 10M NaOH, 1 ml 10% SDS
Tris-EDTA-glucose (TEG) buffer	1.8 ml 25% glucose, 685 µl 2M Tris (pH 8), 1 ml 0.5M EDTA (pH 8), H_2O up to 50 ml

Table 5. Chemicals and media used in DNA methods.

DNA METHODS

Chemicals	Producer	Catalogue number
Agarose	Sigma	A9539
AMPure XP magnetic beads	Beckman	A63881
DNA Stain G	Serva	39803
Ethanol 96%	Lach:ner	64-17-05
Gene ruler DNA ladder mix	Thermo Scientific	SM0333
KAPA PureBeads	Roche	07983280001
Loading dye 6x	NEB	B7024A
Media and buffers	**Composition**	
Agar plates	20 g/l LB broth low salt, 20 g/l agar, kanamycin/ampicillin	
SB buffer 20x	55 g boric acid and 8 g NaOH in 1000 ml H_2O	

Table 6. List of enzymes and buffers used in DNA cloning methods.

DNA CLONING		
Restriction enzyme	**Producer**	**Catalogue number**
BamHI	NEB	R3136L
DpnI	NEB	R0176L
EcoRI	NEB	R3101S
EcoRV	NEB	R3195S
KpnI	NEB	R3142S
NcoI	NEB	R3193L
SalI	NEB	R0138S
SfiI	NEB	R0123S
SspI	Thermo Scientific	ER0772
StuI	NEB	R0187S
Enzymes and others		
7x Pfu polymerase	Thermo Scientific	EP0501
Antarctic Phosphatase	NEB	M0289S
dNTPs mix	VWR	733-1663
Gibson Assembly GeneArt Seamless Cloning and Assembly Enzyme Mix	Invitrogen	A14606, A13288
RNAse A	Omega Bio-Tek	RNA-03
T4 DNA ligase	Thermo Scientific	EL0011
Buffers		
7x Pfu polymerase buffer	Thermo Scientific	EP0501
Antarctic Phosphatase buffer	NEB	M0289
NEBuffer™ r3.1	NEB	B6003S
T4 DNA ligase buffer	Thermo Scientific	B69
rCutSmart™ Buffer	NEB	B6004S

Table 7. Equipment.

EQUIPMENT	
Product	**Producer**
Amersham™ Imager 600	GE Healthcare
Amersham™ Protran™ 0.45 µm NC	GE Healthcare
Artist Pro 16 TP	XPPen Technology Co
Automated Cell Counter & Cell Viability Analyzer NORMA XS	Iprasense
Centrifuge 5415 D	Eppendorf
Centrifuge 5417 R	Eppendorf
Centrifuge 5910 Ri	Eppendorf
Eclipse TE2000-S	Nikon
Environmental Shaker-Incubator ES-20	Biosan
Incubated Shaker SIF6000R	Lab Companion
Infinite M200PRO	Tecan
Leica DMi8 microscope	Leica
Mini Rocker-Shaker	Biosan

Nanodrop 2000	Thermo Scientific
Pierce™ Spin Columns Snap Cap	Thermo Scientific
PowerPac™ HC	Bio-Rad
GenePro Thermal Cycler	Bioer
TransIlluminator InGenius3	Syngene
Trans-Blot® Turbo™ Transfer System	Bio-Rad

3.2. Methods

3.2.1. Cell culture methods

3.2.1.1. Culturing cells

Cells were cultured in humidified atmosphere with 5% CO_2 at 37°C under standard conditions by means of an incubator (Sanyo). Cells were cultivated on polystyrene Petri dishes (see Table 8). The confluence of cells was regularly determined using a light microscope (Nikon), and the cells were passaged once reaching 90-100% confluency to avoid overgrowing.

Table 8. Petri dishes characteristics.

Cell dish size	S [cm^2]	$V_{cell\ culture\ medium}$ [ml]
90 x 20 mm	57.5	8
60 x 18 mm	21.2	4

3.2.1.2. Passaging or splitting cells

Every 2-3 days cultured cells were passaged to achieve a confluence between 20-70%. The protocol of passaging was the following:

- Preheat culture medium to 37°C
- In a laminar air flow cabinet (Telstar) remove medium from the cell dishes using a vacuum pump
- Wash cells in PBS, remove with vacuum pump
- Add trypsin solution on cells, so that it covers the whole surface of the dish (1 ml for a 90 mm dish, 0.5 ml for a 60 mm dish)
- Put the dishes into an incubator for 3-5 minutes to allow cells detaching from plates
- Add fresh cell culture medium (volume equal to the volume of trypsin solution)
- Resuspend the cells, remove part of the suspension according to the desired ratio of confluence (for splitting one cell dish into several, split the suspension equally on as many dishes as needed)
- Add more medium to reach the final volume (see Table 1), and mix the solution by moving the dish from side to side to ensure even distribution

3.2.1.3. Storing cells

Cells were stored long term in liquid nitrogen (-196°C). One cryovial was prepared from one 90 mm Petri dish. The protocol of preparing cells for freezing was the following:

- Prepare cryogenic vials, name them properly
- Prepare freezing medium (FBS and DMSO in a 9:1 ratio, 1 ml total for 1 cryovial)
- In a laminar air flow cabinet remove medium from the dish with a vacuum pump
- Wash cells in PBS, remove with vacuum pump
- Add 1 ml of trypsin solution on cells, so that it covers the whole surface of the dish
- Put the dishes into an incubator for 3-5 minutes to allow cells detaching from plates
- Add 1 ml of fresh cell culture medium
- Resuspend the cells, add culture medium to a final volume of 4 ml and mix
- Transfer cells to a 15 ml falcon tube with and centrifuge for 4 minutes at 180 RCF at room temperature (RT)
- Remove the supernatant with a vacuum pump
- Resuspend the cells in freezing medium and transfer them to cryogenic vials
- Put the vials in Corning®CoolCell® Cell Freezing Container at -80°C freezer
- After 2-3 days move the vials to liquid nitrogen

3.2.1.4. Defrosting cells

To defrost cells after storage in liquid nitrogen, the following protocol was used:

- Preheat water bath and culture medium to 37°C
- Prepare one 15 ml falcon tube with 5 ml of cell culture medium per one cryovial
- Bring cryovials from liquid nitrogen and place them in a water bath to thaw
- Transfer cell suspension from cryovials to the prepared falcon tubes
- Centrifuge for 4 minutes at 180 RCF (1000 RPM) at RT, remove supernatant
- Resuspend the cells in 1 ml of culture medium, transfer them to a 90 mm Petri dish
- Add culture medium to a final volume of 8 ml and mix by moving the dish

3.2.1.5. Transient cell transfection

To prepare transiently transfected cells, the following protocol was used:

- Prepare the transfection solution (counted per one 90 mm dish): 900 µl of culture medium without FBS + 90 µl of LMW PEI + 15 µl of DNA, mix thoroughly using vortex and leave to set for minimum 20 minutes at RT
- Passage cells to 50-60% confluence, add transfection solution
- Incubate overnight (O/N) at 37°C, change medium to a fresh one next morning
- 2-3 days after transfection the cells can be used for experiments

3.2.1.6. QCM™ Gelatine Invadopodia Assay

To determine the ECM degradation abilities of particular cells, the following protocol was used:

A. *Coverslips preparation*:

- Prepare coverslips in EtOH, a fire source, a 12-well plate, parafilm, and sterile PBS
- Mix poly-lysine with dH_2O in 1:1 ratio (35 µl + 35 µl per coverslip)
- Take coverslips out of ethanol, sterilize them by putting on fire for a second, and afterwards onto the lid of a 12-well plate
- Drop 70 µl of poly-lysine-dH_2O solution per coverslip on parafilm, place coverslips on the drops, and incubate 20 minutes
- In a 12-well plate, put ~500 µl of sterile PBS per well, carefully turn coverslips upside down and place in wells, remove PBS with vacuum pump, add new PBS
- Mix glutaraldehyde with PBS to a final concentration of 2% (70 µl per coverslip)
- Drop 70 µl of 2% glutaraldehyde per coverslip on parafilm, place coverslips upside up on the drops, and incubate 15 minutes
- Wash 3x in ~500 µl of sterile PBS in a 12-well plate

B. *Preparation of gelatine* – in a laminar air flow cabinet:

- Stained Cy3-gelatine: 3 µl of Cy3-gelatine per coverslip heat on 60°C for 5 minutes, afterwards mix by vortexing with 9 µl of PBS per coverslip (1:3 ratio)
- Non-stained gelatine: 12 µl of non-stained gelatine per coverslip heat on 60°C for 5 minutes, afterwards mix by vortexing with 36 µl of PBS per coverslip (1:3 ratio)
- Mix Cy3-gelatine with non-stained gelatine

C. *Gelatine coating*:

- Drop 60 µl of prepared gelatine per coverslip on parafilm, place coverslips upside up on the drops, incubate 10 minutes at RT (from this point till the end of the experiment, protect coverslips from light by enveloping the 12-well plate in foil)
- Wash 3x in ~500 µl of sterile PBS in a 12-well plate
- Disinfection of wells with 70% ethanol: 500 µl per well, incubate 30 minutes at RT
- Wash 3x in ~500 µl of sterile PBS in a 12-well plate
- Stop residual aldehydes by DMEM: ~500 µl per well, incubate 30 minutes at RT

D. *Cells seeding*:

- Trypsinise cells on Petri dishes, add culture medium, centrifuge for 4 minutes at 180 RCF, remove supernatant, and resuspend in fresh cell culture medium
- Determine the number of cells in the suspension using the automated cell counter (iPrasense) and appropriate software (Norma XS)
- Calculate the dilution coefficient to achieve the number of 100 000 cells per 1 ml of culture medium, dilute the suspension accordingly
- Seed 1 ml of cells in culture medium per coverslip, incubate 15 minutes at RT
- Leave cells to set for 3-5 hours (time may vary for different cell types, here HT1080 were used) in an incubator at 37°C, to allow for gelatine degradation

E. *Cells fixation and immunolabelling for fluorescence microscopy*:

- Wash 2x in ~500 µl of sterile PBS in a 12-well plate
- Prepare 4% PFA from 8% PFA and PBS (1:1 ratio, 1 ml of 4% PFA per well)
- Fixation of cells: 1 ml of 4% PFA per well, incubate 10-15 minutes at RT

- Wash 2x in ~500 µl of sterile PBS in a 12-well plate
- Prepare 0.2% Triton X-100 from 20% Triton X-100 (1:1 ratio)
- Permeabilization of cells: 150 µl of 0.2% Triton X-100 per well, 10 minutes at RT
- Wash in ~500 µl of sterile PBS in a 12-well
- Blocking: 150 µl of 3% BSA in PBS per well, incubate 30 minutes – 1 hour at RT
- Incubation with primary antibody (here FLAG 1:1000) in 1% BSA in PBS for 45 minutes at RT (to economize antibodies, the best is to drop 60 µl of solution per coverslip on parafilm and place coveslips upside up on the drops)
- Wash in sterile PBS 3x for 10 minutes in a 12-well plate
- Prepare a mix of secondary antibody (here CAR488) + SiR-actin + DAPI in 1% BSA in PBS (5:10:1:5000 ratio, 60 µl of mix per coverslip)
- Drop 60 µl of prepared mix per coverslip on parafilm, place coverslips upside up on the drops, incubate 45 minutes at RT
- Wash in sterile PBS 3x for 10 minutes in a 12-well plate
- Prepare microscope slides for each coverslip, name them properly, and drop 9 µl of mounting medium per coverslip on them
- Rinse coverslips with dH_2O: put dH_2O in a glass, take a coverslip out of PBS and level it down into water for a second, then lift it again and put on a drop of prepared mounting medium
- Let the mounting medium to solidify overnight (O/N) in fridge

F. *Fluorescent microscopy*:

- To observe fluorescence of fixed cells on gelatine, the Leica DMi8 fluorescence microscope was used. Images were obtained in 4 channels: to observe gelatine and areas of its degradation (Cy3-gelatine), to observe cells themselves and invadopodia they form (SiR-actin), to observe presence and localization of transfected constructs (primary FLAG antibody + secondary CAR488 antibody), and to define cellular nuclei (DAPI).

G. *Image Analysis*:

- Image analysis was performed in ImageJ to determine gelatine degradation areas per particular cells, the obtained data were transferred to Microsoft Excel for statistical analysis.

3.2.1.7. Immunofluorescence

To assess the presence and/or localization of the transfected proteins with fluorescent tags, the following protocol was used:

- Seed cells onto ibidi 8-well / glass cover slips
- Incubate O/N at 37°C
- Wash 2x with chilled PBS
- Put the ibidi 8-well on ice, fixate the cells with 150 µl of 4% PFA in PBS per well for 10 minutes
- Wash with PBS
- Permeabilize with 150 µl of 0.2% Triton X-100 per well for 10 minutes

- Wash with PBS
- Block with 150 µl of 3% BSA in PBS per well for 1 hour
- Incubate with primary antibody in 1% BSA in PBS for 45 minutes
- Wash in PBS 3x for 10 minutes
- Incubate with secondary fluorescent antibody in 1% BSA in PBS 45 minutes
- Wash in PBS 3x for 10 minutes
- Incubate with DAPI (1:500 in PBS) for 20 minutes
- Wash in PBS 3x for 10 minutes
- Take images on microscope (see 3.2.1.6.F.)

3.2.2. Protein methods

3.2.2.1. Cell surface proteins crosslinking

To capture not only stable, but also transient interactions of the studied protein, crosslinking of cell surface proteins was used. The protocol of the procedure was the following:

- Prepare 5mM Dimethyl pimelimidate dihydrochloride (DMP) in PBS (pH 8.0)
- Wash cell dish with PBS
- Wash cell dich with PBS of pH 8.0
- Put ~3 ml of 5mM DMP in PBS of pH 8.0 per one 90 mm cell dish, incubate 10 minutes at 37°C
- Wash cell dish with TBS at RT to allow DMP neutralization by Tris
- Wash cell dish with TBS at 4°C
- Continue with cells lysis and immunoprecipitation

3.2.2.2. Cells lysis

To prepare lysates from cells, the following protocol was used:

A. *Lysates preparation*:

- Pre-cool centrifuge to 4°C, prepare ice, prepare lysis buffer (RIPA + mammalian protease inhibitors (100x))
- Put cells on ice, remove medium, wash 2x with PBS, remove all liquid
- Add lysis buffer (1 ml per 90 mm dish, 400 µl per 60 mm dish), lyse max 3 minutes
- Scrape lysate off the plate, transfer to 1.5 ml tube, scrape rest and add to the tube
- Homogenize with 26G syringe
- Spin 10-15 minutes at 15 000 RCF at 4°C
- Transfer clear lysate (supernatant) to a new tube

B. *Adjusting protein concentration*:

- Label a 96-well plate, take out BSA reference solutions
- Mix reagents A and S (24.5 µl + 0.5 µl per well), put 25 µl of premix into each well
- Add 2-5 µl of lysate or BSA reference solution + 1 blank (lysis buffer) – in triplicate
- Add 200 µl of reagent B
- Incubate in dark for 15 minutes
- Turn on Tecan, insert the 96-well plate, and measure relative concentrations

- In Microsoft Excel, average the triplicats, make graph with linear trendline, and show the equation $y = ax + b$
- Calculate concentrations, as $c = (average - b) / a$, define the lowest c as *desired c*
- To mix final lysate: *(desired c / current c) * desired V = V* of lysate to use, *desired V – V of lysate to use = V of lysis buffer to add*
- Add 6x Laemmli buffer, 20x DTT, boil at 95°C for 10 minutes
- Freeze the samples at -20°C or continue with SDS-PAGE, immunoprecipitation, or pulldown experiments

3.2.2.3. Co-immunoprecipitation

3.2.2.3.1. Proximity-dependent biotinylation and streptavidin affinity purification

To biotinylate the proteins in close proximity to biotin ligase, and precipitate the biotinylated ones, the following protocol was used:

- Use 3x 10cm plates per variant, (subconfluent to maximize cell-ECM contacts instead of cell-cell)
- Incubate in serum-free DMEM with 50 µM biotin for 18-24 hrs
- Wash the cells 3x in PBS at RT (lysis at RT prevents precipitation of SDS)
- Lyse with 400 µl per dish of 0.2% SDS lysis buffer
- Add 40 µl per plate of 20% Triton X-100 (2% final concentration), mix by pipetting (addition of Triton prevents precipitation at low temperature and aids solubilization of proteins)
- Move to ice, triturate by passing through needle (4x 25 G, then 4x 21 G)
- Add 360 µl of Tris-Cl per plate, then pass 4x through 19 G needle
- Centrifuge at 14k RCF for 15 minutes at 4°C
- Collect all lysates from each condition into 5 ml tubes
- Measure and adjust lysate concentration (see 3.2.2.2.B)
- Put 15 µl of magnetic streptavidin beads per condition on magnet in 1.5 ml tubes
- Wash beads 2x in 400 µl of equilibration buffer
- Collect 100 µl of adjusted lysate as *"whole cell lysate" (WCL)* samples for WB
- Use ~500 µl of lysate to collect beads from each 1.5 ml tube and transfer them into a 5 ml tube
- Add the rest of adjusted lysate to washed beads
- Resuspend beads by inverting tubes, rotate at 4°C O/N
- Briefly spin down, separate lysates with beads into 2x 1.5 ml tubes (800 µl for WB, the rest for mass spectrometry)
- Place on magnetic rack
- Collect 100 µl as *"flow through" (FT)* samples for WB to check how efficient affinity purification is, remove the rest of the supernatant
- Add 500 µl of wash buffer 1 (2% SDS), rotate 5 minutes at RT
- Wash again in 1 ml of wash buffer 1, rotate 5 minutes at RT
- Wash in wash buffer 2, rotate 5 minutes at RT
- Wash 2x in wash buffer 3, rotate 5 minutes at RT

- Wash again in wash buffer 3, rotate 5 minutes at RT
- Elute the samples at 70°C in 30 µl of 2.5x Laemmli buffer (to maximize dissociation of biotinylated proteins and minimalize streptavidin leaching)
- Freeze the beads for mass spectrometry

3.2.2.3.2. Immunoprecipitation using Strep-Tactin® Super Flow® beads

Using specialised columns (Pierce™ Spin Columns Snap Cap) will prevent samples loss during multiple washing steps and produce higher yield

To pull down proteins with Strep tags, the following protocol was used:

- Use 2x 90 mm dishes per variant, cells should be of 50-70% confluence to minimize cell-to-cell contacts
- Put plates on ice, wash 2x with pre-cooled PBS to 4°C
- Lyse with 600 µl per dish of 0.5% Triton X-100 lysis buffer
- Triturate 5x with 26G needle
- Centrifuge 15 minutes at 13000 RCF at 4°C, transfer cleared lysates to new tubes
- Measure and adjust lysates concentration (see 3.2.2.2.B.)
- Take out 50 µl of each cleared, concentration-adjusted lysate, and put into new tubes for *"whole cell lysate" (WCL)* samples, prepare them for SDS-PAGE by adding 6x Laemmli buffer, 20x DTT, and boiling 10 minutes at 95°C

If performing lysate preclearing:

- *Wash nProtein A Sepharose™ 4 Fast Flow beads (25 µl of beads per 500 µl of lysate from one 90 mm dish) in 500-700 µl of 0.5% Triton X-100 lysis buffer: add buffer to the beads, carefully resuspend, centrifuge 2 minutes at 1000 RCF, remove supernatant with 26G/29G needle; repeat twice*
- *Transfer 500 µl of cleared lysate onto the beads, rotate 40 minutes at 4°C*
- *Centrifuge 2 minutes at 1000 RCF, transfer the supernatant onto newly prepared (2x washed in lysis buffer) nProtein A Sepharose™ 4 Fast Flow beads; repeat 3x*

- Wash Strep-Tactin beads (15 µl per one dish) in 500-700 µl of 0.5% Triton X-100 lysis buffer: add the buffer to the beads, carefully resuspend, and centrifuge 2 minutes at 1000 RCF, remove supernatant with 26G/29G needle; repeat twice
- Transfer cleared, concentration-adjusted lysates onto the beads, rotate O/N at 4°C
- Centrifuge 2 minutes at 1000 RCF, take out 50 µl of supernatant and put into new tubes for *"flow through" (FT)* samples, prepare them for SDS-PAGE by adding 6x Laemmli buffer, 20x DTT, and boiling 10 minutes at 95°C
- Wash beads 2x in 500-700 µl of 0.5% Triton X-100 lysis buffer: add the buffer to the beads, carefully resuspend, and centrifuge 2 minutes at 1000 RCF, remove supernatant with 26G/29G needle, repeat
- Wash beads 1x in TBS, take out 50 µl of supernatant and put into new tubes for *"wash"* samples, prepare them for SDS-PAGE by adding 6x Laemmli buffer, 20x DTT, and boiling 10 minutes at 95°C; remove all the remaining supernatant

- Add 75 µl per sample of Strep-Tactin beads elution buffer and incubate 3-10 minutes, gently shaking the tubes occasionally
- Centrifuge 2 minutes at 1000 RCF, and transfer 70 µl of each elute into new tubes for *"elute"* samples, prepare them for SDS-PAGE by adding 6x Laemmli buffer, 20x DTT, and boiling 10 minutes at 95°C
- To check efficiency of elution, wash beads 2x with TBS and boil them in 35 µl of 2x Laemmli buffer, 20x DTT to elute remaining proteins from beads into the buffer – *"beads"* samples

3.2.2.3.3. Immunoprecipitation using Anti-FLAG® M2 magnetic beads

To pull down proteins with FLAG tags, the following protocol was used:

- Use 2x 90 mm dishes per variant, cells should be of 50-70% confluence to minimize cell-to-cell contacts
- Put plates on ice, wash 2x with pre-cooled PBS to 4°C
- Lyse with 600 µl per dish of 0.5% Triton X-100 lysis buffer
- Triturate 5x with 26G needle
- Centrifuge 15 minutes at 13000 RCF at 4°C, transfer cleared lysates to new tubes
- Measure and adjust lysates concentration (see 3.2.2.2.B.)
- Take out 50 µl of each cleared, concentration-adjusted lysate, and put into new tubes for *"whole cell lysate" (WCL)* samples, prepare them for SDS-PAGE by adding 6x Laemmli buffer, 20x DTT, and boiling 10 minutes at 95°C

If performing lysate preclearing:

- *Wash nProtein A Sepharose™ 4 Fast Flow beads (25 µl of beads per 500 µl of lysate from one 90 mm dish) in 500-700 µl of 0.5% Triton X-100 lysis buffer: add buffer to the beads, carefully resuspend, centrifuge 2 minutes at 1000 RCF, remove supernatant with 26G/29G needle; repeat twice*
- *Transfer 500 µl of cleared lysate onto the beads, rotate 40 minutes at 4°C*
- *Centrifuge 2 minutes at 1000 RCF, transfer the supernatant onto newly prepared (2x washed in lysis buffer) nProtein A Sepharose™ 4 Fast Flow beads; repeat 3x*

- Take 20 µl per sample of Anti-FLAG® M2 magnetic bead suspension (10 µl per sample of packed resin), put them into prepared tubes and place in magnetic stand
- After the beads attach to the magnet, remove supernatant
- Equilibrate beads with 200 µl of TBS, place in magnet, discard supernatant
- Repeat the previous step one more time
- Transfer 500 µl of cleared lysate onto beads, rotate 3 hours – O/N at RT on a rotator
- Place in magnetic stand, take out 50 µl of supernatant and put into new tubes for *"flow through" (FT)* samples, prepare them for SDS-PAGE by adding 6x Laemmli buffer, 20x DTT, and boiling 10 minutes at 95°C; discard the rest of the supernatant
- Wash beads 3x in 500 µl of TBS, during the 3rd wash place the tubes on rotator for 10 minutes at RT, then place in magnet and take out 50 µl of supernatant for *"wash"*

samples, prepare them for SDS-PAGE by adding 6x Laemmli buffer, 20x DTT, and boiling 10 minutes at 95°C

- Elute by adding 50 µl of Pierce™ 3X DYKDDDDK Peptide solution, incubate at RT for 30 minutes in orbital shaker
- Place in magnet and transfer all the supernatant (eluted fraction) into new tubes for *"elute"* samples, prepare them for SDS-PAGE by adding 6x Laemmli buffer, 20x DTT, and boiling 10 minutes at 95°C
- To check efficiency of elution, wash beads 2x with TBS and boil them in 20 µl of 2x Laemmli buffer to elute remaining proteins from beads into the buffer – *"beads"* samples

3.2.2.3.4. Immunoprecipitation with GFP antibody-coupled protein A sepharose beads

Using specialised columns (Pierce™ Spin Columns Snap Cap) will prevent samples loss during multiple washing steps and produce higher yield

To pull down proteins fused to GFP (EGFP), the following protocol was used:

- Use 1x 90 mm dish per variant, cells of 90-100% confluence
- Put plates on ice, wash 2x with pre-cooled PBS to 4°C
- Lyse with 300-600 µl per dish of 0.5% Triton X-100 lysis buffer
- Triturate 5x with 26G needle
- Centrifuge 15 minutes at 13000 RCF at 4°C, transfer cleared lysates to new tubes
- Measure and adjust lysates concentration (see 3.2.2.2.B.)
- Take out 50 µl of each cleared, concentration-adjusted lysate, and put into new tubes for *"whole cell lysate" (WCL)* samples, prepare them for SDS-PAGE by adding 6x Laemmli buffer, 20x DTT, and boiling 10 minutes at 95°C

If performing lysate preclearing:

- *Wash nProtein A Sepharose™ 4 Fast Flow beads (25 µl of beads per 500 µl of lysate from one 90 mm dish) in 500-700 µl of 0.5% Triton X-100 lysis buffer: add buffer to the beads, carefully resuspend, centrifuge 2 minutes at 1000 RCF, remove supernatant with 26G/29G needle; repeat twice*
- *Transfer 500 µl of cleared lysate onto the beads, rotate 40 minutes at 4°C*
- *Centrifuge 2 minutes at 1000 RCF, transfer the supernatant onto newly prepared (2x washed in lysis buffer) nProtein A Sepharose™ 4 Fast Flow beads; repeat 3x*

- Add anti-GFP antibody (1:1000) to the prepared lysates, rotate O/N at 4°C
- Wash nProtein A Sepharose™ 4 Fast Flow beads (25 µl of beads per 500 µl of lysate from one 90 mm dish) in 500-700 µl of 0.5% Triton X-100 lysis buffer: add the buffer to the beads, carefully resuspend, and centrifuge 2 minutes at 1000 RCF, remove supernatant with 26G/29G needle; repeat twice
- Transfer 500 µl of cleared lysate onto the beads, rotate 2 hours at 4°C on a rotator
- Centrifuge 2 minutes at 1000 RCF, take out 50 µl of supernatant and put into new tubes for *"flow through" (FT)* samples, prepare them for SDS-PAGE by adding 6x Laemmli buffer, 20x DTT, and boiling 10 minutes at 95°C

- Wash beads 3x in 500 µl of TBS, during the 3rd wash place the tubes on rotator for 10 minutes at RT, then centrifuge 2 minutes at 1000 RCF, take out 50 µl of supernatant and put into new tubes for *"wash"* samples, prepare them for SDS-PAGE by adding 6x Laemmli buffer, 20x DTT, and boiling 10 minutes at 95°C
- Elute by adding 30-60 µl of 0.1M glycine (pH 3.5), incubate at RT for 15 minutes, occasionally shaking the tubes
- Add 0.05x volume of glycine 1M Tris pH 9.2 (3 µl of Tris per 60 µl of glycine) for neutralization, centrifuge 2 minutes at 1000 RCF
- Transfer all the supernatant (eluted fraction) into new tubes for *"elute"* samples, prepare them for SDS-PAGE by adding 6x Laemmli buffer, 20x DTT, and boiling 10 minutes at 95°C
- To check efficiency of elution, wash beads 2x with TBS and resuspend them in the same volume as elute of TBS, prepare the samples for SDS-PAGE by adding 6x Laemmli buffer, 20x DTT, and boiling 10 minutes at 95°C – *"beads"* samples

3.2.2.4. SDS-polyacrylamide gel electrophoresis (SDS-PAGE)

To separate proteins based on their molecular weight, SDS-PAGE was performed. Table 9 shows the recipe that was used to prepare the gels.

Table 9. Tris-glycine PAGE gel recipe. Counted for one 0.75 mm / 1.00 mm thick gel.

Chemicals	10% Separation gel	Stacking gel
H_2O	2.08 ml	1.55 ml
4x Tris, SDS	1.25 ml (pH 8.8)	0.625 ml (pH 6.8)
Acrylamide	1.67 ml	0.325 ml
TEMED	3.40 µl	2.50 µl
10% APS	16.50 µl	12.50 µl

The protocol of the procedure was the following:

A. *Casting*:

- Assemble glass plates in casting frame and clamp them into the casting stand
- Mix H_2O, Tris/SDS buffer, acrylamide for both stacking and separation gels
- Add TEMED and 10% APS to separation gel, mix thoroughly, and immediately pipette into the casting "sandwich" up to the tops of the flaps on the casting frame
- Overlay with H_2O and leave to set for ~30-45 minutes
- Pour our H_2O, dry with cellulose pads
- Add TEMED and 10% APS to stacking gel, mix thoroughly and immediately pipette into the casting "sandwich" up to the top
- Insert comb avoiding formation of bubbles, leave to set for ~30 minutes

B. *Running*:

- Assemble sandwich and electrodes into the clamping frame
- Place clamping frame in tank, remove comb, and fill the chamber between the gels with SDS buffer
- Load ladder (0.5-2 µl) and samples (15 µl)

- Fill outer chamber with SDS buffer so that it covers the electrode
- Place lid properly (red and black must match)
- Run: 10 mA / gel for stacking gel, 20 mA / gel for separation gel

3.2.2.5. Gradient SDS-polyacrylamide gel electrophoresis

To separate proteins with considerably different molecular weights (including those, whose molecular weight is lower than 20 kDa), gradient SDS-PAGE was performed. Table 10 shows the recipe used to prepare the gels.

Table 10. Gradient (6-15%) PAGE gel recipe. Counted for one 0.75 mm / 1.00 mm thick gel.

Chemicals	6% Separation gel	15% Separation gel	Stacking gel
H_2O	2.65 ml	1.125 ml	1.55 ml
4x Tris, SDS	1.25 ml (pH 8.8)	1.25 ml (pH 8.8)	0.625 ml (pH 6.8)
Acrylamide	1 ml	2.5 ml	0.325 ml
TEMED	4 µl	4 µl	2.5 µl
10% APS	20 µl	20 µl	12.5 µl

The protocol of the procedure was the following:

A. Casting:

- Assemble glass plates in casting frame and clamp them into the casting stand
- Mix H_2O, Tris/SDS buffer, acrylamide for both stacking gels and separation gel
- Add TEMED and 10% APS to both separation gels, mix thoroughly, take 2.3 ml of 6% separation gel into a 5 ml pipette, fill up to 4.6 ml with 15% separation gel
- Let 2-3 air bubbles go through the gels to allow partial mixing and gradient, then immediately pipette into the casting "sandwich" up to the tops of the flaps on the casting frame
- Overlay with H_2O and leave to set for ~30-45 minutes, then follow the protocol of regular SDS-PAGE (see 3.2.2.4.) till the end

3.2.2.6. Immunoblotting

A. Western blot (WB):

- Prepare cassette, cut nitrocellulose membrane
- Wet blotting sponges in Transfer Turbo buffer and place one per gel in tray
- Take membrane out of protective paper, wet it in buffer, and place over the sponge
- Take the gel out from the sandwich, remove the stacking gel, and place separation gel on membrane
- Cover the gel with a second sponge
- Remove bubbles from stack using a roller
- Close cassette and decant excess buffer
- Insert cassette in the Trans-Blot® Turbo™ Transfer System (Bio-Rad), adjust the number of gels, set I = 2.5 A, U = 25 V, t = 9 minutes

B. Western blot ("wet") – for proteins of molecular weight higher than 100 kDa:

- Insert blotting insert and iced gel pack into tank
- Pour transfer buffer into a tray, place cassette into tray black side down
- Assemble sandwich in the tray, wetting every layer well in the following order: sponge, Whatman filter paper, gel (flipped!), membrane, Whatman filter paper, sponge
- Use blot roller to remove bubbles after adding gel, membrane and second layer of filter paper
- Close and lock the cassette and insert it into blotting insert in the tank (black to black)
- Pour transfer buffer from tray to tank, top it up with recycled buffer, if available
- Place the whole tank in a tray with ice slush in it or in the fridge
- Run with constant voltage – 25 V O/N or 100 V for 1h

C. Immunolabelling (proteins visualization by antibodies):

- Put membranes into TBS, cut them according to the sizes of proteins
- Block for 1 hour in 5% milk in TBS at RT, constantly shaking the tank
- Mix primary antibodies in 2% milk in TTBS, incubate with membranes O/N at 4°C
- Wash the membranes in TTBS 3x 10 minutes
- Mix secondary antibodies in 2% milk in TTBS, incubate with membranes for 1 hour
- Wash the membranes in TTBS 3x 10 minutes
- Rinse in TBS, prepare everything needed for visualization
- Visualize the chemiluminescence of antibodies using Amersham Imager 600 by WesternBright^{TM}ECL kit according to the manufacturer´s protocol

D. Stripping:

- Prepare stripping buffer
- Wash the membranes in TBS 2x 10 minutes
- Put membranes into the stripping buffer for maximum 20 minutes
- Wash the membranes in TBS 3x 5 minutes
- Block again for 10 minutes, continue with immunolabelling and visualizing

3.2.3. Bacterial culture methods

3.2.3.1. Preparation of chemically competent bacterial culture

To prepare a competent bacterial culture, the following protocol was used:

- Plate 5 µl of DH5α onto an agar plate without antibiotic and incubate at 37°C O/N
- Using a pipette tip, pick a single colony from the agar plate and transfer it to a 15 ml tube containing 12 ml of LB medium with antibiotic (1000x)
- Incubate at 37°C for ~12 hours in a shaking incubator
- Inoculate the prepared culture into 400 ml of LB medium to final $OD_{595} = 0.1$
- Incubate at 37°C on a shaker to $OD_{595} = 1$
- Cool the culture on ice and divide into 8x 50 ml falcons
- Centrifuge at 3000 RPM for 15 minutes at 4°C
- Remove the supernatant and resuspend the pellet in 4 ml of 0.1M $MgCl_2$
- Merge the suspensions in two 50 ml falcons, fill up to 50 ml with 0.1M $MgCl_2$ and centrifuge at 3000 g for 15 minutes at 4°C

- Remove the supernatant and resuspend the pellet in 5 ml of 0.1M $CaCl_2$
- Fill up to 50 ml with 0.1M $CaCl_2$ and incubate 20 minutes on ice
- Centrifuge at 3000 RPM for 15 minutes at 4°C
- Remove the supernatant and resuspend the pellet in 5 ml of 0.1M $CaCl_2$ and 14% glycerol
- Aliquot the suspension into 50 µl, 100 µl, or 150 µl samples and freeze quickly on dry ice
- Store the bacterial aliquots at -80°C freezer

3.2.3.2. Bacterial transformation

To transform bacteria while preparing a new construct, the following protocol was used:

- Prepare ice, dry agar plates with the appropriate antibiotic at -37°C in an incubator
- Bring competent DH5α (TOP10) bacteria from -80°C freezer and put them on ice
- Pre-heat heat block at 42°C
- Label a 1.5 ml tube, put 50 µl of bacteria per one ligation or PCR reaction product, add 5 µl of the reaction product (max 1/10 of the volume of bacteria), mix by stirring with a pipette tip
- Place in a heat block at 42°C for 1 minute, then place back on ice
- Add 500 µl of SOC medium, and rotate in an incubator at 37°C for 1 hour
- Centrifuge at 3000 RPM for 1 minute
- Remove most of the medium (so that only 70-100 µl is left) and resuspend
- Spread evenly on the preheated agar plate with an antibiotic (here kanamycin) using a glass stick under sterile conditions (flame)
- Incubate at 37°C O/N in an incubator

To transform bacteria with a construct, for the purpose of amplifying the existing construct, the following protocol was used:

- Prepare ice and KB medium with antibiotic (diluted 1000x)
- Under sterile conditions (flame), put 12 ml of KB medium with an added antibiotic into each 50 ml falcon tube
- Bring competent DH5α (TOP10) bacteria from -80°C freezer and put them on ice
- Pre-heat heat block at 42°C
- Label a 1.5 ml tube, put 25-30 µl of bacteria per one construct, add 200-1000 ng of DNA, mix by stirring with a pipette tip
- Place in a heat block at 42°C for 1 minute, then place back on ice
- If using plasmids with kanamycin resistance, add 500 µl of SOC medium, and rotate in an incubator at 37°C for 1 hour, then proceed with transferring the suspension under sterile conditions (flame) into the prepared tubes with KB medium and kanamycin (1000x diluted)
- If using plasmids with ampicillin resistance, simply transfer the suspension under sterile conditions (flame) into the prepared tubes with KB medium and ampicillin
- Incubate at 37°C O/N in an incubator

3.2.3.3. Bacterial culture inoculation

To inoculate bacterial culture from an agar plate into the medium, the following protocol was used:

- Prepare KB medium with an appropriate antibiotic diluted 1000x
- On an agar plate, choose several bacterial clones (usually 6 to 10 clones) of different sizes (to compare different examples) that are separated from others (each clone has to be grown from a single bacterial cell) by circling them with a marker and numbering
- Prepare corresponding number of 10 ml falcon tubes, label them, and under flame put 3 ml of the prepared KB medium with antibiotic into each one
- To provide sterile conditions, continue under flame with picking single colonies from the agar plate using a pipette tip, and placing them into the prepared falcons
- Incubate at 37°C for ~12 hours in a shaking incubator

3.2.3.4. Plasmid isolation

Transformed *Echerichia coli* strain DH5α were spread on agar plates and incubated O/N at 37°C. Afterwards, selected bacterial clones were inoculated into KB medium and incubated ~12 hours at 37°C with constant shaking. To isolate plasmid DNA from prepared transformed bacteria, the following protocol was used:

- Prepare lysis solution
- Centrifuge 1.5 ml of bacterial culture in 2 ml tube at 13,000 RPM for 1 minute, repeat if necessary (1 if isolating new constructs – leave 500 µl of culture in fridge for future inoculation)
- Remove medium with a vacuum pump, resuspend pellet in 150 µl TEG (use 100 µl of TEG if only 1.5 ml of culture was centrifuged) by vortexing 2 tubes together
- Lyse by adding 280 µl of lysis solution while gently vortexing
- After ~1 minute, add 420 µl of NH_4Ac while gently vortexing (mix by pipetting)
- In the fume hood, add 280 µl of phenol-chloroform, vortex each tube for 10 seconds
- Centrifuge at 13,000 RPM for 5 minutes, remove supernatant with vacuum pump
- Transfer upper colourless phase (750 µl if 150 µl TEG; 700 µl if 100 µl TEG) into new tube
- Add 0.7x of transferred volume of isopropanol, vortex, incubate 15 minutes at RT
- Centrifuge at 13,000 RPM for 15 minutes, remove supernatant with vacuum pump
- Add ~600 µl of 80% ethanol and shake tubes to dislodge pellet
- Centrifuge at 13,000 RPM for 1 minute, remove supernatant with vacuum pump
- Leave the tubes opened for 30 minutes at RT to dry pellet
- Dissolve pellet in 20 µl of RNAse-Tris-EDTA solution for 15-60 minutes at 37°C

3.2.4. DNA methods

3.2.4.1. Polymerase chain reaction (PCR)

Polymerase chain reaction was used to amplify DNA segments. The protocol of the procedure was the following:

- Set PCR program (Table 11) on Thermal Cycler (Bioer), preheat it to 98°C

Table 11. PCR program. Primer annealing temperature depends on the T_m of the primer. Time required for the synthesis of DNA depends on the length of the sequence (PfuX7 synthesizes ~1000 kb in 45 seconds).

Process	Temperature	Time	
Initial DNA denaturation	98°C	3 min	
Template denaturing	98°C	30 sec	20 cycles
Primer annealing	55-72°C	45 sec	
DNA synthesis	72°C	**x** min	
Final extension of fragments	72°C	10 min	
Cooling	4°C	∞	

- Mix reagents (Table 12) to a total reaction volume of 20 µl

Table 12. PCR mix.

Chemicals	Volume, µl
H_2O	13.2
Pfu buffer	2
dNTPs (10 mM)	1
each primer (10 µM)	1.25
DNA (10 ng/µl)	1
PfuX7	0.3

- Put the mixed reagents into PCR microtubes and place them into the Thermal Cycler, run the program
- After the program finishes, add 0.5 µl of DpnI to each reaction in order to chop up the template DNA, incubate the microtubes at 37°C for 1 hour

3.2.4.2. Gibson Assembly

The protocol provided by the manufacturer was used for GeneArt® Seamless Cloning and Assembly:

- In a 0.5 ml microcentrifuge tube, set up the reaction (Table 13)

Table 13. The seamless cloning and assembly reaction. If using multiple inserts, add 200 ng of each.

Components	Volume, µl
Insert(s) – 200 ng of each	x
Linear cloning vector – 50 ng	1
ddH_2O	to 5

- Quickly thaw the GeneArt® 2X Enzyme Mix and mix thoroughly by pipetting up and down, add 5 µl to the reaction
- Mix the reaction components completely by pipetting them up and down
- Incubate the reaction mix at RT for 15-30 minutes, not longer
- Place the reaction mix on ice for 2-5 minutes
- Use 2.5 µl of the seamless cloning and assembly reaction to transform 50 µl of TOP10 competent bacteria

3.2.4.3. Restriction enzyme digestion

To test the sequence of newly synthesized DNA, digestion with a restriction enzyme was used. The protocol of the procedure was the following:

- Choose the appropriate enzyme/enzymes using specialized software (here SnapGene was used), choose suitable buffer
- Mix the reaction with a total volume of 15 µl in a 0.5 ml tube (Table 14)

Table 14. Restriction reaction. If using multiple enzymes, add the same volume of each.

Chemicals	Volume, µl
chosen buffer	1.5
chosen restriction endonuclease	0.2
H_2O	12.8
DNA (1000 ng/µl)	0.5

- Incubate the tube at 37°C O/N

3.2.4.4. DNA gel electrophoresis

To separate DNA fragments according to their size, DNA gel electrophoresis was used. The protocol of the procedure was the following:

- Prepare 1% agarose gel in Erlenmeyer flask (50 ml for small cast, 100 ml for large cast): weight 1 g agarose, add 100 ml SB buffer – for large cast
- Cover the flask with lid and heat in a microwave until agarose is completely melted
- Let it cool or cool it under steam of cold water until it is not hot to touch
- Add 1.5 µl of DNA stain G (Serva) per 100 ml and mix
- Pour gel into tray (dammed by tape) and insert comb, leave to set for 20-30 minutes
- Remove tape and comb, place tray in chamber
- Add ~5 µl of DNA dye to the "+" part of the chamber, mix into the buffer
- Add loading dye to samples
- Load 4 µl of ladder and appropriate amount of samples (15-20 µl)
- Run gel at 120-150 V (should not exceed 100 A)

3.2.4.5. DNA purification

To purify isolated DNA using KAPA PureBeads, the following protocol was used:

- Completely resuspend the beads and equilibrate them to RT
- Pre-heat heat block to 37°C
- Add appropriate volume of beads to the isolated DNA (~5 µl of beads per 10 µl of DNA of size larger than 1 kbp), mix well by pipetting up and down
- Incubate at RT for 5-15 minutes
- Place on a magnet and wait for beads to separate (~2 minutes), remove liquid
- Wash 2x in ~500 µl of 70% ethanol removing it with vacuum pump
- Leave tubes open to dry beads (~3-5 minutes depending on the amount of beads)
- Take tubes off the magnet, add the appropriate amount of H_2O (20 µl per sample), resuspend, then wait 2-10 minutes for DNA to elute
- Incubate in the heat block at 37°C for 10 minutes
- Return to magnet and wait for the beads to separate
- Transfer eluted DNA to a new tube

To purify isolated DNA using AM Pure XP Beads, the following protocol was used:

- Completely resuspend the beads
- Pre-heat heat block to 65°C
- Add appropriate volume of beads to the isolated DNA (~18 µl of beads per 10 µl of DNA), mix well by pipetting up and down
- Incubate at RT for 5-10 minutes
- Place on a magnet and wait for beads to separate (~2 minutes), remove liquid
- Wash 2x in ~500 µl of 70% ethanol removing it with vacuum pump
- Leave tubes open to dry beads (~5-10 minutes depending on the amount of beads)
- To allow DNA elution, take tubes off the magnet, add the appropriate amount of H_2O (20 µl per sample), wait 1 minute, then resuspend the beads
- Incubate in the heat block at 65°C for 10 minutes
- Return to magnet and wait for the beads to separate
- Transfer eluted DNA to a new tube

3.2.4.6. DNA concentration measurement

To measure the concentration of isolated, purified DNA, was measured using NanoDrop 2000 Spectrophotometer.

3.2.4.7. Sequencing analysis

Samples for sequencing were prepared according to the specifications of the Laboratory of DNA sequencing. 200 ng of DNA was mixed with appropriate primers (10µM) to a total reaction volume of 8 µl, labelled properly, and sent to the facility. Primers were designed using GeneRunner and SnapGene softwares and provided by the KRD trading company.

4. Results

4.1. Investigation of MT1-MMP's interactions pool and identification of the potential novel MT1-MMP binding partners

The general experimental design of this step is schematically represented in Figure 9. The idea behind it is that MT1-MMP interaction partners can be isolated when bound to MT1-MMP using a proximity-dependent biotinylation (PDB) approach. Lately PDB approaches coupled with mass spectrometry (MS) have emerged as powerful techniques to study proximal protein interactions in living cells (Samavarchi-Tehrani et al., 2020). For our study we chose *E. coli* biotin ligase BirA, which is "highly specific in covalently attaching biotin to the 15 amino acid AviTag peptide, giving a homogeneous product with high yield" (Fairhead & Howarth, 2015). AviTag is a biotin-acceptor peptide of the GLNDIFEAQKIEWHE amino acid sequence. Therefore, the plan was to 1) insert AviTag sequences into MT1-MMP plasmids, 2) prepare BirA-encoding plasmids, 3) transfect both constructs into mammalian cells, 4) allow for PDB of AviTag-ed MT1-MMP, 5) perform affinity purification (AP) on streptavidin-conjugated resin, and 6) identify the isolated proteins isolated via mass spectrometry.

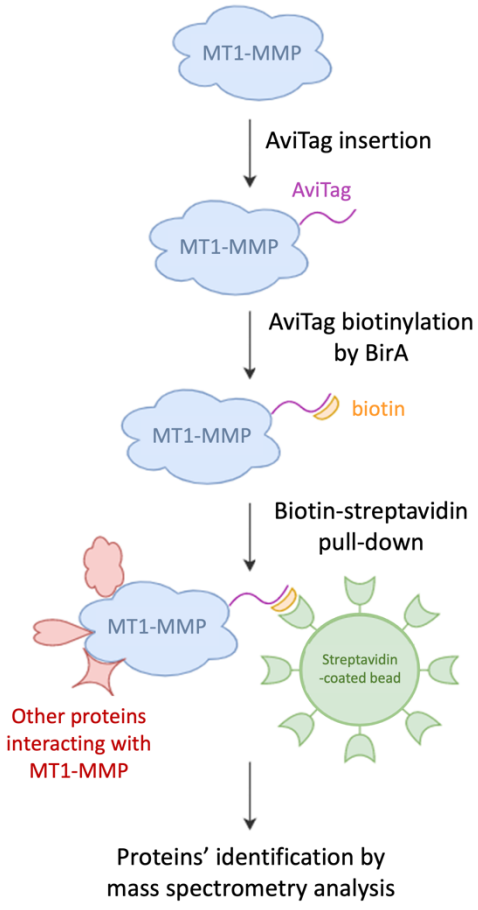

Figure 9. Simplified scheme of the "PDB-AP-MS" experimental design. Firstly, AviTags are inserted into MT1-MMP sequences to allow for biotin binding during the proximity biotinylation step. Secondly, BirA biotin ligase is cloned into IRES vector. Both pIRESpuro3_BirA and a variant of MT1-MMP-Avi constructs are transfected into HT1080 cells. During proximity-dependent biotinylation, BirA ligase attaches biotin to the AviTag peptide, and the biotinylated MT1-MMP-Avi, along with its interaction partners, is immunoprecipitated on Streptavidin-coated beads. After purification, the precipitated proteins are identified by mass spectrometry.

4.1.1. DNA constructs preparation

4.1.1.1. Introducing AviTag into cytoplasmic tail of MT1-MMP of the available MT1-MMP DNA plasmids

In this thesis, I follow up the work of my colleague, Katerina Strouhalova, MSc., who investigated the trafficking of MT1-MMP, and provided me with the plasmids, which contained MT1-MMP DNA sequence, as well as the ones with the mutant variants of the enzyme. A depiction of the plasmid with MT1-MMP *wild type* sequence is shown in Figure 10, and the mutated sequences of MT1-MMP used in this work are schematically represented in Figure 11.

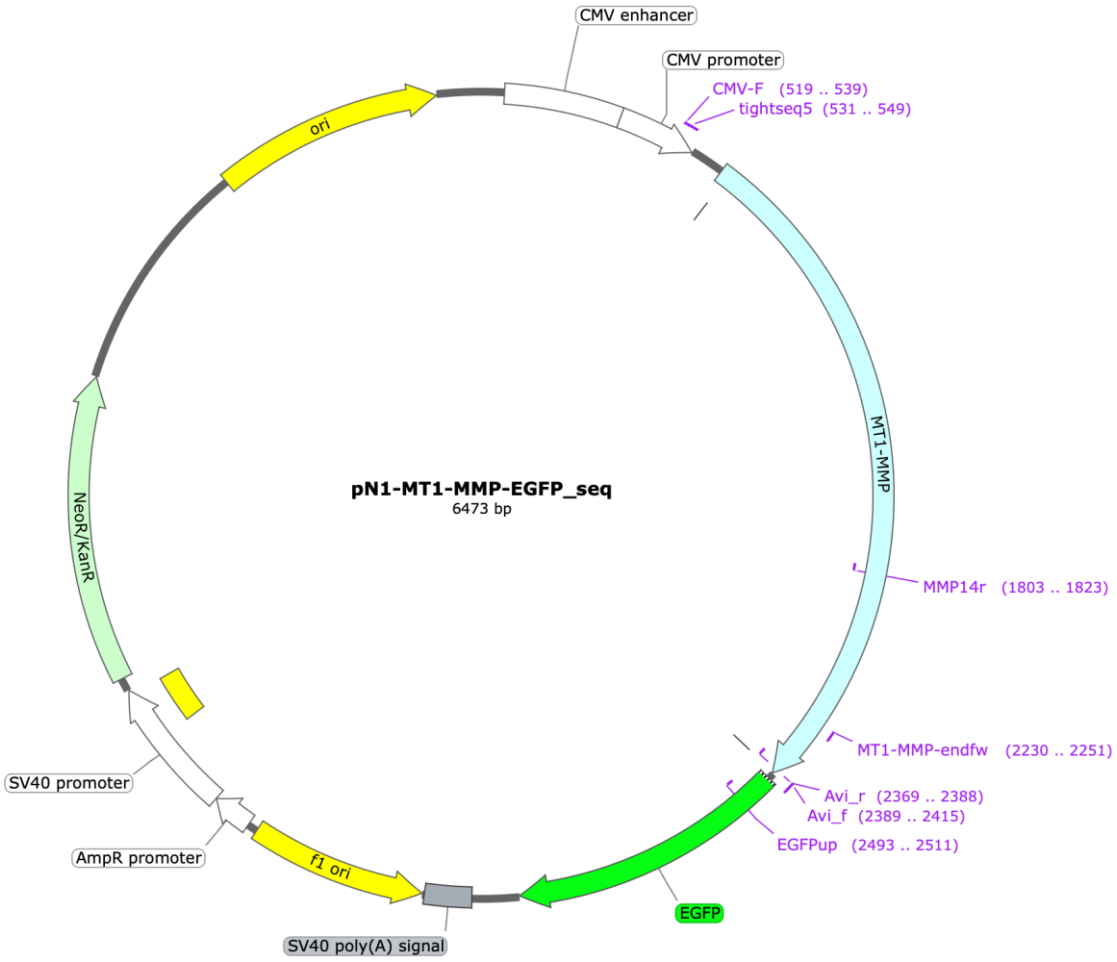

Figure 10. A schematic representation of the pN1-MT1-MMP-EGFP plasmid available in our laboratory, shown in the SnapGene Viewer software. The plasmid contains origin of replication (ori), CMV enhancer and CMV promoter, *wild type* MT1-MMP sequence, EGFP sequence, SV40 poly(A) signal, f1 ori, AmpR promoter, SV40 promoter and SV40 ori (represented by a yellow rectangle), and a gene for neomycin or kanamycin resistance (NeoR/KanR). PRO = MT1-MMP prodomain; CAT = catalytic domain; HPX = hemopexin domain.

The chosen mutants were all previously reported to have impaired MT1-MMP endocytosis (Anilkumar et al., 2005; Uekita et al., 2001). To be precise, under normal conditions, the LLY^{573} sequence binds AP-2, an adaptor protein which induces clathrin-mediated endocytosis (Uekita et al., 2001; Anilkumar et al., 2005). Apart from this, these amino acids are key for MT1-MMP interaction with actin and invadopodia formation (Yu et al., 2012), and the last tyrosine is phosphorylated by Src, which triggers MT1-MMP association with FAK and p130Cas and its recruitment to focal adhesions (Wang and McNiven, 2012). Cys^{574} is necessary for Src-induced binding of caveolin-1 to MT1-MMP (Labrecque et al., 2004) and needs to be palmitoylated for clathrin-mediated endocytosis (Uekita et al., 2001; Anilkumar et al., 2005). Therefore, when these amino acids are mutated or the cytoplasmic tail is absent completely, MT1-MMP endocytosis is altered, which might affect the function of the enzyme, and thus cell migration and/or invasion.

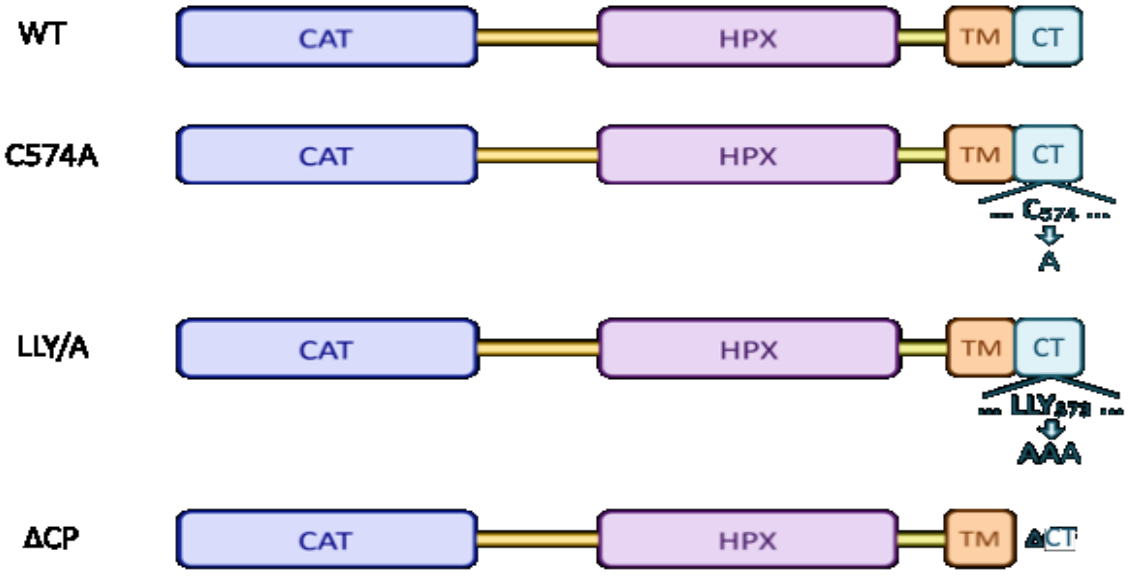

Figure 11. Simplified schemes of the main MT1-MMP mutant variants used in this work. WT = wild type form of the enzyme; C574A = C-terminal amino acid replacement mutant with Cys^{574} substituted for Ala; LLY/A = C-terminal amino acid replacement mutant with LLY^{573} substituted for AAA; ΔCP = cytoplasmic domain deletion mutant. Created by Katerina Strouhalova, MSc.

In order to perform the proximity-dependent biotinylation (Figure 9), we firstly needed to insert AviTags into the mentioned MT1-MMP constructs. We have chosen an insertion target site in the MT1-MMP's cytoplasmic tail sequence in such a way that it would not disrupt any of the known other proteins' binding sites (Figure 12).

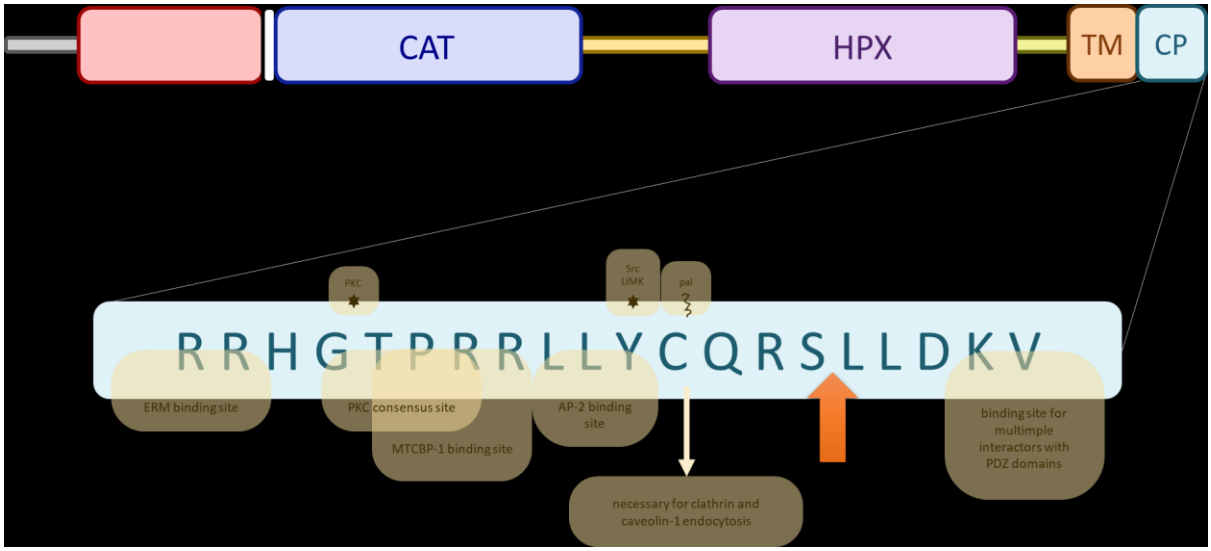

Figure 12. Target site for AviTag insertion was chosen between Ser[577] and Leu[578], since we supposed that sequence disruption at this site would not affect any known interactors binding. Slightly transparent yellow boxes outline amino acid sites known to be involved in different cellular processes and interactions. Specifically, RRH[565] is the binding site of moesin – one of ERM proteins; Thr[567] is phosphorylated by PKC, whereas TPR[569] is a supposed PKC consensus sequence; PRR[570] motif is a known binding site of MTCBP-1; LLY[573] motif interacts with the μ2 subunit of AP-2, and Tyr[573] in particular is phosphorylated by means of either Src kinase or LIMK1/2; Cys[574] is important for clathrin and caveolin-1 endocytosis; and the final DKV[582] motif is a binding site for multiple interactors. Created by Katerina Strouhalova, MSc.

Next, we have designed primers (Attachment 2) containing AviTag sequence and the sequence complementary to the plasmids we had (Figure 13). Since our plasmids contained a mutation of terminal Val[582] → Asp, we also aimed to reverse this mutation with the prepared primers.

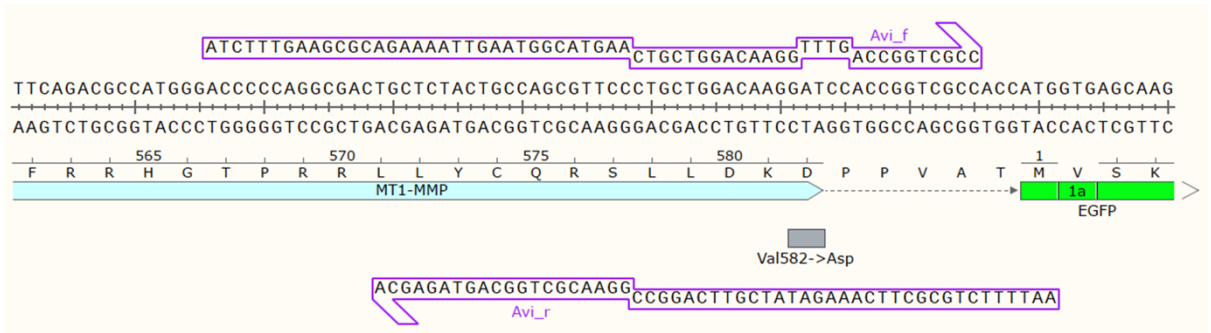

Figure 13. A schematic representation of primers synthesized for AviTag insertion into pN1 plasmid containing *wild type* MT1-MMP sequence. Primers contain Val[582] instead of an

Asp[582] in order to reverse the MT1-MMP sequence mutation in one step. The figure was made using the SnapGene Viewer software. Avi_f = forward primer; Avi_r = reverse primer.

After running a PCR of the described MT1-MMP plasmids with the prepared primers, we verified the obtained sequence corresponded to the expected through transforming bacteria with the prepared constructs, seeding them on kanamycin plates, inoculation of selected clones into KB medium, plasmid isolation, restriction enzyme digestion, and DNA electrophoresis. Enzymes SalI and EcoRV were chosen for verification of AviTag presence, whereas BamHI restriction was chosen to make sure the stop codon was recovered (Figure 14).

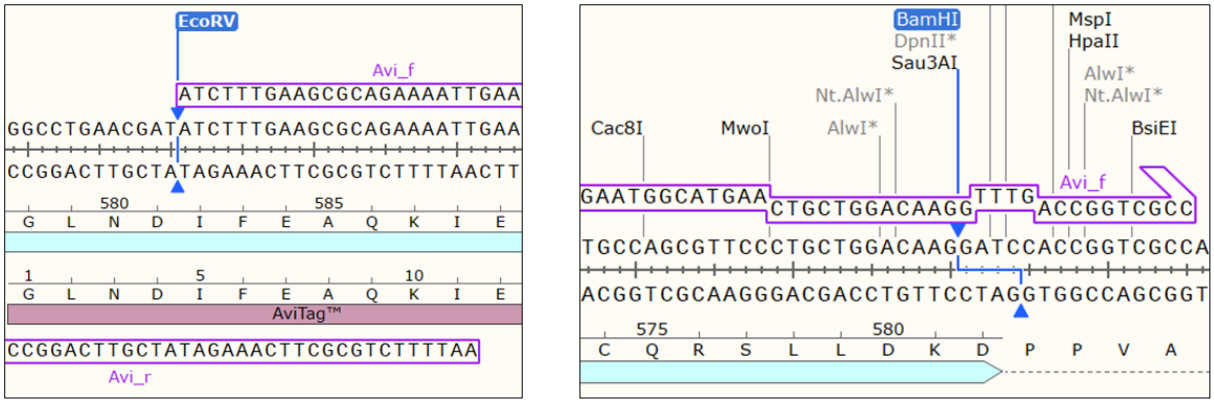

Figure 14. Restriction sites of the enzymes. First (left) picture shows the restriction sequence GAT↓ATC of EcoRV, which, if present, verifies the accuracy and presence of inserted AviTag sequence. Second (right) picture shows the BamHI restriction sequence G↓GATTC, which should be eliminated if the mutagenesis succeeds. The figure was made using the SnapGene Viewer software. Avi_f = forward primer; Avi_r = reverse primer.

The expected results of *wild-type* MT1-MMP-Avi DNA restriction analysis were:

1st reaction (to confirm proper cloning of AviTag into MT1-MMP-WT): 2 restriction sites, expected fragments 4727 bp and 1761 bp long;

2nd reaction (to confirm DKV mutation correction & stop-codon insertion): 1 restriction site, expected fragment 6518 bp long (BamHI site is eliminated).

The obtained DNA gel is displayed in Figure 15.

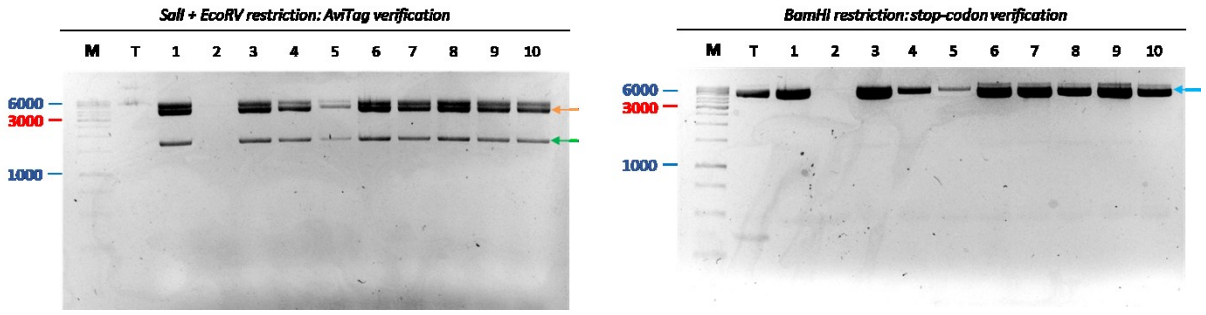

Figure 15. Restriction analysis of the DNA isolated from the bacterial clones. First (left) gel shows results from the restriction with SalI and EcoRV; second (right) – from the restriction with BamHI. Arrows indicate the sizes of expected fragments: orange = 4727 bp, green = 1761 bp, blue = 6518 bp. M = marker; T = template; 1-10 = numbers of particular clones.

The same restriction analysis was repeated for the plasmids of the mutated variants of MT1-MMP, the results are shown in Figure 16. The sizes of expected fragments were:

1st reaction (to confirm proper cloning of AviTag into MT1-MMP) – SalI + EcoRV:

- C574A: 4757 bp + 1761 bp (template size 6473 bp);
- LLY/AAA: 4757 bp + 1761 bp (template size 6473 bp);
- dCP: 4745 bp + 1731 bp (template size 6413 bp).

2nd reaction (to confirm DKV mutation correction & stop-codon insertion) – BamHI:

- C574A: 6518 bp (template 6103 bp + 370 bp);
- LLY/AAA: 6518 bp (template 6103 bp + 370 bp).

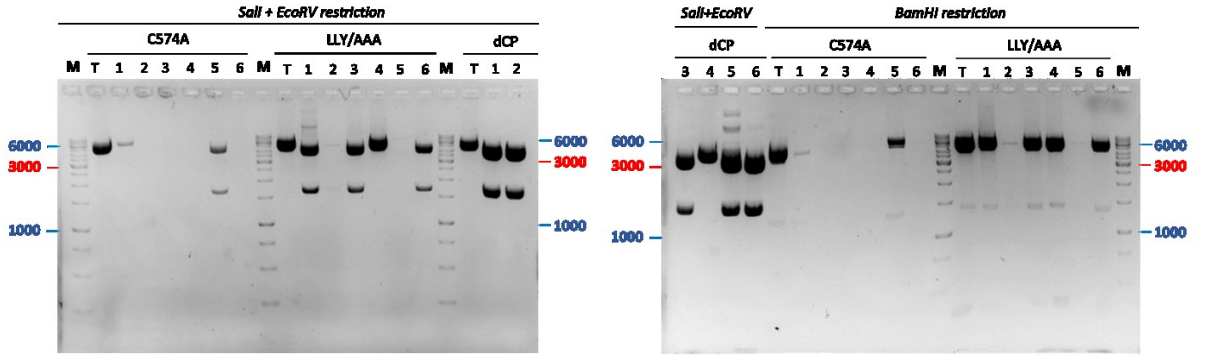

Figure 16. Restriction analysis of the DNA isolated from the bacterial clones transfected with the mutated MT1-MMP variants. First (left) gel and left part of the second (right) gel show results from the restrictions with SalI and EcoRV; right part of the second (right) gel shows the result of the restriction with BamHI. M = marker; T = template; C574A, LLY/AAA, dCP = MT1-MMP mutant variants; 1-10 = numbers of particular clones.

Based on the electrophoresis results, the clones with fragments' sizes corresponding to those expected were selected as successful: clone #3 for MT1-MMP-Avi-WT, clone #5 for MT1-MMP-Avi-C574A, clone #3 for MT1-MMP-Avi-LLY/AAA, clone #1 for MT1-MMP-Avi-ΔCP. DNA of these particular clones was purified, its concentration measured, and DNA sequencing using tightseq5, MMP14r, and EGFPup primers (Attachment 2) confirmed the sequences precisely corresponded to those expected.

4.1.1.2. *E. coli* biotin ligase (BirA) cloning into IRES vector

According to the plan (Figure 9), our next step was the preparation of plasmids encoding BirA. pIRESpuro3 vector available in our laboratory was chosen as backbone (Figure 17).

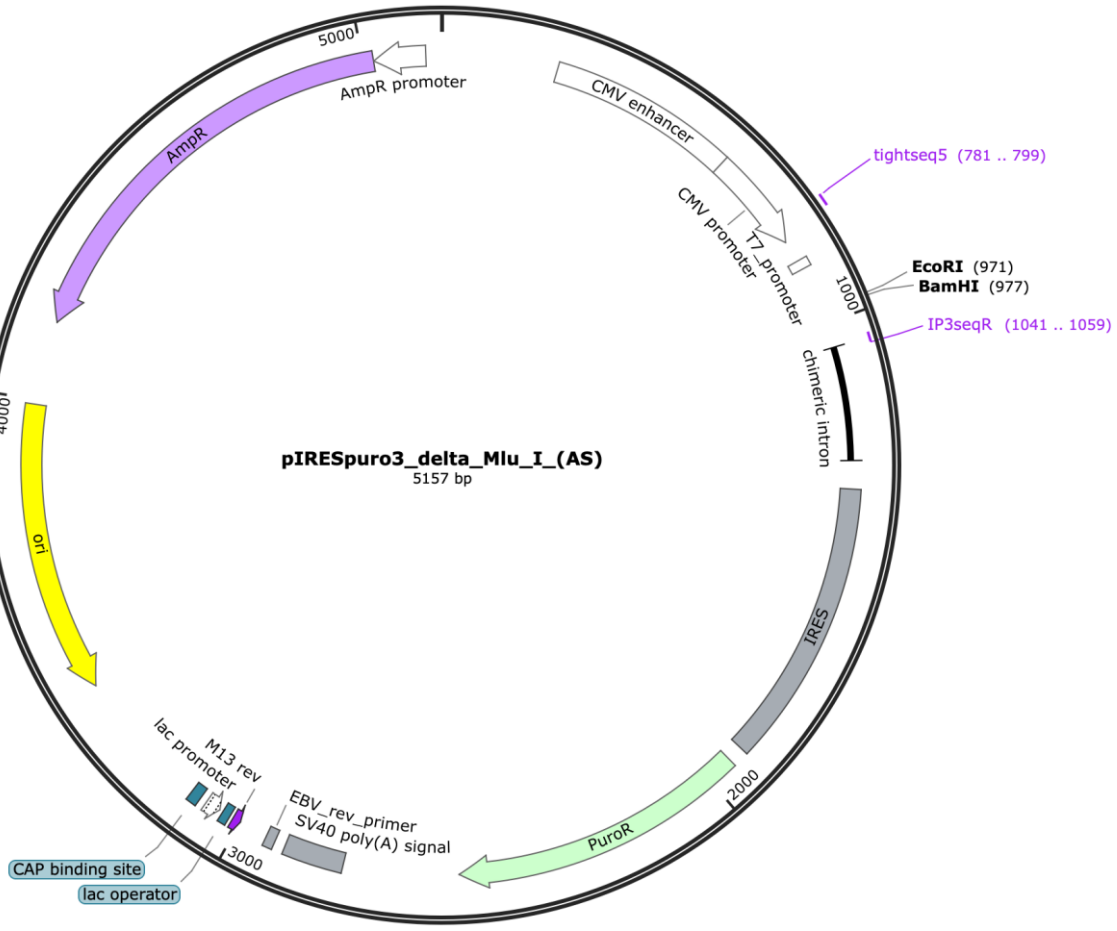

Figure 17. pIRESpuro3 vector available in our laboratory.

We have designed primers BirA_IRES_f and BirA_IRES_r (Attachment 2) for PCR of the BirA sequence so that they comprised 20 bp complementary with template (predicted sequence of the combined BirA insert and IRES vector), a restriction site (EcoRI and BamHI for the BirA_IRES_f and BirA_IRES_r primers correspondingly), and 2-3 bp based on

enzymes' nucleotides' preferences. BirA_IRES_r also contained the 6x His-tag to allow for its insertion in frame with BirA insert as well.

Next, restriction enzymes digestion using EcoRI and BamHI was performed with both the prepared BirA insert sequence and pIRESpuro3 backbone vector to create mutually fitting ends. Afterwards, DNA gel electrophoresis was done with the BirA restriction product, the DNA of corresponding size was extracted from the gel. The backbone vector DNA was purified; concentrations of both insert and vector were measured. Then Antarctic phosphatase was added to the backbone DNA and the tube was incubated with Antarctic phosphatase reaction buffer for 1 hour at 37°C. To inactivate the phosphatase, the tube was next incubated at 80°C for 2 minutes. Ligation of BirA into IRES vector was done using T4 DNA Ligase in T4 DNA Ligase reaction buffer, the reaction was mixed according to the measured vector and insert concentrations and incubated for 2,5 hours at RT. The ligation product was then used to transform bacteria, which we seeded on plates with ampicillin. We inoculated selected clones from the plate into medium, performed plasmid isolation and DNA restriction analysis using SspI. The sizes of the expected fragments were 4213 bp and 1949 bp; the template expected size was 5157 bp. The resulting DNA gel is shown in Figure 18.

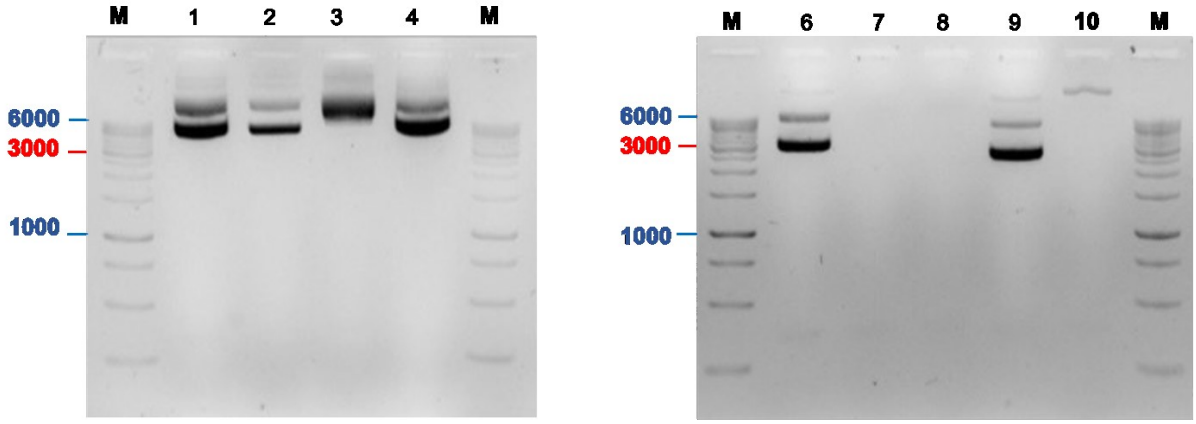

Figure 18. Restriction analysis of the DNA isolated from bacterial clones transfected with the prepared pIRESpuro3_BirA construct. Restriction was done with SspI enzyme, the expected fragments were 4213 bp and 1949 bp long. M = marker; 1-10 = numbers of particular clones.

As can be seen, the resulting fragments are much bigger than those expected, approximately 3000 bp and 6000 bp, in most of the clones. For this reason, we have repeated the restriction analysis with clones #6 and #9 in order to eliminate a possible technical errors' effect (Figure 19).

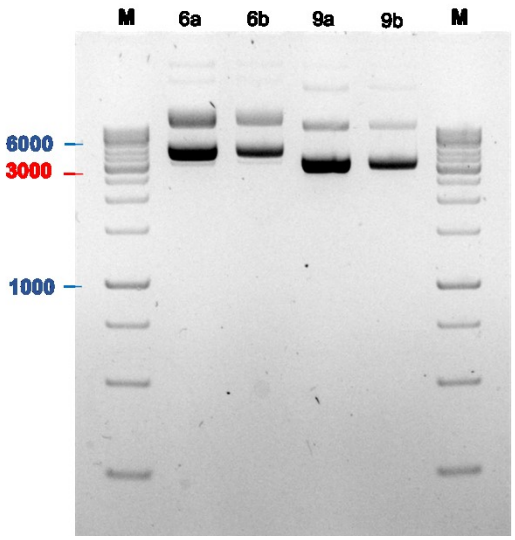

Figure 19. Restriction analysis of the DNA isolated from bacterial clones #6 and #9 transfected with the prepared pIRESpuro3_BirA construct. Restriction was done with SspI enzyme, the expected fragments were 4213 bp and 1949 bp long. M = marker; 6a = clone #6, 10 μl of sample; 6b = clone #6, 5 μl of sample; 9a = clone #9, 10 μl of sample; 9b = clone #9, 5 μl of sample.

The resulting fragments did not correspond to those expected, which we could not explain, and so we have performed DNA sequencing using primers tightseq5 and IP3seqR (Attachment 2). My colleague Katerina Strouhalova, who analysed the sequencing results, found that in clone #6, when sequencing started from tightseq5 primer (bases 781-799), the bases corresponded to those of the predicted sequence until 845-900 bp, when the sequence continued with bases from 3500 bp in the predicted sequence. Meaning that not only the desired BirA insert sequence is absent, but also part of the source vector is deleted. In clone #9 both primers produced no product. So, we may conclude that the molecular cloning did not work properly, and thus the construct cannot be used in future steps.

Later we have decided to employ another method using BioID2, which will be explained in next chapters (see 5.1.3.).

4.1.2. Transient transfection of HT1080 cells with the prepared constructs

In order to avoid misunderstandings, this part of the work, as well as the following chapters 4.1.3., 4.1.3.1., and 4.1.4. were conducted mainly by my colleague Katerina Strouhalova, MSc., as a part of her PhD studies and are presented here for the purpose of complete explanation of all of the experiments, thoughts and decisions flow.

To check the expression of the prepared MT1-MMP-Avi constructs, we have transfected them into HT1080 cells, prepared the lysates and performed immunoblotting analysis with anti-AviTag, anti-MT1-MMP and (after stripping) anti-GAPDH antibodies (Figure 20). As can be seen, anti-AviTag antibody detects AviTag in positive control, as well as some other proteins, suggesting its low specificity or cross-reactivity/recognition. MT1-MMP active form is clearly detected in the transfected cells, but also in control, indicating low

difference between expression of MT1-MMP from the transfected constructs and its endogenous levels. We concluded that the expression of the prepared constructs in HT1080 cells is very low and needs to be optimized (discussed in 5.1.1.).

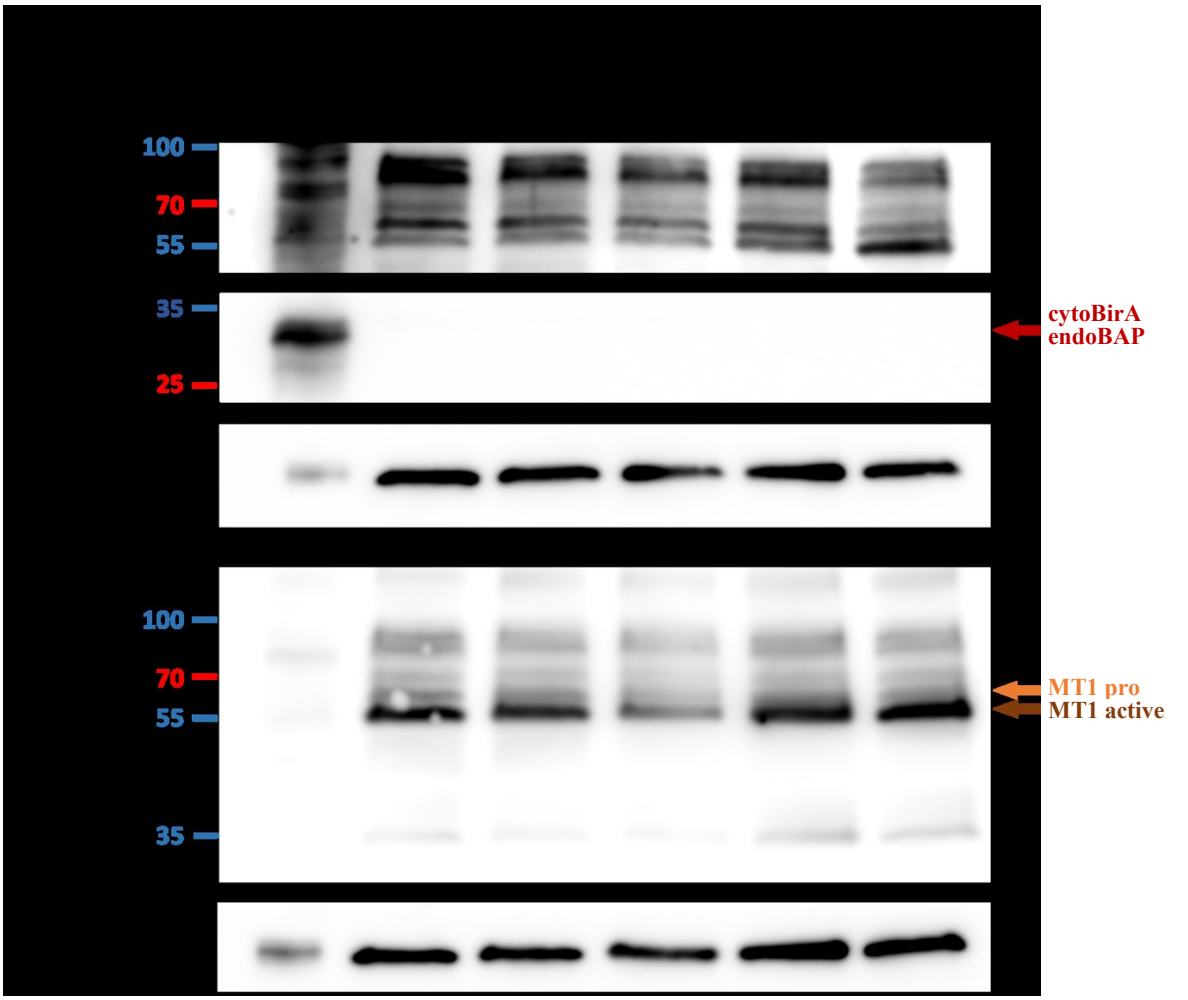

Figure 20. Western blot of the lysates prepared from MT1-MMP-Avi constructs-transfected HT1080 cells. Top membranes show detection with anti-AviTag antibody (1:5,000), bottom membrane – anti-MT1-MMP antibody detection (1:10,000). GAPDH (1:5,000) served as a loading control. CytoBirA endoBAP Dolezal construct encoding an Avi-tagged protein of 32kDa was used as a positive control. Arrows indicate the expected sizes of proteins: red = 32 kDa cytoBirA endoBAP; orange = 60-63 kDa MT1-MMP "pro" or "cleaved pro" forms; brown = 55 kDa MT1-MMP "active" form. Ctrl no tf = control non-transfected HT1080 cells; WT = MT1-MMP-WT-Avi; C574A = MT1-MMP-C574A-Avi; LLY/A = MT1-MMP-LLY/AAA-Avi; ΔCP = MT1-MMP-dCP-Avi.

4.1.3. Isolation of MT1-MMP along with its interactors

Since we were not able to create the pIRESpuro3_BirA construct and the pN1-MT1-MMP-Avi constructs were not expressed properly in cells, we have decided to use the BioID2 method for proximity-dependent biotinylation (discussed in 5.1.3.). My colleague Katerina Strouhalova has prepared and verified the constructs of *wild type* MSC-MT1-MMP-BioID2-HA (Figure 21) and the cytoplasmic tail deletion mutant MSC-MT1-MMP-dCP-BioID2-HA (not shown).

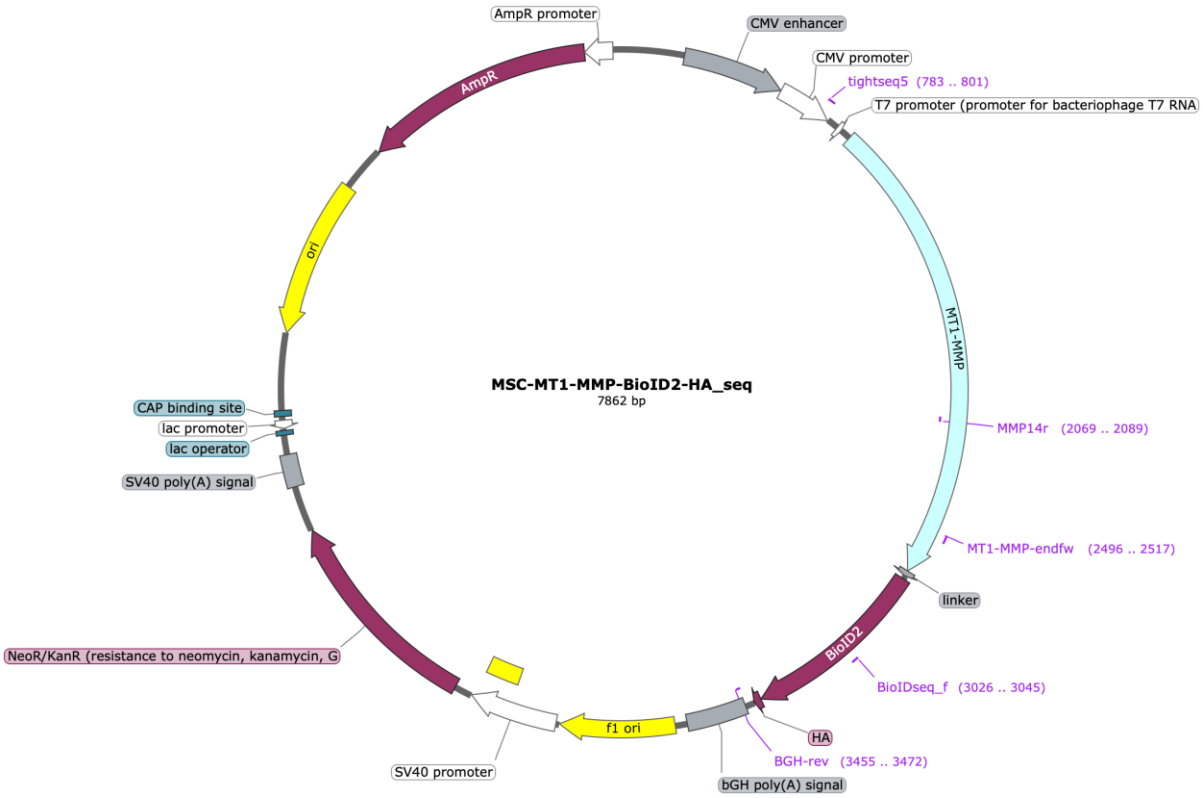

Figure 21. A schematic representation of the MSC-MT1-MMP-BioID2-HA plasmid created by my colleague, shown in the SnapGene Viewer software. The plasmid contains origin of replication (ori), CMV enhancer and CMV promoter, *wild type* MT1-MMP sequence, BioID2 sequence, HA-Tag, bGH poly(A) signal, f1 ori, SV40 promoter, a gene for neomycin or kanamycin resistance (NeoR/KanR), SV40 poly(A) signal, lac operator, lac promoter, catabolite activator protein (CAP) binding site, AmpR promoter, and AmpR gene.

4.1.3.1. Proximity-dependent biotinylation and streptavidin affinity purification

HT1080 cells were transfected with *wild type* MSC-MT1-MMP-BioID2-HA and MSC-MT1-MMP-dCP-BioID2-HA constructs, non-transfected cells served as a control. Proximity-

dependent biotinylation of MT1-MMP and its close surrounding was performed according to the protocol (see 3.2.2.3.1.). Lysates of ~2300 µl were divided in two parts: 800 µl were used for streptavidin affinity purification (AP) and following immunoblotting analysis of "WCL", "flow through" and "pulldown" samples (Figure 22); the rest (~1500 µl) underwent streptavidin AP without the elution step, resulting beads with the bound proteins were frozen for further mass spectrometry analysis.

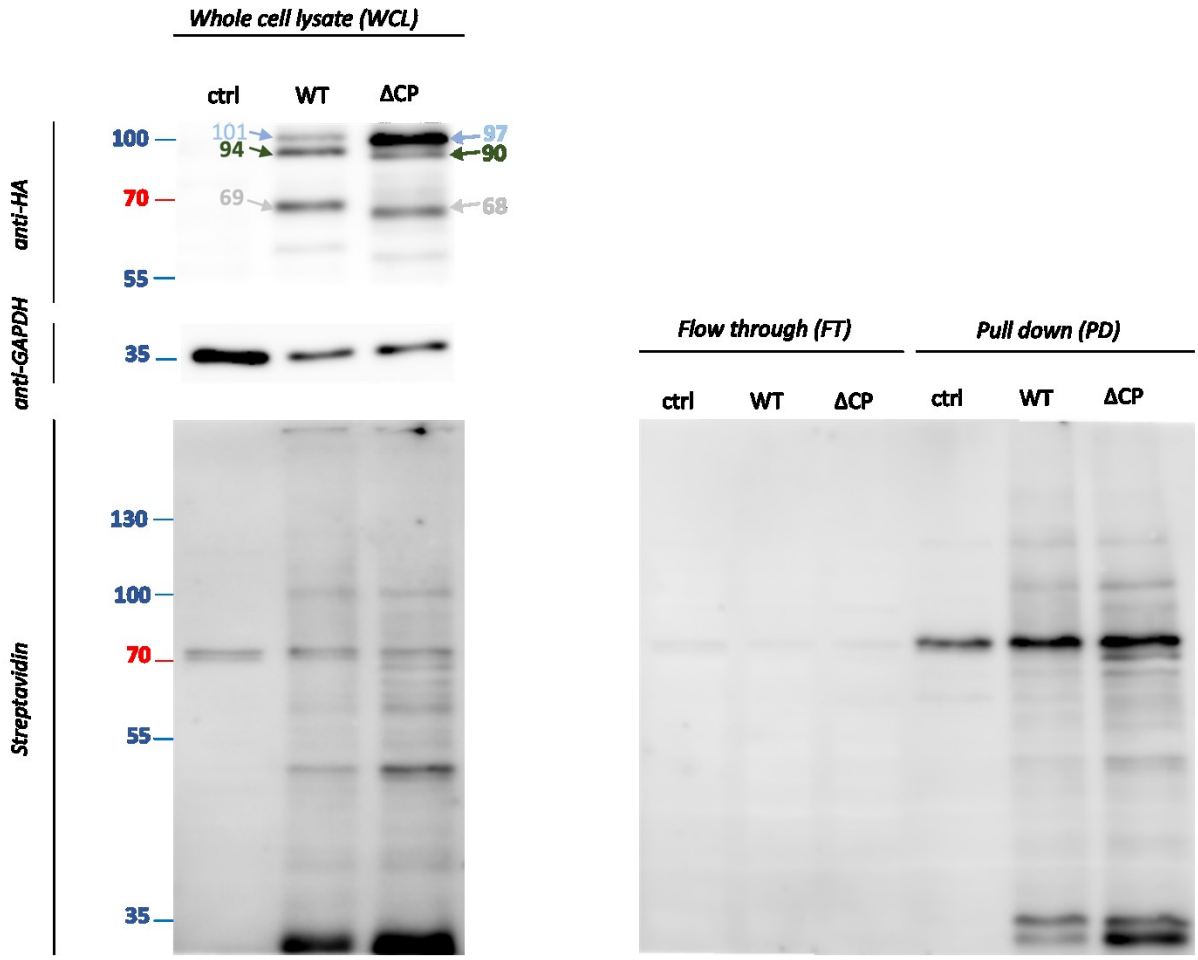

Figure 22. Western blot of the samples resulting from PDB followed by streptavidin AP. Top membranes show detection with anti-HA and anti-GAPDH antibodies, bottom membranes were detected with streptavidin-peroxidase polymer. GAPDH served as a loading control. Arrows indicate the expected sizes of proteins: light blue = 101 kDa MSC-MT1-MMP-WT-BioID2-HA (MT1-MMP-WT with HA tag, pro form); dark green = 94 kDa MSC-MT1-MMP-WT-BioID2-HA (MT1-MMP-WT with HA tag, active/cleaved pro form); grey = 69 kDa MSC-MT1-MMP-WT-BioID2-HA (MT1-MMP with HA tag, inactive form). Ctrl no tf = control non-transfected HT1080 cells; WT = MT1-MMP-WT-BioID2-HA; ΔCP = MT1-MMP-dCP-BioID2-HA.

As can be seen from GAPDH detection, the lysates' concentrations were not adjusted properly. *"Flow through"* almost does not contain any proteins, which suggests that the precipitation worked and most of them bound to the beads. *"Pull down"* samples (here they correspond to the eluted fraction) show that some of the biotinylated proteins were successfully precipitated and eluted. The band of proteins around MT1-MMP size precipitated from the non-transfected control cells is supposed to be endogenous MT1-MMP.

4.1.4. Identification of the isolated proteins by mass spectrometry

As it was mentioned before, during the PDB-AP, samples were divided into two: for the following immunoblotting analysis and for mass spectrometry (MS). The beads with bound proteins from MS samples were sent for MS analysis, which revealed notable differences in the biotinylated proteins identified in *wild-type* MT1-MMP-transfected cells and those in MT1-MMP-dCP-transfected cells. Particularly, the following proteins demonstrated reduced enrichment in the dCP sample compared to the WT sample: AHNAK, AHNAK2, desmoglein-2, Nectin-2, EPHA2, CD44, ZO-2 (TJP2), Integrin β1, Pinin, Filamin-A, Myosin-9 and more (discussed in 5.2.2.).

4.2. Verification of the supposed interaction with desmoglein-2 by coimmunoprecipitation

As it has been told, my colleague and I have identified several proteins to be potential interaction partners of MT1-MMP. At the same time, another my colleague, RNDr. Ondrej Tolde, PhD., has identified desmoglein-2 as one of MT1-MMP transient interactors, in his immunoprecipitation experiments (Figure 23). Before cells lysis, he used a crosslinking molecule (dimethyl pimelimidate, Figure 24), which linked proteins in close proximity to each other on cell surface, enabling to capture not only stable, but also transient interactions.

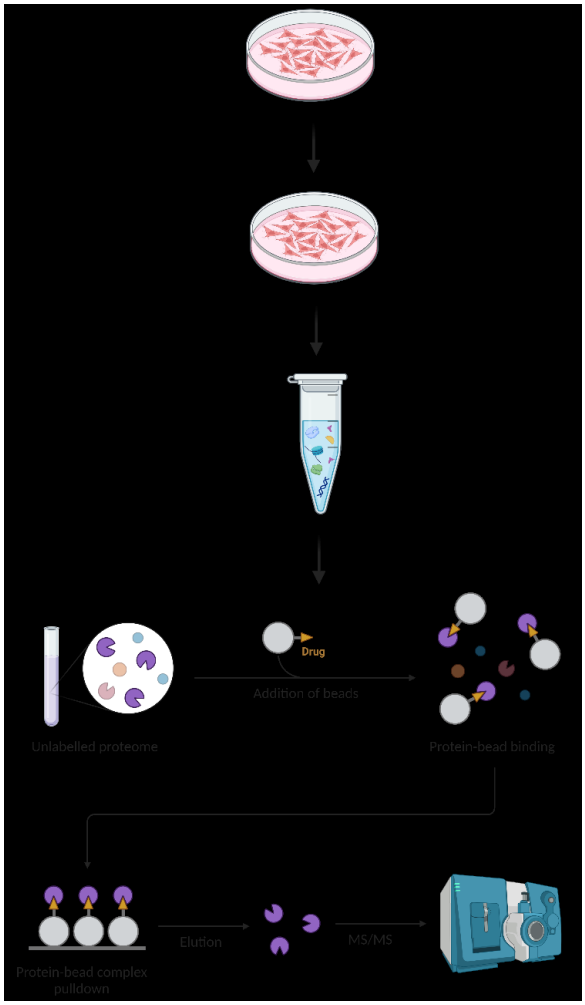

Figure 23. Schematic representation of Ondrej Tolde's experiment. Cell surface proteins crosslinking using DMP was done before cells lysis. IP with following MS were performed. Created in BioRender.

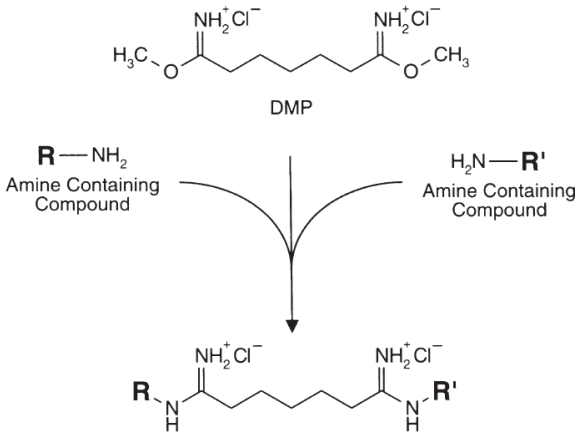

Figure 24. Dimethyl pimelimidate (DMP) crosslinking mechanism (Hermanson, 2013).

Since both described experiments captured desmoglein-2 being not in a stable contact, but only in close proximity of MT1-MMP, the aim of my work was to establish whether this interaction truly happens in cancer cells. To achieve this, we came up with the following plan: synthesis of MT1-MMP-FLAG/Strep-tag constructs (*wild type* and 3 mutant variants), verification of their expression and enzymatic activity in mammalian cells, coimmunoprecipitation of FLAG/Strep-tagged MT1-MMP and its interactors with StrepTactin or anti-FLAG® M2 magnetic beads. We have chosen FLAG/Strep-tags because they allow for Tandem Affinity Purification, as well as separate immunoprecipitations using different tags.

4.2.1. Insertion of FLAG/Strep-tags into the available MT1-MMP DNA plasmids

To prepare the constructs, we have again used the plasmids available in our laboratory (Figure 10). We have chosen two possible regions for FLAG/Strep-tag insertion, namely the "Hinge" and the "Linker" regions. Hinge region is located between catalytic and hemopexin domains of MT1-MMP, while Linker region is the one between hemopexin and transmembrane domains (Figure 6). Both of them are linkers by function, so the disruption of their sequences

should not affect any important functions of the enzyme or interfere with its known interactions. Hence, we designed primers (Attachment 2,) for synthesis of different fragments and performed PCR with subsequent confirmation of the expected fragments' sequences by DNA electrophoresis and sequencing (not shown). To be precise, primers 46+47 were used to synthesize Linker-FFSS fragment; primers 48+49 for Linker-MT1-MMP (C-terminal part) fragment for WT, C574A and LLY/A; primers 47+50 for Hinge-FFSS fragment; primers 52+53 for Hinge-MT1-MMP (C-terminal part) fragment for WT, C574A and LLY/A; primers 54+55 for Linker-MT1-MMP (C-terminal part) fragment for dCP; primers 56+57 for Hinge-MT1-MMP (C-terminal part) fragment for dCP.

Once the fragments' sequences were confirmed, a Gibson Seamless Cloning and Assembly was used to put the synthesized fragments together, and the sequences were again verified by DNA restriction analysis (Figure 25) and sequencing.

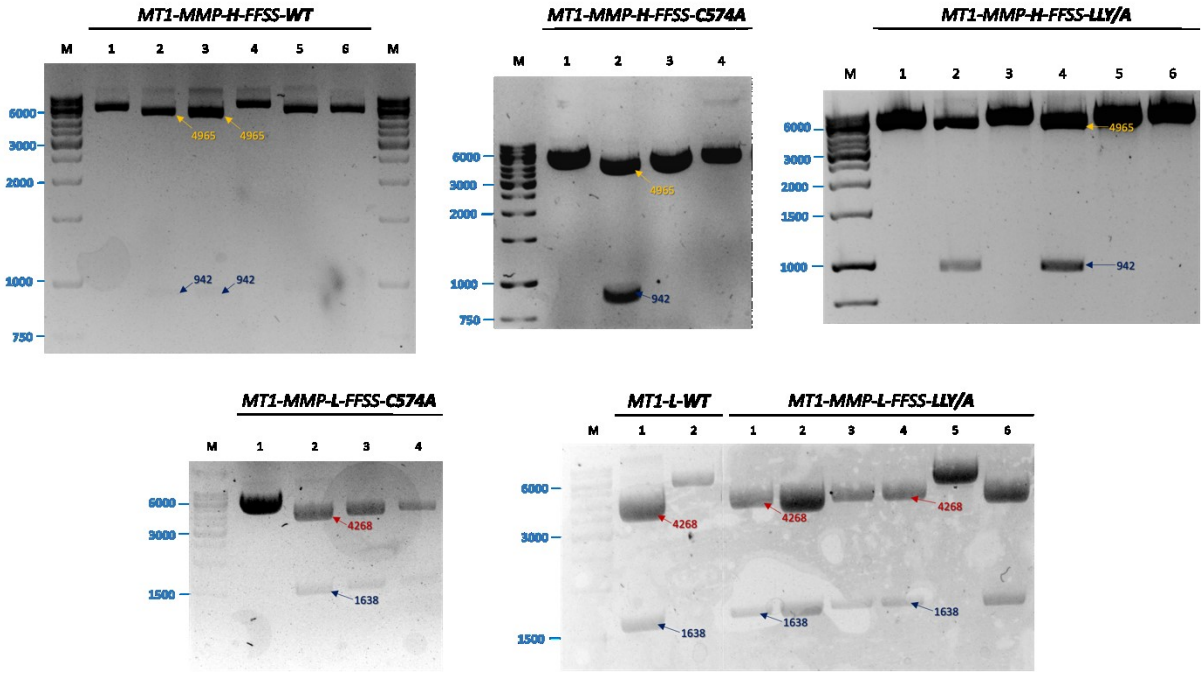

Figure 25. Restriction analysis of the DNA isolated from bacterial clones transfected with the prepared constructs (left to right, top to bottom): MT1-MMP-Hinge-FFSS-WT, MT1-MMP-Hinge-FFSS-C574A, MT1-MMP-Hinge-FFSS-LLY/A, MT1-MMP-Linker-FFSS-C574A, MT1-MMP-Linker-FFSS-WT, MT1-MMP-Linker-FFSS-LLY/A. Restriction was done with KpnI enzyme, the sizes of the expected fragments were: **942 bp** and 4965 bp (for all "Hinge" constructs), **1638 bp** and 4268 bp (for all "Linker" constructs). M = marker; 1–6 = numbers of particular clones.

Since none of the prepared MT1-MMP-Hinge-FFSS-dCP, MT1-MMP-Linker-FFSS-dCP constructs (not shown) showed proper fragment sizes on restriction analysis, we used another method to produce them: the successfully prepared variants of MT1-MMP-Hinge-FFSS-WT, MT1-MMP-Linker-FFSS-WT were mutagenized to delete the cytoplasmic tail. Figure 26 demonstrates the DNA gel resulting from restriction with NcoI.

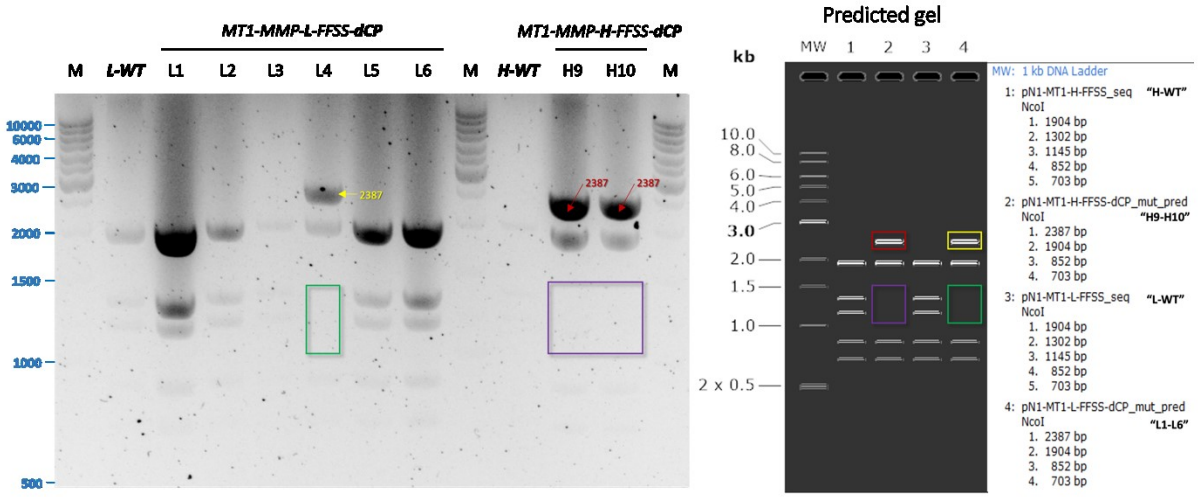

Figure 26. *Left:* restriction enzyme digestion of the DNA isolated from bacterial clones transfected with the prepared constructs (left to right): MT1-MMP-Linker-FFSS-WT, MT1-MMP-Linker-FFSS-dCP; MT1-MMP-Hinge-FFSS-WT, MT1-MMP-Hinge-FFSS-dCP. Restriction was done with NcoI enzyme, the sizes of the expected fragments were: 2387 bp, 1904 bp, 852 bp and 703 bp (for all "dCP" constructs); 1904 bp, 1302 bp, 1145 bp, 852 bp and 703 bp (for all "WT" constructs). *Right:* predicted gel showing all the expected fragments sizes (created in SnapGene software). M = marker; 1–10 = numbers of particular clones.

To sum up, the following clones were chosen as successful based on DNA restriction and sequencing analyses: clones #2 and #3 for MT1-MMP-Hinge-FFSS-WT, clone #2 for MT1-MMP-Hinge-FFSS-C574A, clone #4 for MT1-MMP-Hinge-FFSS-LLY/A, clones #9 and #10 for MT1-MMP-Hinge-FFSS-dCP; clone #1 for MT1-MMP-Linker-FFSS-WT, clone #2 for MT1-MMP-Linker-FFSS-C574A, clones #1 and #4 for MT1-MMP-Linker-FFSS-LLY/A, clone #4 for MT1-MMP-Linker-FFSS-dCP.

4.2.2. Verification of plasmids expression and enzyme functioning in mammalian cells

4.2.2.1. Assessing the constructs expression levels in HT1080 mammalian cell line

In order to verify, whether the prepared MT1-MMP-Hinge/Linker-FFSS constructs are expressed properly in mammalian cell line, we have transfected them into HT1080 MT1-MMP KO (F3) cells, prepared the lysates and performed immunoblotting analysis (Figure 27).

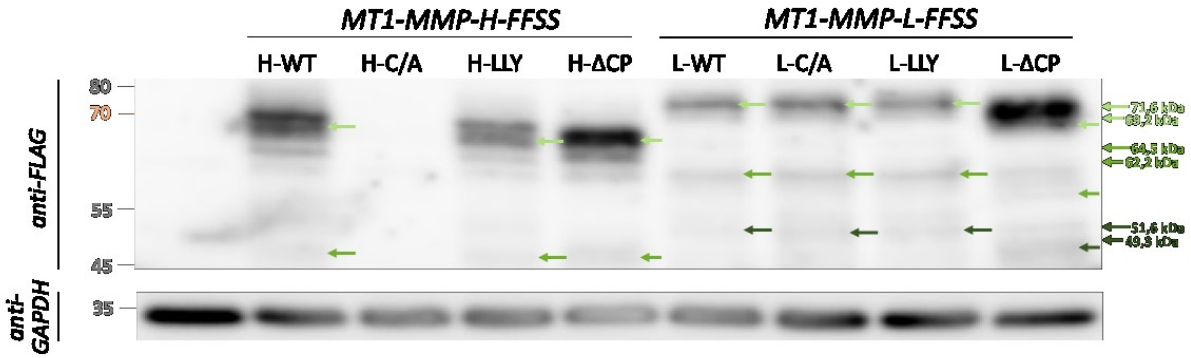

Figure 27. Western blot of the lysates prepared from HT1080 MT1-MMP KO (F3) cells transfected with the produced constructs. Anti-FLAG antibody (F1804-200UG, Ms, 1:1,000) was used to detect FLAG/Strep-tag, anti-GAPDH antibody (MA5-15738, Ms, 1:10,000) served as a loading control. Arrows indicate sizes of different MT1-MMP forms (Hernandez-Barrantes et al., 2000; Cho et al., 2008): uncleaved pro (light green), cleaved pro (green), and active form (dark green).

As can be seen (Figure 27), FLAG is not detected in lysate prepared from the cells transfected with MT1-MMP-Hinge-FFSS-C574A construct, and all of the "Hinge" constructs show generally smaller sizes of the expressed MT1-MMP variants than the "Linker" constructs, which mostly correspond to the expected sizes (discussed in 5.4.). For this reason, we decided to work only with the "Linker" constructs in further experiments, i.e. MT1-MMP-L-FFSS-WT, MT1-MMP-L-FFSS-C574A, MT1-MMP-L-FFSS-LLY/A, MT1-MMP-L-FFSS-dCP.

4.2.2.2. Testing the enzyme functioning with gelatine degradation assays

To establish whether the insertion of FLAG/Strep-tags affected the main function of MT1-MMP – ECM degradation, – cells transfected with these constructs were tested for gelatine degradation ability using gelatine degradation assays. The experiment was performed according to the protocol (see 3.2.1.6.), Figure 28 shows the resulting microscopy images.

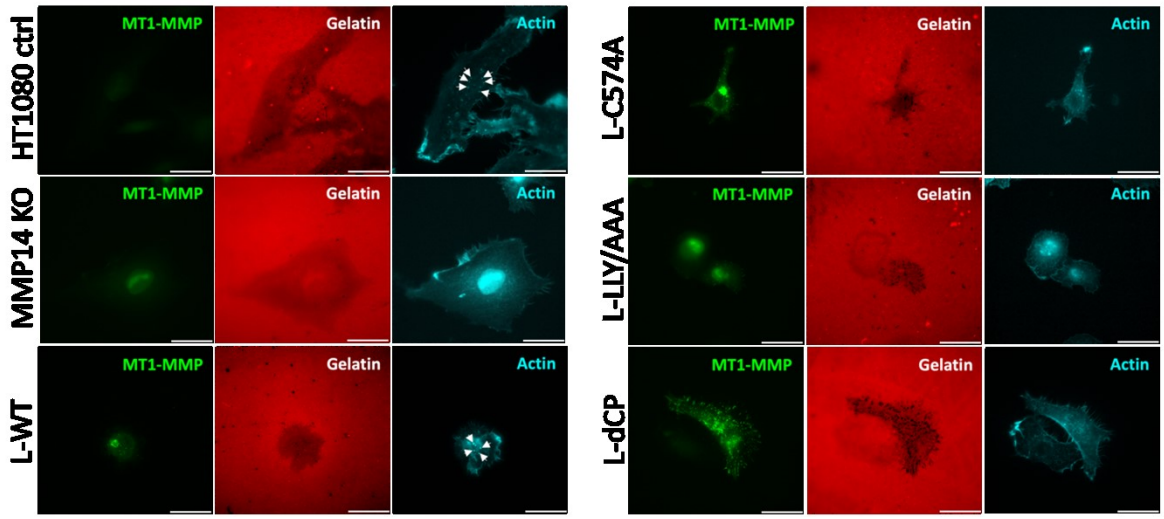

Figure 28. Gelatine degradation assay of human HT1080 MMP14 KO cells transfected with the "Linker" constructs. Images were obtained using widefield fluorescence microscopy and edited in ImageJ for brightness/contrast adjustment. MT1-MMP was detected using primary antibody against FLAG peptide and Alexa Fluor 488 dye, gelatine was labelled with Cy3 dye, actin was stained with SiR-actin probe. Black spots on gelatine indicate the degraded areas. Arrows point to the invadopodia of invading cells. HT1080 ctrl = non-transfected *wild-type* HT1080 cells; MMP14 KO = non-transfected HT1080 MMP14 KO (F3 clone) cells; L-WT, L-C574A, L-LLY/AAA, L-dCP = HT1080 MMP14 KO (F3) cells transfected with MT1-MMP-L-FFSS-WT, MT1-MMP-L-FFSS-C574A, MT1-MMP-L-FFSS-LLY/A, and MT1-MMP-L-FFSS-dCP constructs, correspondingly. Scale bar, 30 µm.

The degraded area (in the form of black – degraded – spots on gelatine) was measured for over 30 cells per each variant using ImageJ tool, which calculates the fraction of degraded area versus the area occupied by a cell. The values obtained from three independent biological replicates (Attachment 3) were then put together and normalized each to its' negative control (non-transfected MT1-MMP KO cells). Figure 29 shows the resulting graph.

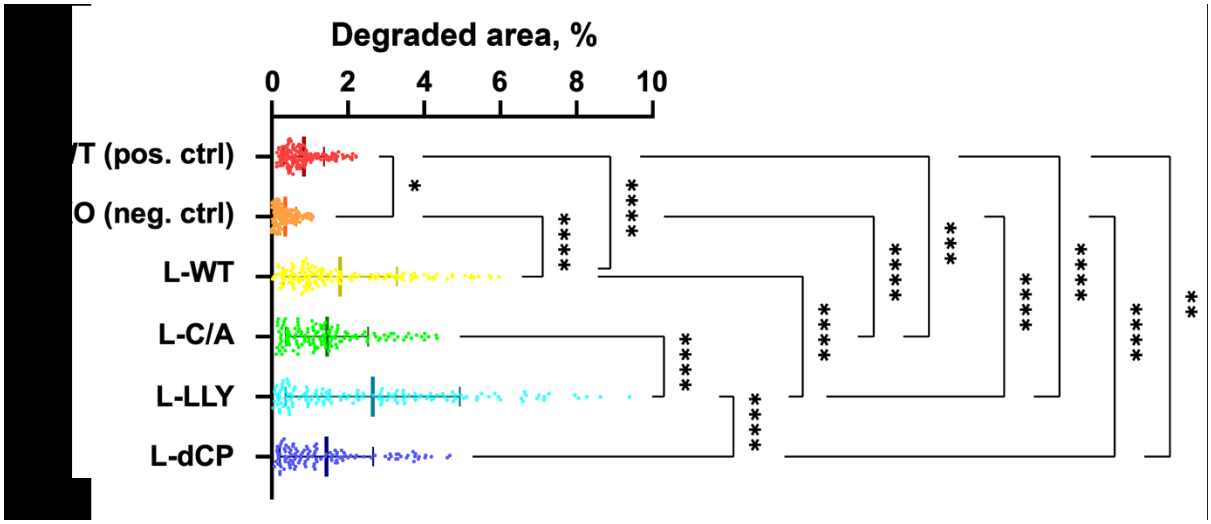

Figure 29. Statistical analysis of the mutagenized protein's ability to degrade gelatine. X-axis shows the percentage of the degraded gelatine area from the total gelatine area occupied by a corresponding cell. On the Y-axis there are different variants of cells analysed: WT (pos. ctrl) = non-transfected *wild-type* HT1080 cells, which served as positive control since they express only endogenous MT1-MMP; KO (neg. ctrl) = non-transfected HT1080 MMP14 KO (F3 clone) cells serving as a negative control since they should not express any MT1-MMP; L-WT, L-C574A, L-LLY/AAA, L-dCP = HT1080 MMP14 KO (F3) cells transfected with MT1-MMP-L-FFSS-WT, MT1-MMP-L-FFSS-C574A, MT1-MMP-L-FFSS-LLY/A, and MT1-MMP-L-FFSS-dCP constructs, correspondingly. Asterisks illustrate statistical significance of mean difference: * = $p < 0.05$, ** = $p < 0.01$, *** = $p < 0.001$, **** = $p < 0.0001$.

The graph clearly demonstrates that the level of degradation by endogenous MT1-MMP expressed in non-transfected *wild-type* HT1080 cells is much lower than in HT1080 MMP14 KO (F3) cells transfected with the prepared constructs, indicating functional MT1-MMP protein overexpression, which was expected. On the contrary, non-transfected HT1080 MMP14 KO (F3) cells almost do not degrade the gelatine, as expected in cells which do not express any MT1-MMP. Interestingly, particular mutated variants of MT1-MMP showed significantly different degradation rates – presumably, owing to different effects of mutations (discussed in 5.5.). To conclude, we have verified that the insertion of FLAG/Strep-tags into Linker region of *wild-type* MT1-MMP and its mutated variants does not affect the functioning of the enzyme in mammalian cells.

4.2.3. Transfection of the prepared constructs into HT1080 cells, lysates preparation

Now, when the constructs' sequences were confirmed and we have verified the enzyme's function, they were transfected into HT1080 cells, and the lysates were prepared.

4.2.4. Coimmunoprecipitation of MT1-MMP and DSG2, immunoblotting analysis

4.2.4.1. StrepTactin pulldown

Immunoprecipitation using StrepTactin beads was performed, and the obtained samples were analysed through immunoblotting. The resulting membranes prepared by Kateřina Strouhalová, MSc., are shown in Figure 30.

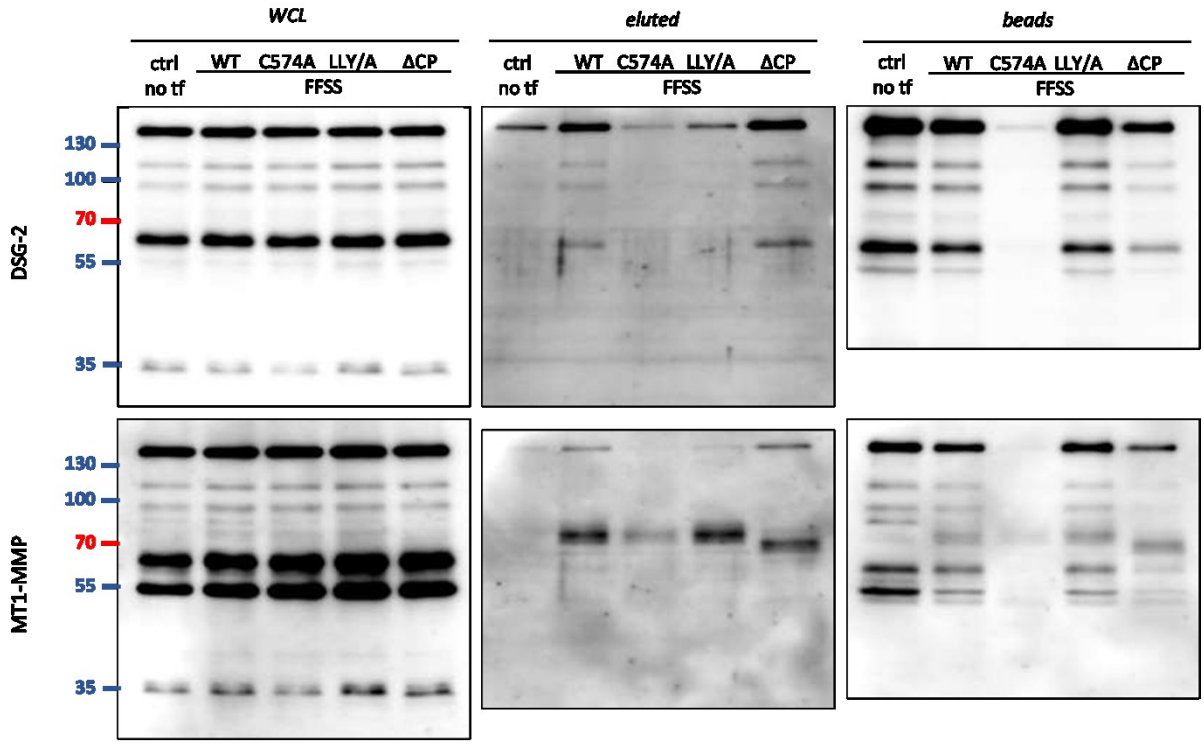

Figure 30. Western blot of the IP samples prepared from HT1080 cells transfected with the produced MT1-MMP-L-FFSS constructs. Anti-DSG2 antibody was used to detect desmoglein-2, then the membranes were stripped, and anti-MT1-MMP antibody was used to detect MT1-MMP (endogenous and transfected). WCL = whole cell lysate; ctrl no tf = non-transfected *wild-type* HT1080 cells; WT, C574A, LLY/A, ΔCP = HT1080 cells transfected with MT1-MMP-L-FFSS-WT, MT1-MMP-L-FFSS-C574A, MT1-MMP-L-FFSS-LLY/A, and MT1-MMP-L-FFSS-dCP constructs, correspondingly.

According to the anti-DSG2 antibody manufacturer, DSG2 migrates in a position corresponding to 150 kDa (discussed in 5.7.1.). As can be seen from the figure, DSG2 is highly expressed in HT1080 cells (WCL samples), and the signal is quite strong. C574A sample was probably lost during the experiment. MT1-MMP binds the beads and is quite well eluted. DSG2 elutes along with MT1-MMP-WT and MT1-MMP-dCP, although the band in dCP sample is stronger than in WT (mass spectrometry showed stronger coprecipitation of the two proteins in WT than in dCP). DSG2 band in LLY/A eluted sample is weaker than in control cells, suggesting it does not elute along with MT1-MMP-LLY/A, which is abundant in the eluted sample. The membranes also clearly show that DSG2 binds the beads non-specifically and remains bound even after the elution.

Next, we have repeated the experiment in HT1080 MMP-14 KO cells to eliminate the background of endogenous MT1-MMP. Also, since anti-MT1-MMP antibody was previously shown in our laboratory to exhibit cross-reactivity, we continued with anti-FLAG antibody, which is supposed to detect the transfected MT1-MMP-FFSS constructs only. The obtained Western blot is shown in Figure 31.

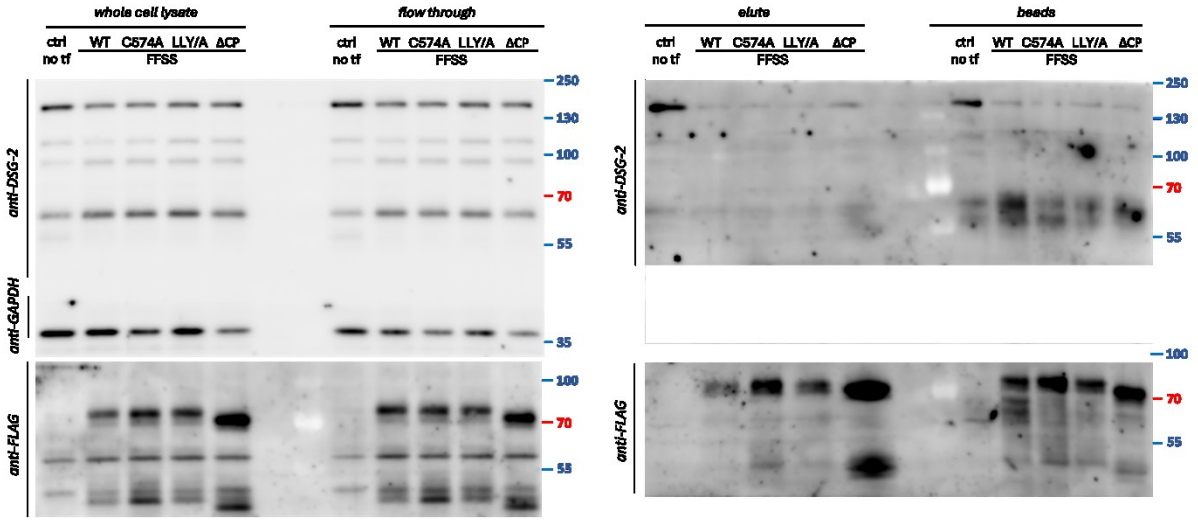

Figure 31. Western blot of the IP samples prepared from HT1080 MMP-14 KO cells transfected with the produced MT1-MMP-L-FFSS constructs. Anti-DSG2 antibody was used to detect desmoglein-2, anti-FLAG antibody detected the transfected MT1-MMP-FFSS constructs, GAPDH served as a loading control. Ctrl no tf = non-transfected HT1080 MMP-14 KO cells; WT, C574A, LLY/A, ΔCP = HT1080 MMP-14 KO cells transfected with MT1-MMP-L-FFSS-WT, MT1-MMP-L-FFSS-C574A, MT1-MMP-L-FFSS-LLY/A, and MT1-MMP-L-FFSS-dCP constructs, correspondingly.

Most of the sample remained in "flow through", although significant amount of MT1-MMP-FFSS bound the beads and was successfully eluted. Strong DSG2 bands in "elute" and "beads" control samples indicates non-specific binding of DSG2 to StrepTactin beads. "Elute" from the transfected cells almost did not contain any DSG2 implying low elution efficiency.

What is also noticeable, DSG2 bands in WCL and FT at sizes of approximately 95 kDa and 65 kDa are stronger in transfected cells compared to control. We supposed this could be caused by MMP-2 cleavage of DSG2 (discussed in 5.3.2.), since MMP-2 is activated by MT1-MMP (and TIMP2), which is overexpressed in the transfected cells while absent in the control. We performed another round of IP and analysed the blots using MMP-2 and TIMP2 antibodies, but detection showed no sign of MMP-2 or TIMP2 in any of the analysed samples (not shown).

4.2.4.2. Immunoprecipitation using Anti-FLAG® M2 magnetic beads

We next employed another IP method using anti-FLAG® M2 magnetic beads. MT1-MMP-FFSS-E240A, a MT1-MMP variant with Glu → Ala substitution in the active site, was added to explore potential differences in the pattern of DSG2 bands, since catalytically inactive MT1-MMP is not able to activate MMP-2, and thus the supposed DSG2 cleavage should not occur. HT1080 MMP-14 KO cells were transfected with MT1-MMP constructs (WT, ΔCP and E240A) and the experiment was performed according to the protocol (see 3.2.2.3.3.).

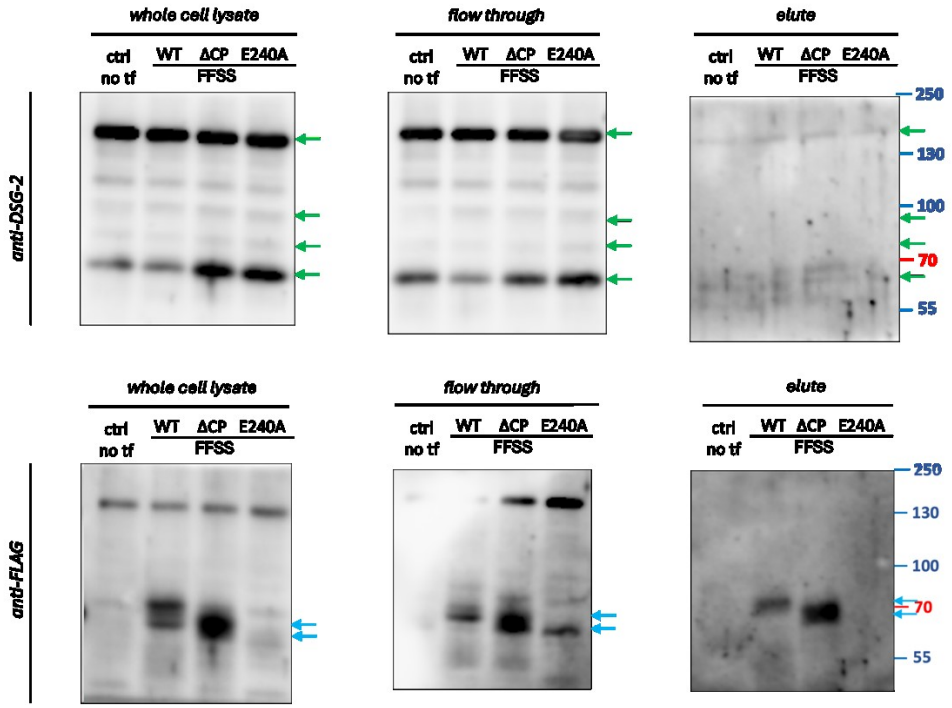

Figure 32. Western blot of the anti-FLAG® M2 magnetic beads IP samples prepared from HT1080 MMP-14 KO cells transfected with the produced MT1-MMP-L-FFSS constructs.

Anti-DSG2 antibody was used to detect desmoglein-2, anti-FLAG antibody detected MT1-MMP-FFSS constructs. Ctrl no tf = non-transfected HT1080 MMP-14 KO cells; WT, ΔCP, E240A = HT1080 MMP-14 KO cells transfected with MT1-MMP-L-FFSS-WT, MT1-MMP-L-FFSS-dCP, MT1-MMP-FFSS-E240A constructs, correspondingly. Arrows indicate the expected sizes of the proteins: green for DSG2 (main band of 150 kDa and the supposed cleavage products of approximately 65 kDa, 78 kDa, and 92 kDa); blue for MT1-MMP-FFSS (pro form, 72 kDa for MT1-MMP-FFSS-WT and mutant variants C574A, LLY/A, and 69 kDa for MT1-MMP-FFSS-dCP).

This time ~ 65 kDa DSG2 band in WCL and FT (Figure 32) was weaker in "WT" compared to control, the ~ 95 kDa band pattern remained similar to the previous result. DSG2 bands in MT1-MMP-FFSS-E240A-transfected cells did not differ from the ones in MT1-MMP-FFSS-transfected cells, therefore we concluded that the 65 kDa fragment is not a product of MMP-2 or MT1-MMP cleavage. In the "elute" samples, DSG-2 band was weaker in control than in the transfected cells, but the eluted fraction still remained tiny.

Trying to minimize the non-specific interaction of DSG2 with agarose-coated beads (discussed in 5.7.2., 5.7.3.), we have tested different lysis buffer compositions including different detergents (Nonidet P-40 and Triton X-100) at different concentrations (0.5%, 1 %), adding 100 mM KCl, 3.5 mM $MgCl_2$ ions, 1 mM Na_2ATP and 10 mM HEPES. In the end, we concluded that the standard 0.5% Triton X-100 buffer worked best.

4.2.4.3. New constructs: DSG2-FLAG-EGFP and DSG2-mCherry

For the purposes of coimmunoprecipitation and colocalization assays, we have ordered two DSG2 constructs: DSG2-FLAG-EGFP and DSG2-mCherry (Figure 33).

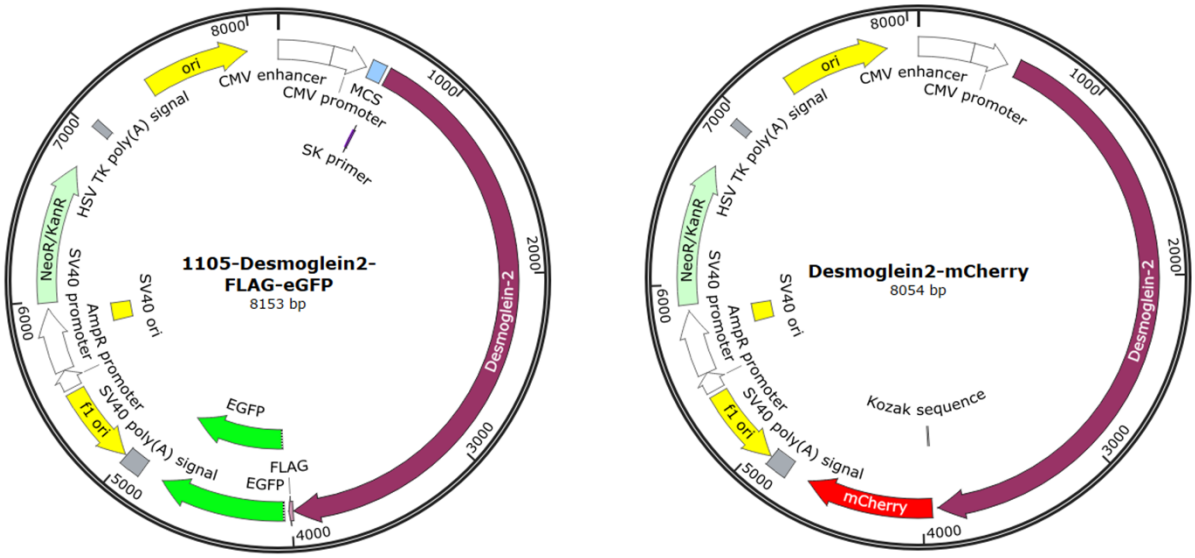

Figure 33. A schematic representation of the plasmids containing DSG2 protein sequence, shown in the SnapGene Viewer software. DSG2-FLAG-EGFP plasmid contains the DSG2 sequence itself, FLAG-tag, EGFP sequence; DSG2-mCherry plasmid contains DSG2 sequence, mCherry tag. Both plasmids also contain a gene for neomycin or kanamycin resistance (NeoR/KanR) and other components important for their replication and expression.

Both plasmids were verified by DNA restriction analysis (Figure 34) to be as expected.

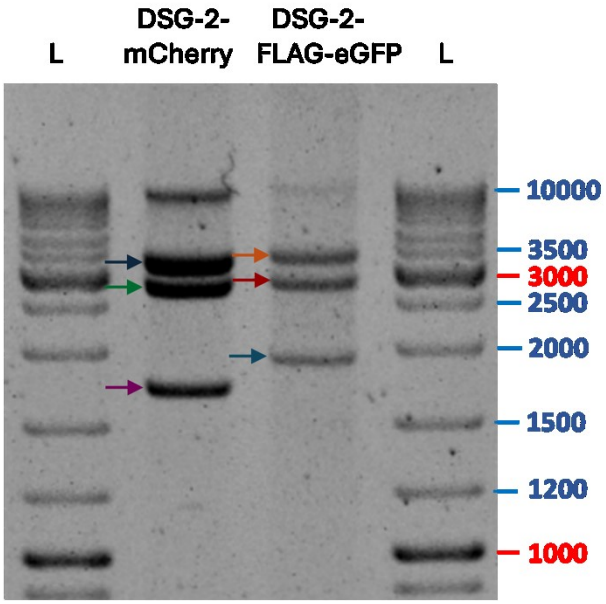

Figure 34. Restriction analysis of the DNA isolated from the bacteria transformed with the two DSG2 constructs. DSG2-mCherry restriction was done with EcoRI and SfiI, the expected fragments were 1732 bp, 2921 bp, and 3401 bp. DSG2-FLAG-EGFP restriction was done with KpnI and SfiI, the expected fragments were 1932 bp, 2850 bp, and 3371 bp. Arrows indicate the sizes of expected fragments: 1732 bp, 2921 bp, 3401 bp for DSG2-mCherry; 1932 bp, 2850 bp, 3371 bp for DSG2-FLAG-EGFP. L = DNA ladder.

DNA sequencing proved the plasmids' sequences to be precisely as expected.

To test functionality of the constructs, we have performed immunofluorescence and fluorescent microscopy according to the protocol (see 3.2.1.7.). HT1080 MMP-14 KO cells were co-transfected either with MT1-MMP-EGFP and DSG2-mCherry, or with DSG2-FLAG-EGFP and DSG1-mCherry constructs. After cells fixation, permeabilization and blocking, SiR-actin staining was performed. The images obtained are represented in Figure 35.

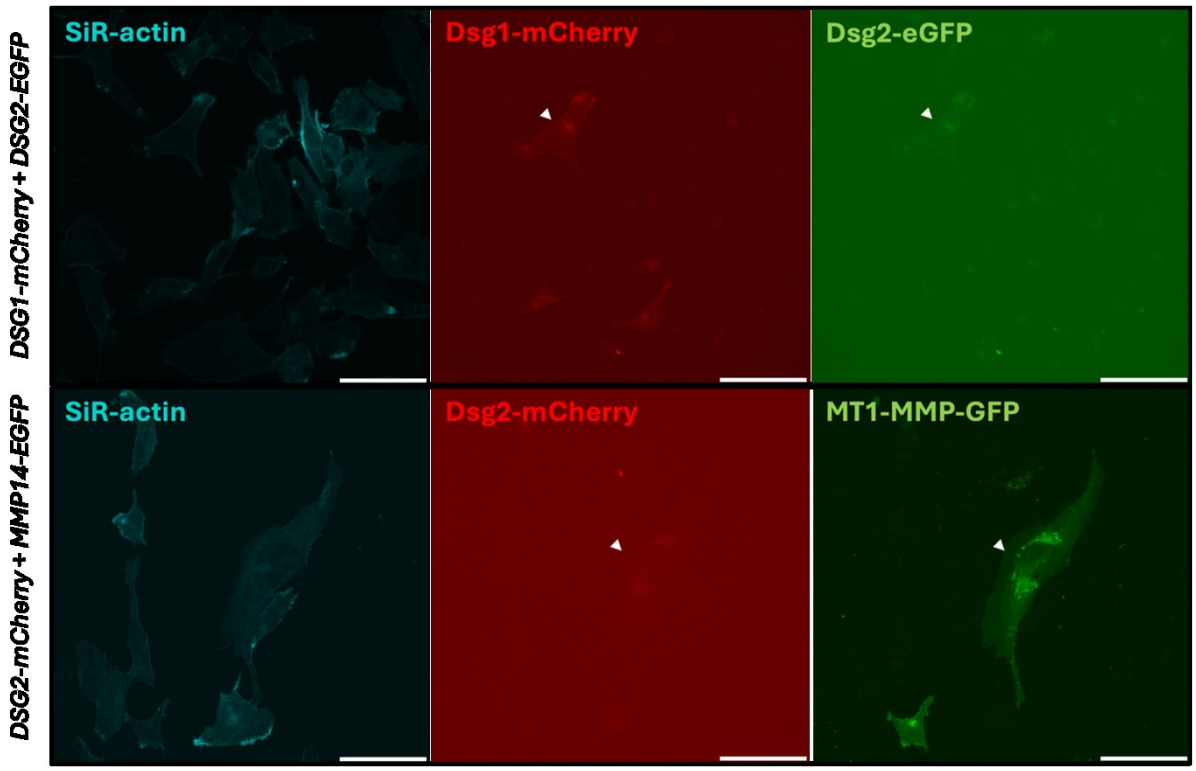

Figure 35. Fluorescence imaging of HT1080 MMP-14 KO cells co-transfected with *(top line)* DSG1-mCherry and DSG2-FLAG-EGFP, *(bottom line)* DSG2-mCherry and MT1-MMP-EGFP. SiR-actin staining was used to detect actin. Imaging was performed using widefield fluorescence microscopy, the resulting images were edited in ImageJ for brightness/contrast adjustment. White arrows point to presumably co-transfected cells. Scale bar, 30 µm.

The imaging showed the constructs' (especially DSG2-mCherry) expression is either low, or the expressed DSG2 variants emit less fluorescence than the control constructs.

When we transfected DSG2-FLAG-EGFP and MT1-MMP-EGFP constructs into HT1080 MMP-14 KO cells, immunoblotting did not detect any DSG2-FLAG-EGFP expression (Figure 36).

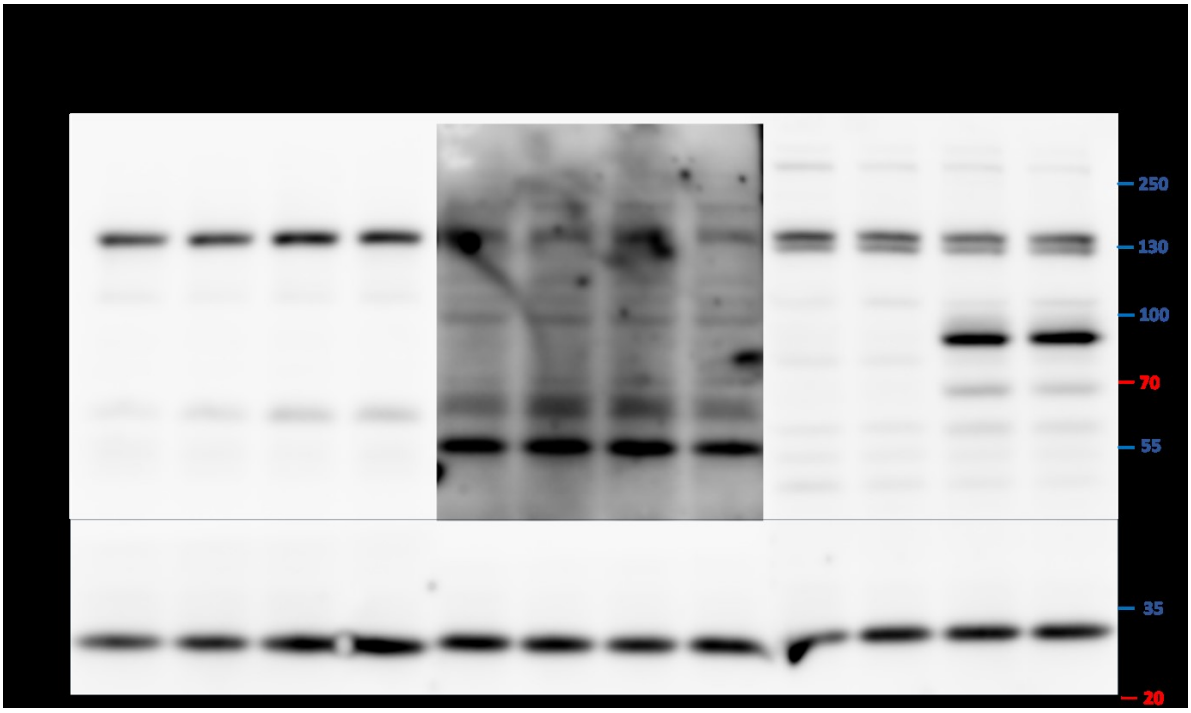

Figure 36. Western blot of the lysates prepared from HT1080 MMP-14 KO cells transfected with DSG2-FLAG-EGFP and MT1-MMP-EGFP constructs. Anti-DSG2 antibody was used to detect desmoglein-2, anti-FLAG antibody detected FLAG-tag present in DSG2-FLAG-EGFP construct, anti-GFP was used to detect GFP in both constructs. Ctrl no tf = non-transfected HT1080 MMP-14 KO cells; DSG-2-FLAG-GFP = HT1080 MMP-14 KO cells transfected with DSG2-FLAG-EGFP; MMP-14-GFP = HT1080 MMP-14 KO cells transfected with MT1-MMP-EGFP; co-transfection = HT1080 MMP-14 KO cells transfected with both constructs.

DSG2 bands are similar in all of the samples, suggesting they come from endogenous DSG2 with only a slight increase of ~ 65 kDa fragment in the transfected cells. Detection with anti-FLAG antibody revealed an identical pattern in all samples, GFP was only detected in cells transfected with MT1-MMP-EGFP. Collectively, the data suggests that DSG2-FLAG-EGFP is not expressed properly in HT1080 MMP-14 KO cells.

Therefore, we decided to test the constructs expression in another cell line. HEK293 cells were transfected with MT1-MMP-EGFP, MT1-MMP-E240A, DSG2-FLAG-EGFP, DSG2-mCherry and their co-transfection mixes. Figure 37 demonstrates Western blots of the prepared lysates.

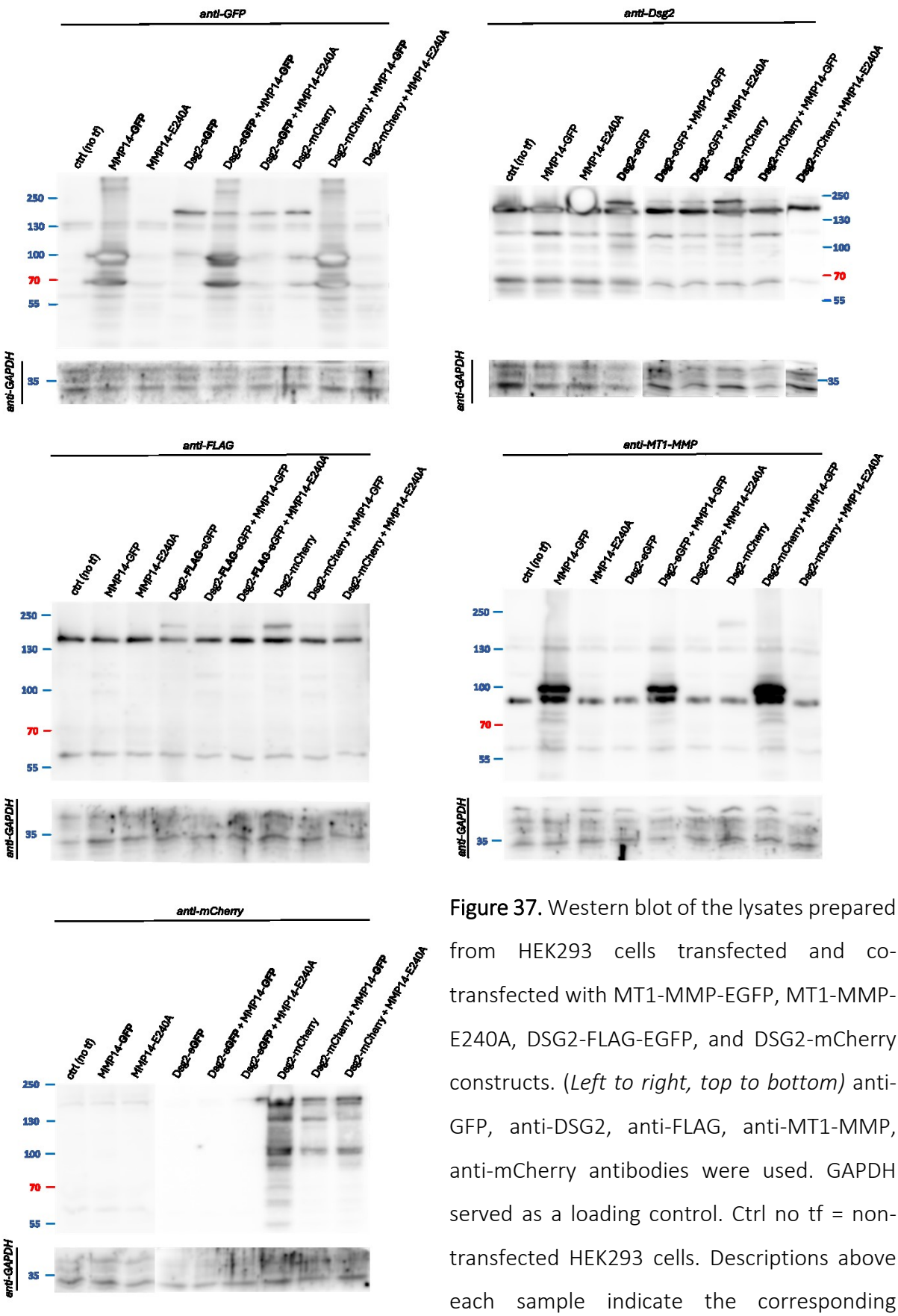

Figure 37. Western blot of the lysates prepared from HEK293 cells transfected and co-transfected with MT1-MMP-EGFP, MT1-MMP-E240A, DSG2-FLAG-EGFP, and DSG2-mCherry constructs. (*Left to right, top to bottom)* anti-GFP, anti-DSG2, anti-FLAG, anti-MT1-MMP, anti-mCherry antibodies were used. GAPDH served as a loading control. Ctrl no tf = non-transfected HEK293 cells. Descriptions above each sample indicate the corresponding construct(s) transfected into it.

In HEK293 cells, DSG2-FLAG-EGFP is detected by anti-GFP, anti-DSG2 and anti-FLAG antibodies. DSG2-mCherry is detected by anti-mCherry antibody, but also with anti-FLAG and anti-GFP antibodies in cells transfected only with DSG2-mCherry construct. This might be due to antibodies cross-reactivity, since DSG2-mCherry plasmid was checked for containing either FLAG or GFP sequence, and none were found. What is also interesting, upon detection with anti-DSG2, anti-GFP and anti-FLAG antibodies, DSG2 band of ~190 kDa is significantly weaker in cells co-transfected with DSG2-FLAG-EGFP and MT1-MMP-EGFP or MT1-MMP-E240A than in those transfected with DSG2 only. Similarly, in anti-mCherry antibody detection, DSG2 bands are generally less intensive in cells expressing MT1-MMP, either regular or mutated.

In general, the expression of the DSG2 is higher in HEK293 cells than in HT1080, so we continued the coimmunoprecipitation experiments using HEK293 cell line.

4.2.4.4. Coimmunoprecipitations in HEK293 cells

We transfected HEK293 cells with MT1-MMP-L-FFSS constructs, prepared the lysates and performed immunoprecipitation on Anti-FLAG® M2 magnetic beads. Figure 38 demonstrates immunoblotting analysis results.

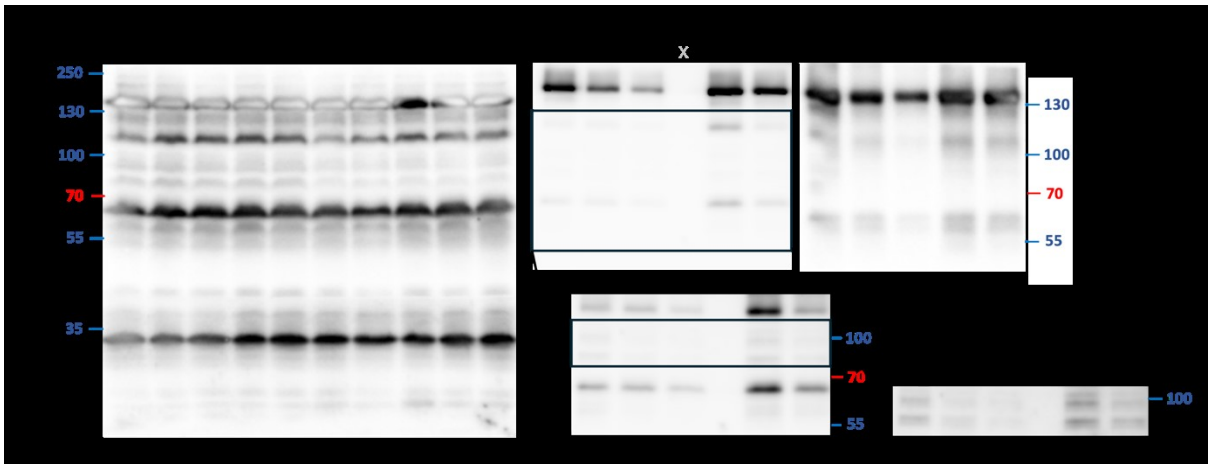

Figure 38. Western blot of the anti-FLAG® M2 magnetic beads IP samples prepared from HEK293 cells transfected with the MT1-MMP-Linker-FFSS constructs. Anti-DSG2 antibody was used to detect desmoglein-2, GAPDH served as a loading control. Ctrl = non-transfected HEK293 cells; WT, C/A, LLY, dCP = HEK293 cells transfected with MT1-MMP-L-FFSS-WT, MT1-MMP-L-FFSS-C547A, MT1-MMP-L-FFSS-LLY/A, and MT1-MMP-L-FFSS-dCP, constructs, correspondingly.

WCL and FT samples show similar DSG2 bands' patterns in the transfected and control cells indicating a high amount of endogenous DSG2 in HEK293, a slight increase in DSG2 levels (~110 kDa band) is present in MT1-MMP-transfected cells. DSG2 signal in elute is stronger in some of the transfected cells, especially in the "LLY" and "dCP" variants. Anti-FLAG detection showed the expected pattern of MT1-MMP-FFSS bands (not shown).

Another IP was performed on StrepTactin beads. HEK293 cells were transfected with MT1-MMP-Linker-FFSS constructs, the lysates were prepared, regular StrepTactin pulldown was performed. The resulting Western blots are shown in Figure 39.

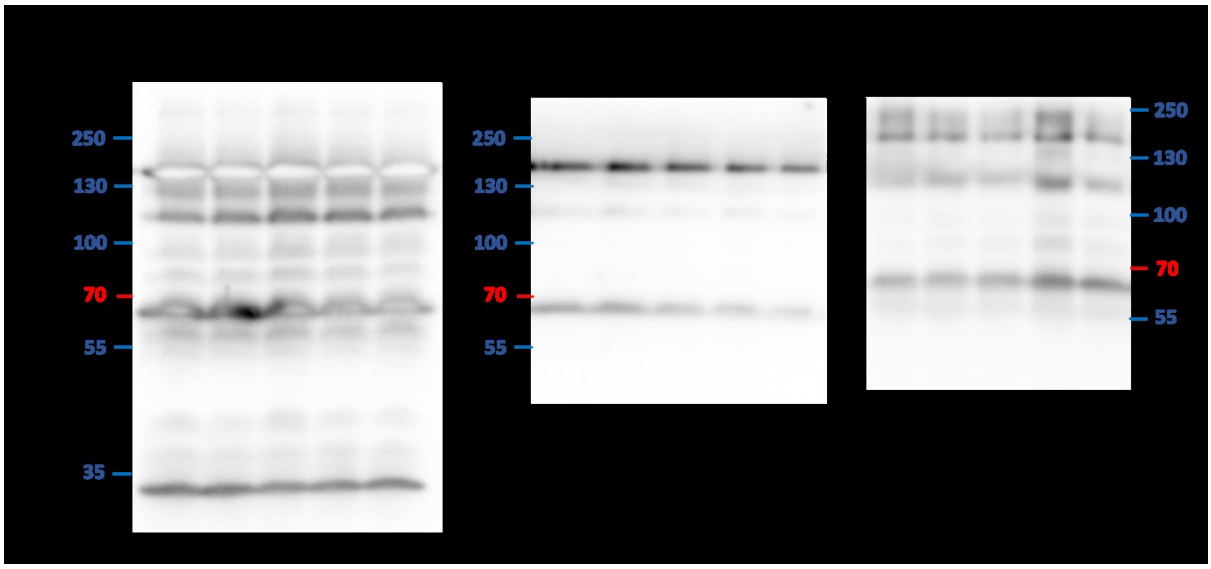

Figure 39. Western blot of the StrepTactin beads IP samples prepared from HEK293 cells transfected with the MT1-MMP-L-FFSS constructs. Anti-DSG2 antibody was used to detect desmoglein-2, GAPDH served as a loading control. Ctrl = non-transfected HEK293 cells; WT, C/A, LLY, dCP = HEK293 cells transfected with MT1-MMP-L-FFSS-WT, MT1-MMP-L-FFSS-C547A, MT1-MMP-L-FFSS-LLY/A, and MT1-MMP-L-FFSS-dCP, constructs, correspondingly.

In this design, elute samples revealed a similar pattern of DSG2 bands without notable differences between the transfected and control cells. However, much more DSG2 remained bound to the beads in cells transfected with "LLY" and "dCP" constructs than in control. Anti-FLAG detection showed the expected pattern of MT1-MMP-FFSS bands (not shown).

Having DSG2-FLAG-EGFP construct enabled us to perform coimmunoprecipitation the other way round: precipitate DSG2 via its GFP tag on anti-GFP antibody-coupled nProtein A Sepharose™ 4 Fast Flow beads and detect the beads fraction for MT1-MMP signal.

HEK293 were co-transfected with DSG2-FLAG-EGFP and MT1-MMP-L-FFSS constructs, immunoprecipitation using GFP antibody-coupled protein A sepharose beads was performed from the prepared lysates according to the protocol (see 3.2.2.3.4.). Samples were analysed with immunoblotting, the resulting membranes are shown in Figure 40.

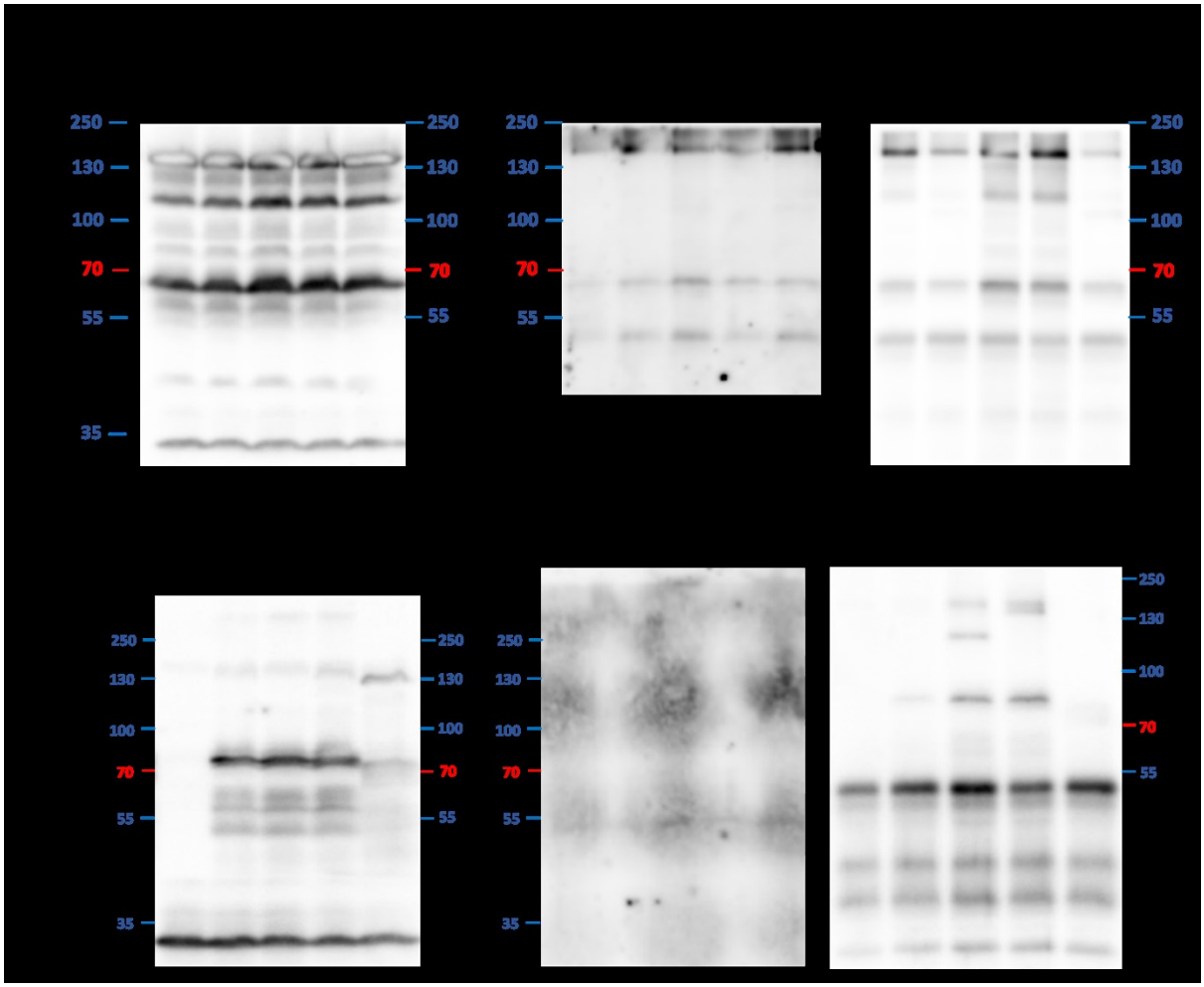

Figure 40. Western blot of the GFP-sepharose IP samples prepared from HEK293 cells transfected with DSG2-FLAG-EGFP and the MT1-MMP-Linker-FFSS constructs. Anti-DSG2 antibody was used to detect desmoglein-2, anti-FLAG antibody detected FLAG-tag, GAPDH served as a loading control. Ctrl = non-transfected HEK293 cells; WT, C/A, LLY, dCP = HEK293 cells co-transfected with DSG2-FLAG-EGFP and MT1-MMP-L-FFSS-WT, DSG2-FLAG-EGFP and MT1-MMP-L-FFSS-C547A, DSG2-FLAG-EGFP and MT1-MMP-L-FFSS-LLY/A, DSG2-FLAG-EGFP and MT1-MMP-L-FFSS-dCP, constructs, correspondingly.

DSG2 bands in WCL of the transfected cells were only slightly stronger than in control, indicating low transfection efficiency. A lot of DSG2 bound the beads in C/A and LLY variants, but also some DSG2 is present in control, indicating a non-specific interaction with

beads. MT1-MMP (detected by anti-FLAG antibody) precipitated well in the transfected cells but considering that DSG2 signal is quite weak in the WT and dCP variants, this result cannot be qualified representable.

4.2.4.4.1. Lysates preclearing step and incorporating EGTA in the lysis buffer

In order to minimize non-specific DSG2 binding to the beads (discussed in 5.7.2.), we have added EGTA, a chelating agent with a higher affinity for Ca^{2+} than EDTA, to the lysis buffer. In addition, a lysates preclearing step (Figure 41) was established prior to IP.

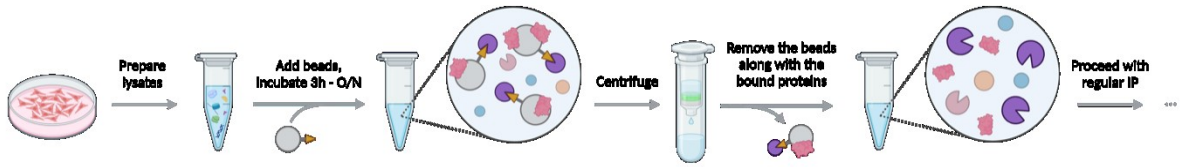

Figure 41. Schematic representation of the lysates preclearing step added to the protocol. *Left to right:* lysates are prepared, beads are added to the lysates and the mix is incubated at 4°C (for 3 hours – O/N), the mix is centrifuged, beads are discharged, the precleared lysate can be used for regular immunoprecipitation.

Using this modified protocol, I have performed StrepTactin IP preclearing the lysates 3x for 1-2 hours on the same StrepTactin beads, which are used in the IP itself. The resulting membranes are shown in Figure 42.

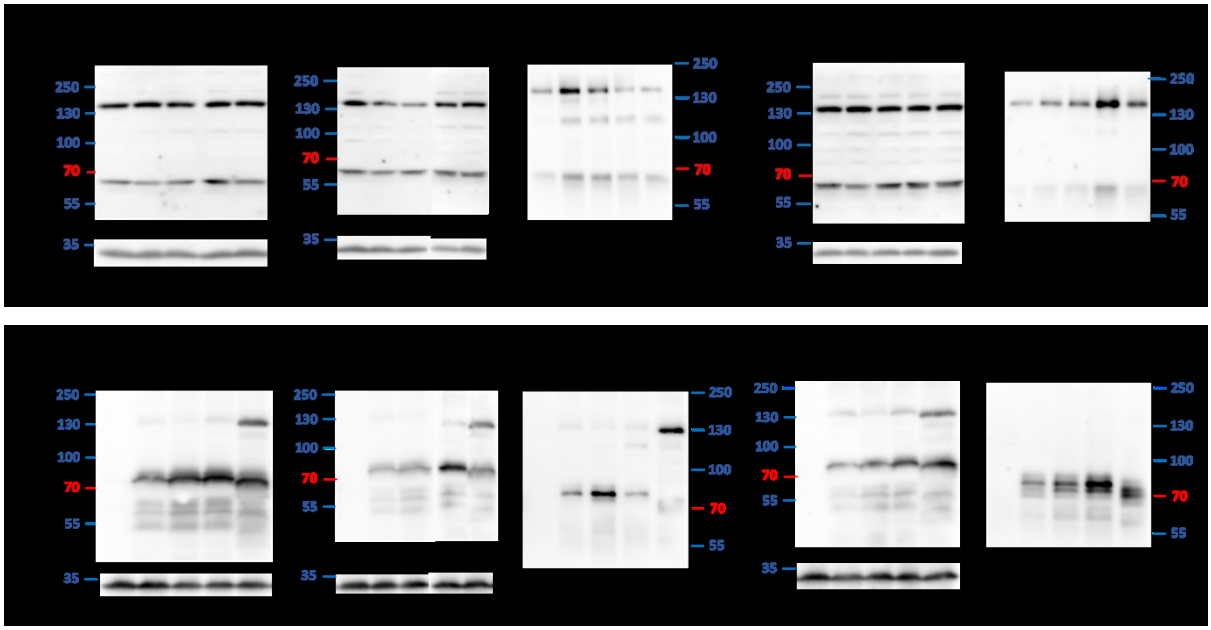

Figure 42. Western blot of the StrepTactin beads IP samples prepared from HEK293 cells transfected with the MT1-MMP-L-FFSS constructs. Anti-DSG2 antibody was used to detect

desmoglein-2, anti-FLAG antibody detected MT1-MMP-L-FFSS, GAPDH served as a loading control. Ctrl = non-transfected HEK293 cells; WT, C/A, LLY, dCP = HEK293 cells transfected with MT1-MMP-L-FFSS-WT, MT1-MMP-L-FFSS-C547A, MT1-MMP-L-FFSS-LLY/A, and MT1-MMP-L-FFSS-dCP, constructs, correspondingly.

Anti-FLAG antibody detected an expected pattern of bands this time, except for ~ 130 kDa band in most of dCP samples; we suppose this could be due to MT1-MMP-dCP form's proneness to form dimers more than other variants. After the 3rd preclearing, anti-DSG2 antibody detection showed DSG2 signal in beads samples from the transfected cells is stronger than in control, which marks a notable advancement compared to earlier findings (Figure 39). However, we concluded that preclearing on StrepTactin beads is not suitable since it might affect specific streptavidin – Strep-tag interactions.

Then we performed another StrepTactin IP with lysates preclearing 4x for 40 minutes on plain protein A sepharose beads with no specific tags, which thus should not affect the specific interactions. A new variant was added – MT1-MMP-FFSS-dCAT, a MT1-MMP construct with Strep/FLAG-tag insertion in the Linker region and catalytic domain deletion prepared by my colleague RNDr. Ondřej Tolde, Ph.D. The resulting samples' immunoblotting analysis is represented in Figure 43.

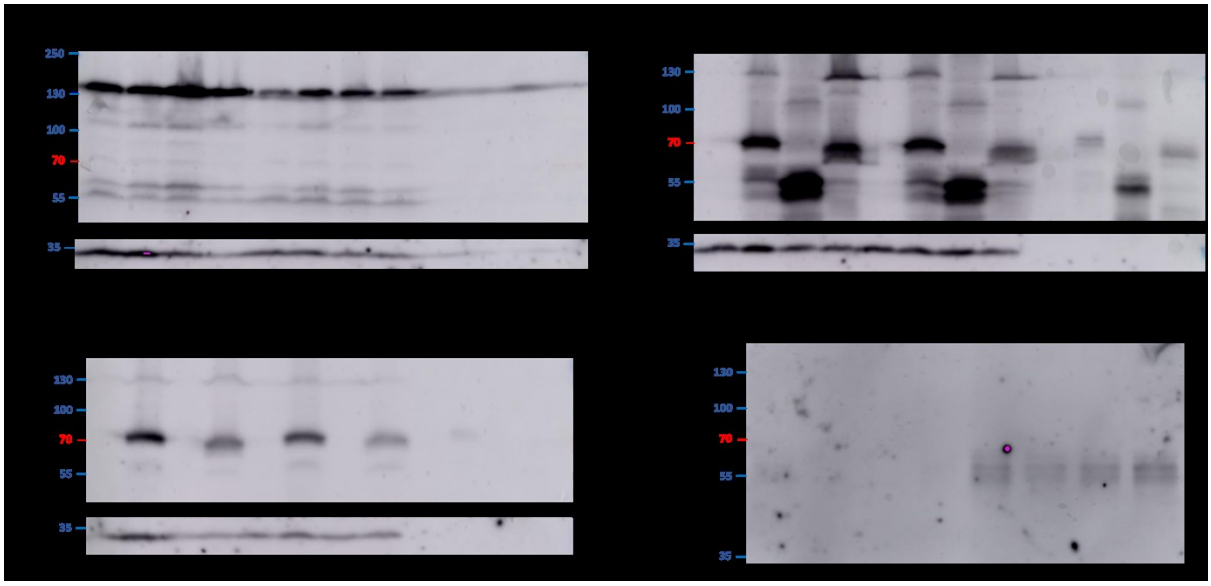

Figure 43. Western blot of the StrepTactin beads IP samples prepared from HEK293 cells transfected with the MT1-MMP-L-FFSS constructs. Anti-DSG2 antibody was used to detect desmoglein-2, anti-MT1-MMP detected MT1-MMP, anti-FLAG detected both DSG2-FLAG-EGFP and MT1-MMP-L-FFSS. GAPDH served as a loading control. Ctrl = non-transfected HEK293

cells; WT, dCAT, dCP = HEK293 cells transfected with MT1-MMP-FFSS-WT, MT1-MMP-FFSS-dCAT, MT1-MMP-FFSS-dCP constructs, correspondingly.

In this case, adding the preclearing step obviously improved the result, considering that DSG2 band's intensity in precleared control lysate decreased significantly compared to non-precleared WCL. Nevertheless, anti-DSG2 antibody did not detect much DSG2 bound to the beads (after repeating DSG2 detection of the "beads" samples *(right bottom membrane)*, the bands' intensity was generally low with control prevailing over MT1-MMP-FFSS-WT). Anti-FLAG detection yielded expected results with bands of dCAT variant demonstrating smaller protein size due to the whole catalytic domain deletion. Similarly, anti-MT1-MMP detection corresponded to our expectations (since anti-MT1-MMP antibody is specific to MT1-MMP's catalytic domain, it should not detect any MT1-MMP in dCAT variants).

Another experiment was performed on anti-GFP-coupled sepharose beads. Membranes resulting from samples analysis by immunoblotting are shown in Figure 44.

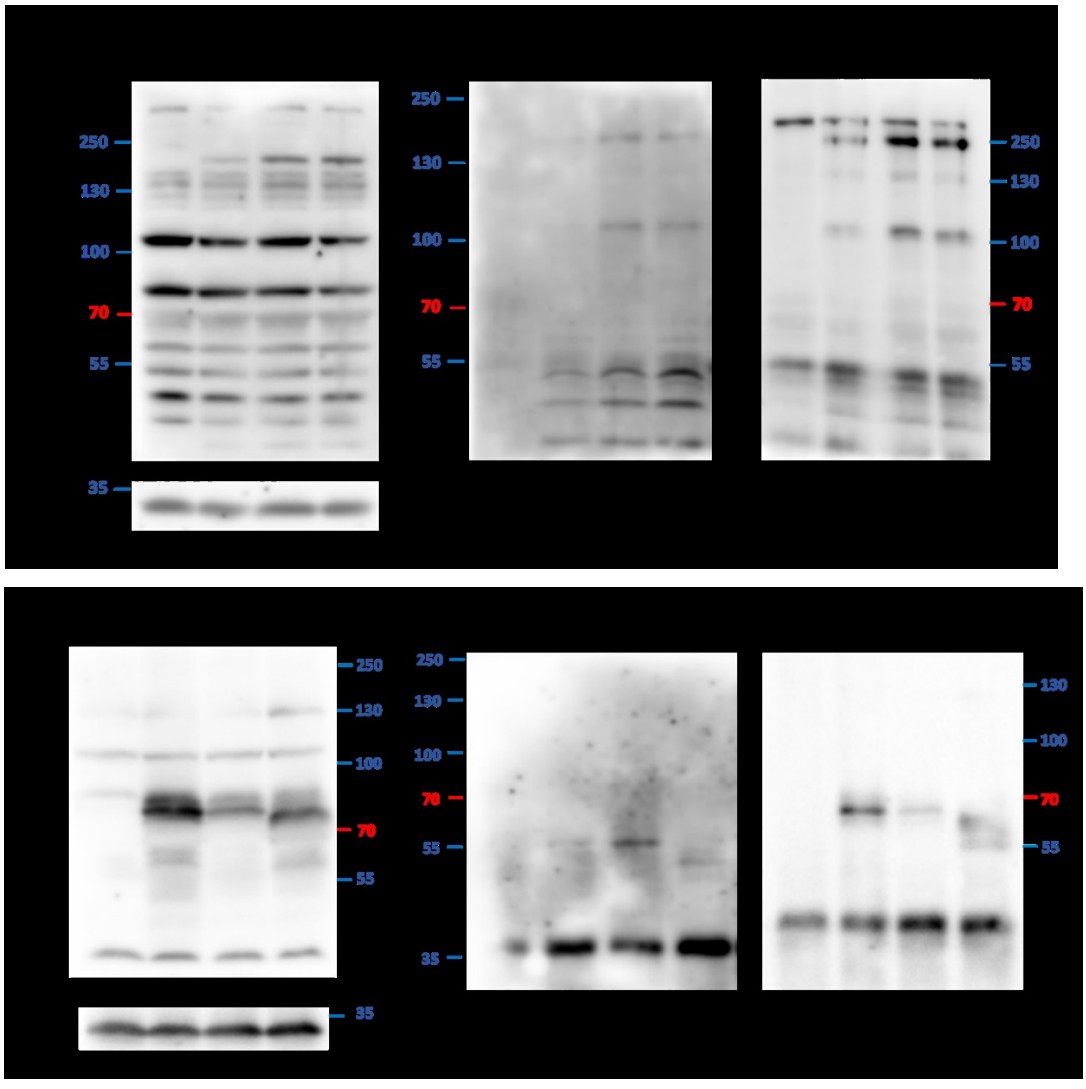

Figure 44. Western blot of the GFP-sepharose IP samples prepared from HEK293 cells transfected with DSG2-FLAG-EGFP and the MT1-MMP-Linker-FFSS constructs. Anti-GFP antibody was used to detect DSG2-GFP, anti-MT1-MMP detected MT1-MMP, GAPDH served as a loading control. Ctrl = non-transfected HEK293 cells; WT, C/A, LLY, dCP = HEK293 cells co-transfected with DSG2-FLAG-EGFP and MT1-MMP-L-FFSS-WT, DSG2-FLAG-EGFP and MT1-MMP-L-FFSS-C547A, DSG2-FLAG-EGFP and MT1-MMP-L-FFSS-LLY/A, DSG2-FLAG-EGFP and MT1-MMP-L-FFSS-dCP, constructs, correspondingly.

This finding initially looked promising: beads samples' anti-GFP detection yielded obvious bands of ~110 kDa and ~190 kDa in the transfected cells, but not in the control, confirming the construct was expressed properly. MT1-MMP was successfully precipitated and eluted along with DSG2 in the transfected cells. Interestingly, the MT1-MMP band detected in WT was considerably stronger than the mutant variants, suggesting a potential interaction of its cytoplasmic domain with desmoglein-2. Nevertheless, because control cells were not transfected with MT1-MMP and endogenous MT1-MMP levels were quite low (WCL, ctrl), anti-MT1-MMP detection of the beads samples from the transfected and control cells are not comparable.

The experiment was repeated with control cells co-transfection by MT1-MMP and plain EGFP vector to verify that MT1-MMP is not precipitated along with GFP, but with DSG2. The resulting Western blot (not shown) demonstrated that DSG2-FLAG-EGFP construct is not expressed properly in these cells, since anti-GFP antibody detected only plain EGFP (band of ~ 26 kDa in control cells), and no expected bands of about DSG2 size were seen.

4.2.4.5. DSG2-FLAG-EGFP DNA verification

Considering that in the latter (not shown) experiment anti-GFP antibody did not detect any DSG2-FLAG-EGFP constructs transfected in WCL of the corresponding transfected cells, we hypothesized this could be a simple transfection/protein expression problem. We tried to optimize the transfection in HEK293 cells testing different DNA to LMW PEI ratios and concluded that the conditions we used before were the most optimal ones. Than we also transfected other cell lines (HEK293, HeLa and U2OS) and imaged them at fluorescent microscopy in order to verify the fluorescent signal from EGFP in DSG2-FLAG-EGFP construct, but this showed either extremely weak or no fluorescent signal in all the tested variants. Finally, we have decided to verify whether DSG2-FLAG-EGFP DNA remained intact after many rounds of its amplification in bacteria. Therefore, we have taken all the samples of

the amplified DSG2-FLAG-EGFP DNA and performed a restriction analysis with KpnI and StuI. The resulting DNA gel is shown in Figure 45.

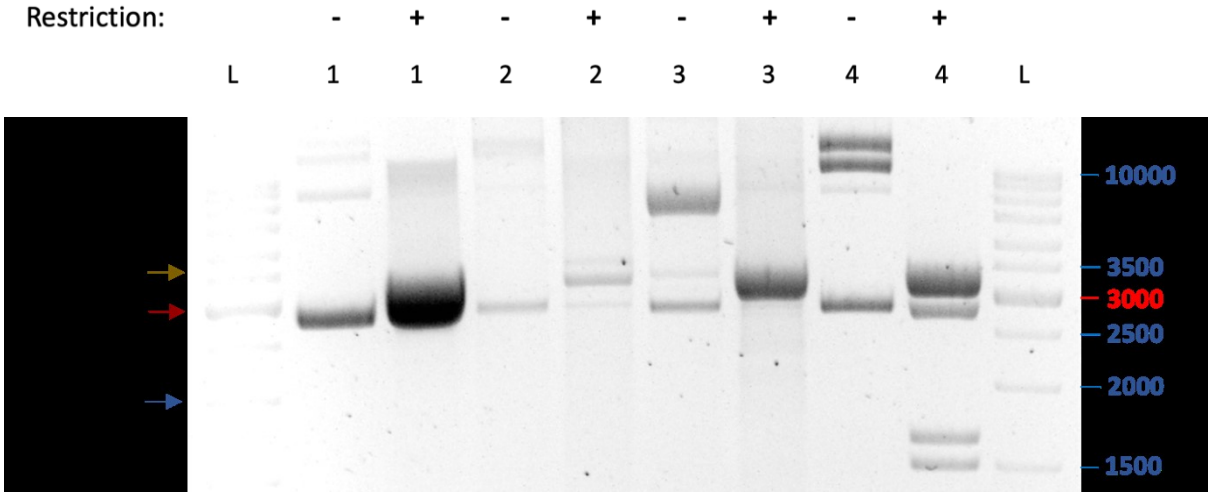

Figure 45. Restriction analysis of the DSG2-FLAG-EGFP construct DNA variants available after numerous amplifications of the original plasmid. The restriction was done with KpnI and StuI, the expected fragments were 1932 bp, 2804 bp, and 3417 bp long. Arrows indicate the sizes of expected fragments via corresponding colours. L = DNA ladder; 1-4 = DNA samples numbers; "+" = restriction performed; "-" = restriction not performed, non-cleaved DNA only.

The restriction analysis clearly demonstrated that the DSG2-FLAG-EGFP DNA we were now using in all the experiments differs a lot from the expected and from what the plasmid DNA looked like before the amplifications (see Figure 34). This result has clarified the reason of improper DSG2-FLAG-EGFP expression in human cells.

We have later found two other samples including a potential original plasmid and performed the same procedure. Restriction analysis was this time performed with KpnI and StuI, as well as with KpnI and SfiI. The resulting DNA gel in shown in Figure 46.

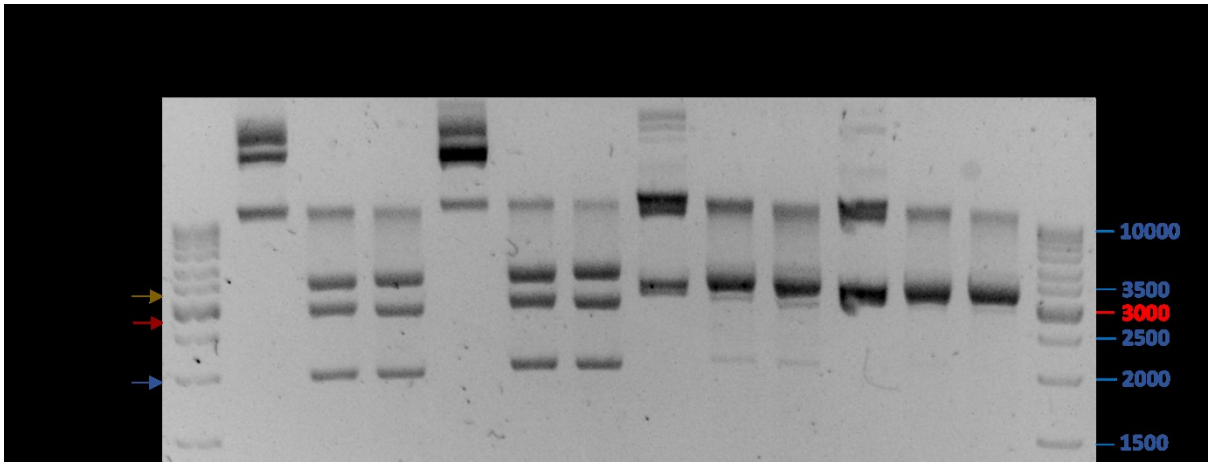

Figure 46. Restriction enzyme digestion of the DSG2-FLAG-EGFP construct DNA variants available after numerous amplifications of the original plasmid. The restriction was done with KpnI and StuI, the expected fragments were 1932 bp, 2804 bp, and 3417 bp; as well as with KpnI and SfiI, the expected fragments were 1932 bp, 2850 bp, 3371 bp. Arrows indicate the sizes of expected fragments via corresponding colours. L = DNA ladder; 1-4 = DNA samples numbers; "-" = restriction not performed, non-cleaved DNA only; StuI = restriction using KpnI + StuI enzymes; SfiI = restriction using KpnI + SfiI.

DNA fragments produced from samples 1 and 2 restriction analysis corresponded for our expectations, so we have sent them for sequencing analysis. The sequencing analysis confirmed that DNA sequences of these samples complied with the predicted sequence.

4.2.5. Fluorescent microscopy of living cells

4.2.5.1. DSG2-FLAG-EGFP construct expression verification

To test the expression of the newly verified DSG2-FLAG-EGFP construct, it was transfected into HEK293 cells. Firstly, at 400x magnification we observed distinct fluorescence of the transfected cells compared to control (not shown). Then the cells were stained with SPY650-FastAct probe, which labels dynamic actin in living cells. After 1 hour of incubation at 37°C, fluorescence imaging was performed at 1000x magnification (Figure 47).

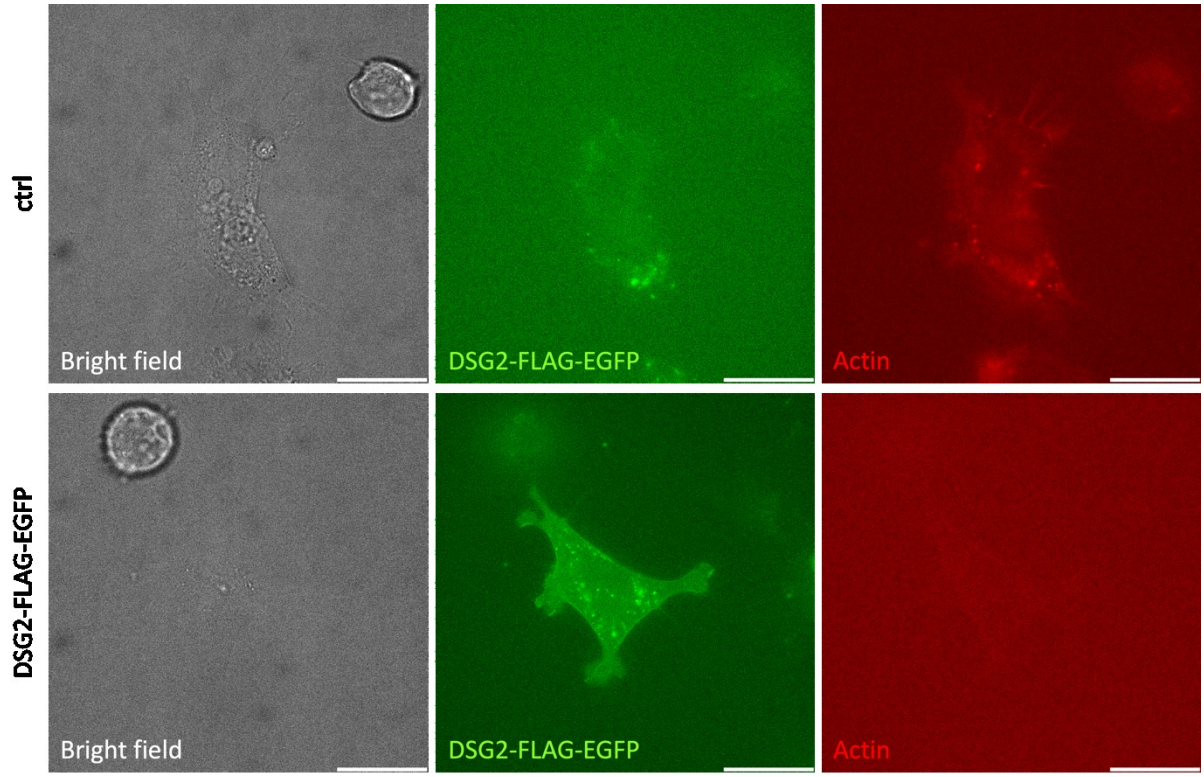

Figure 47. Fluorescence imaging of HEK293 cells transfected with DSG2-FLAG-EGFP. Imaging was performed using widefield fluorescence microscopy, SPY650-FastAct staining was used to detect actin. Ctrl = non-transfected HEK293 cells; DSG2-FLAG-EGFP = HEK 293 cells transfected with DSG2-FLAG-EGFP plasmid. Scale bar, 30 µm.

The imaging revealed strong fluorescence, and thus, expression, of DSG2-FLAG-EGFP. Compared to the previous result (Figure 35), this represented a significant improvement.

4.2.5.2. Desmoglein-2 localisation within cells

HEK293, HeLa and U2OS cells were transfected with the verified DSG2-FLAG-EGFP plasmid. Similarly to the previous experiment, the cells were stained with SPY650-FastAct probe, incubated at 37°C for 1 hour, and imaged on a fluorescent microscope. Figure 48 demonstrates the results obtained from the transfected U2OS cells.

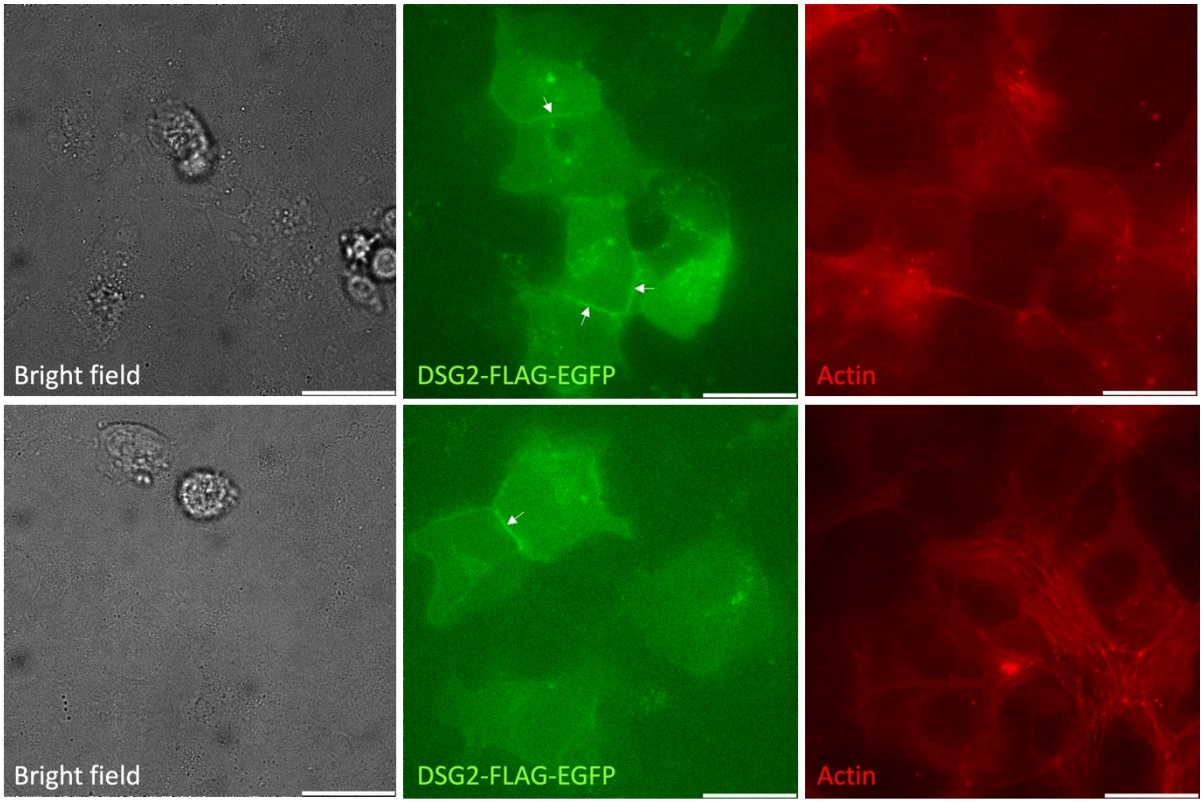

Figure 48. Fluorescence imaging of U2OS cells transfected with DSG2-FLAG-EGFP. Imaging was performed using widefield fluorescence microscopy, SPY650-FastAct staining was used to detect actin. White arrows point to the intercellular adhesions. Scale bar, 30 µm.

Consistent with the literature, the imaging *in vivo* confirmed desmoglein-2 localisation in the regions of intercellular adhesions.

5. Discussion

In this study, we sought to identify novel interaction partners of MT1-MMP, a key ECM-degrading enzyme involved in cancer cell progression. To achieve this, we employed proximity-dependent biotinylation, followed by streptavidin affinity purification and mass spectrometry analysis. This approach led to the identification of desmoglein-2 as a potential binding partner of the cytoplasmic tail of MT1-MMP. To further validate this finding, we conducted multiple coimmunoprecipitation assays. Throughout the process, we encountered several challenges, and addressing these obstacles forms the central focus of this chapter.

5.1. Addressing the challenges of BirA proximity labelling

A key goal of this work was to explore MT1-MMP interactions and identify potential new binding partners. We employed proximity-dependent biotinylation (PDB), which uses a biotin ligase to label nearby proteins, combined with streptavidin affinity purification (AP) to isolate these biotin-labelled proteins. Initially, we chose *E. coli* biotin ligase BirA, which biotinylates the 15-amino acid AviTag peptide. This required constructing MT1-MMP with AviTag insertions to allow BirA-mediated biotinylation and creating a plasmid encoding BirA, both of which would next be transfected into HT1080 cells to enable PDB and IP experiments.

5.1.1. Low MT1-MMP-Avi constructs expression in HT1080 cells (see 4.1.2.)

According to the plan, we have prepared MT1-MMP constructs (*wild type* and C574/A, LLY/A, dCP mutant variants) with inserted AviTags. Restriction analysis and DNA sequencing confirmed the preparation to be successful. However, when we transfected MT1-MMP-Avi constructs into HT1080 cells, and performed immunoblotting, we observed low differences in MT1-MMP signal between control cells and the transfected ones, suggesting expression of MT1-MMP from the transfected constructs is low comparing to the endogenous levels. We supposed the low expression could be due to quite a big distance between MT1-MMP-Avi construct and poly(A) sequence, which was separated from it by EGFP sequence. It was shown that mRNA stability gradually decreases with increasing distance between terminal codon and poly(A) tail (Eberle et al., 2008). Therefore, it is reasonable to assume that 720 nucleotides of EGFP DNA sequence estrange the poly(A) tail too far from MT1-MMP-Avi construct's stop codon.

5.1.2. Unsuccessful BirA-IRES cloning into IRES vector (see 4.1.1.2.)

In order to perform proximity-dependent biotinylation, we needed to prepare plasmids for the expression of a biotin ligase, which would biotinylate AviTag-ed proteins. BirA insert

was cloned into pIRESpuro3 vector. Restriction analysis of constructs has shown fragments much bigger than those expected. DNA sequencing has shown not only the absence of the desired BirA insertion, but also extensive deletion of the backbone vector sequence, which leaves unexplained the longer fragments seen on DNA electrophoresis. Because the process of construct preparation was complex and multistep, there are several potential reasons for such aberrant constructs' emergence, which may include incomplete restriction enzyme digestion, ligation or PCR artifacts, or issues related to the vector stability.

5.1.3. Proximity-dependent biotinylation using BioID2 (see 4.1.3.)

Since we did not succeed in preparing pIRESpuro3_BirA construct, and the expression of pN1-MT1-MMP-Avi constructs was very weak, we decided to switch for Biotin-based Identification of Interacting Proteins 2 (BioID2). BioID2 is an improved version of its predecessor, BioID, and employs a mutated form of the BirA biotin ligase, which exhibits improved specificity for biotinylation and has been optimized for proximity labelling and interactome studies. While BirA normally biotinylates a single, highly specific lysine residue within an AviTag sequence fused to a protein of interest and does not biotinylate other nearby proteins, BioID2 catalyses promiscuous biotinylation, biotinylating lysines on neighbouring proteins in ~10 nm spatial range from the fusion protein. Additionally, BioID2 is engineered to function efficiently *in vivo* under physiological conditions, requiring less stringent reaction parameters compared to BirA, which demands tightly controlled conditions and substrate concentrations to function effectively. Moreover, BioID2 is more stable across a broader temperature range due to its hyperthermophilic origin, whereas BirA performs optimally at ~37°C. Lastly, its smaller size makes it less likely to interfere with the normal function, localization, or folding of the protein it is fused to. Overall, BioID2 offers enhanced accuracy, reduced background noise (non-specific biotinylation events that could confound the analysis), and high sensitivity in detecting weak or transient protein interactions, which is particularly advantageous when studying low-abundance proteins or transient protein complexes.

5.2. Mass spectrometry findings rationale

5.2.1. Previous proteomic research of MT1-MMP interaction partners

Identifying binding partners of MT1-MMP has been the focus of several prior investigations. Bork (2020) analysed MT1-MMP-expressing MCF-7 cells using coimmunoprecipitation and mass spectrometry and identified 248 unique proteins enriched in pathways related to RNA transport, mRNA surveillance, protein processing in the endoplasmic

reticulum, endocytosis, and more. A comparison with a cytoplasmic domain deletion mutant revealed that the cytoplasmic domain is essential for protein export, processing in the endoplasmic reticulum, and endocytosis.

(Hwang et al. (2004) discovered that MT1-MMP cleaves apolipoproteins A-I and E, and plasma gelsolin. Similarly, Stegemann et al. (2013) identified novel vascular extracellular matrix (ECM) substrates of MT1-MMP including periostin, emilin-1, and some basement membrane-associated proteins. Both studies employed mass spectrometry through comparison of total protein following incubation with catalytically active or inactive MT1-MMP.

Two other studies utilized isotope-coded affinity tag (ICAT) labelling and tandem mass spectrometry in MT1-MMP-transfected MDA-MB-231 breast carcinoma cells. Tam et al. (2004) found and biochemically confirmed IL-8, pro-TNFα, death receptor-6, and connective tissue growth factor to be the substrates of MT1-MMP, highlighting the enzyme's role as both a matrix remodeler *and* a signaling protease. Butler et al. (2008) revealed and biochemically validated 20 MT1-MMP substrates (including DJ-1, galectin-1, Hsp90α, pentraxin 3, and others) using a broad-spectrum MMP inhibitor, prinomastat, which reduced substrate shedding while increasing accumulation in the plasma membrane.

High-throughput analyses of proteins associating with MT1-MMP have been performed using FLAG-tagged MT1-MMP, affinity purification and tandem mass spectrometry. Tomari et al. (2009) found 158 interacting proteins in A375 melanoma cells, confirming 5T4 antigen and carboxypeptidase D as MT1-MMP substrates through in vitro cleavage and colocalization studies. Niiya et al. (2009) identified 163 proteins associating with MT1-MMP in epidermoid carcinoma A431 cells, of which 18 were validated as MT1-MMP interactors and nine as substrates. Notably, MT1-MMP cleaves the Lutheran blood group glycoprotein, altering its interaction with laminin-511 and affecting cell surface expression.

In summary, various proteomic strategies have been developed to examine MT1-MMP interactions. Previous proteomic research of MT1-MMP binding partners mainly focused on identifying its proteolytic substrates, which illuminated the degradome and substrate specificity of MT1-MMP. However, the role of its cytoplasmic domain remains less understood. The advent of mass spectrometry technology has enabled high-throughput analysis of cellular interactomes, paving the way for further investigation into MT1-MMP's broader functional network and its role in cellular processes.

5.2.2. Mass spectrometry findings (see 4.1.4.)

Using BioID proximity-dependent biotinylation (PDB) followed by affinity purification (AP), MT1-MMP was isolated along with proteins in its close proximity – thus, its potential interactors. Beads with the bound proteins were sent for mass spectrometry (MS) analysis, which revealed the higher enrichment of AHNAK, AHNAK2, desmoglein-2, Nectin-2, EPHA2, CD44, ZO-2 (TJP2), Integrin β1, Pinin Filamin-A, Myosin-9 and other proteins on the beads from *wild-type* MT1-MMP-transfected cells, than from the ones transfected with the cytoplasmic domain deletion mutant (MT1-MMP-L-FFSS-dCP). Some of the identified proteins, namely CD44 receptor, Eph receptor A2, and integrin β1 are well-established MT1-MMP interactors (Grafinger et al., 2020; Mori et al., 2002; Sugiyama et al., 2013), which verifies the reliability of the result. Others, such as AHNAK, AHNAK2, desmoglein-2, and Nectin-2, have not been previously demonstrated to interact with MT1-MMP, and thus might be considered as candidate MT1-MMP interactors.

5.3. Rationale for desmoglein-2 interaction with metalloproteinases

Current research shows that proteinases play a crucial role in the pathobiology of cancer by targeting intercellular junction proteins such as cadherins. A study from 2015 demonstrated that matrix metalloproteinase 9 (MMP-9) and a disintegrin and metalloproteinase domain-containing protein 10 (ADAM10) promote the shedding of desmoglein-2 ectodomains in intestinal epithelial cells, thereby decreasing intercellular adhesion while enhancing cellular proliferation by activation of human epidermal growth factor receptor 2/3 (HER2/HER3) signaling (Kamekura et al., 2015). A recent article investigating DSG2 function in Moyamoya disease has also confirmed the interaction between DSG2 and MMP-9 (Wang et al., 2024).

5.3.1. My colleagues' previous results on MT1-MMP's potential interaction with desmoglein-2

Given that this project started in relation to my colleague's (Kateřina Strouhalová, MSc.) PhD thesis, it's aims and methods were based on her preliminary data. Our joint efforts lead to identifying desmoglein-2 (DSG2) as one of MT1-MMP's interactors in „PDB-AP-MS" experiments (see 5.2.2.). The data we received from mass spectrometry analysis demonstrated significantly higher presence of desmoglein-2 in the fraction precipitated from cells transfected with *wild-type* MT1-MMP than in that from MT1-MMP-dCP-expressing cells. Some well-established MT1-MMP binding partners were also identified, suggesting the data are reliable.

Later my other colleague, RNDr. Ondřej Tolde, Ph.D., has also identified desmoglein-2 to potentially bind MT1-MMP in his immunoprecipitation experiments involving usage of DMP, which cross-links cell surface proteins that are in close proximity to each other. Together, these results provided us with a hypothesis that desmoglein-2 is a potential interactor of MT1-MMP. Therefore, the goal of the second part of this project was to verify whether this interaction truly occurs.

5.3.2. In silico predictions of desmoglein-2 cleavage by MT1-MMP and MMP-2

Considering my colleagues' results regarding a potential interaction of MT1-MMP with DSG2, we have tested the DSG2 amino acid sequence (Attachment 4) for presence of MT1-MMP cleavage sites. Using Procleave (http://procleave.erc.monash.edu), we have identified 6 sites in the extracellular part of DSG2 sequence that MT1-MMP could cleave with probability higher than 50% (Attachment 5). Since MT1-MMP is an activator of type IV collagenase, MMP-2 (also known as Gelatinase A), we have also tested DSG2 sequence for presence of MMP-2 cleavage sites. Procleave software identified 21 cleavage sites in the extracellular part of DSG2 sequence that MT1-MMP could cleave with over 50% probability (Attachment 6).

5.4. MT1-MMP-Hinge-FFSS constructs expression in mammalian cells (see 4.2.2.1.)

Since we have identified DSG2 to be a potential interactor of MT1-MMP, we aimed to verify this interaction through coimmunoprecipitation. To enable this, we have chosen to insert FLAG/Strep-tags (FFSS) into MT1-MMP *wild type* and mutant sequences, which would permit immunoprecipitations on StrepTactin® or anti-FLAG® M2 magnetic beads using Strep- or FLAG-tag, correspondingly.

MT1-MMP constructs with FLAG/Strep-tag insertions in either Linker or Hinge region of the enzyme were prepared, their sequences were verified with DNA restriction and sequencing analyses. During verification of their expression in mammalian HT1080 cells, a notable difference was observed in the molecular sizes of the expressed MT1-MMP variants. Immunoblotting analysis revealed that the MT1-MMP-Hinge-FFSS constructs were of significantly smaller sizes compared to both the expected sizes and the sizes of MT1-MMP-Linker-FFSS constructs. The difference in electrophoretic mobility is likely attributable to the interference of the FFSS insertion with post-translational modifications, particularly O-glycosylation, within the Hinge region.

The Hinge (also known as proline-rich linker) region of MT1-MMP is known to contain multiple potential O-glycosylation sites, as identified by Wu et al. (2004). Namely, these

include Thr^{291}, Thr^{299}, Thr^{300}, and Ser^{301}. O-glycosylation of MT1-MMP has been reported to be a regulation mechanism of the enzyme's activity (Remacle et al., 2006). Particularly, it was determined that incomplete glycosylation stimulates extensive autocatalytic degradation and self-inactivation of MT1-MMP . It is therefore plausible that the insertion of the FFSS tag within the Hinge region disrupted the normal O-glycosylation process, leading to aberrant molecular processing or altered structural stability of the MT1-MMP-Hinge-FFSS constructs. This could account for their increased electrophoretic mobility/decreased apparent size. Given the importance of O-glycosylation in the regulation of MT1-MMP, as highlighted by Remacle et al. (2006), and the apparent disruption caused by FFSS insertion in the Hinge region, we concluded that constructs with FFSS insertions into the Hinge region are unsuitable for further experiments. Moving forward, only the "Linker" variants of MT1-MMP-FFSS constructs were utilized in subsequent investigations, as they appear to preserve the structural and functional integrity of the protein.

5.5. Different degradative abilities of the studied MT1-MMP mutant forms (see 4.2.2.2.)

To confirm whether FLAG/Strep-tag insertions into the Linker region affected the enzymatic function of MT1-MMP, we performed gelatine degradation assays with HT1080 MMP-14 KO cells transfected with MT1-MMP-L-FFSS constructs. The analysis revealed that while the tagged constructs retained their gelatine-degrading ability, significant differences were observed between specific mutants. These variations likely originate from the distinct structural and functional impacts of each mutation, highlighting the critical roles of specific residues in MT1-MMP degradative activity.

As it is seen from the graph (Figure 29), MT1-MMP-L-FFSS-LLY, which contains LLY^{573}/AAA substitution in MT1-MMP's cytoplasmic tail, exhibits the highest degradative ability of all the tested variants (degrading significantly higher than positive control non-transfected *wild-type* HT1080 cells ($p < 0.0001$), negative control non-transfected HT1080 MMP14 KO cells ($p < 0.0001$), "L-WT" ($p < 0.0001$), "L-C/A" ($p < 0.0001$), and "L-dCP" ($p < 0.0001$)). LLY^{573} motif has been reported to interact with the μ2 subunit of AP-2, a clathrin-coated pit cargo adaptor protein, leading to MT1-MMP endocytosis in CCPs (Uekita et al., 2001). Therefore, we may hypothesize that the disruption of this motif in MT1-MMP-LLY mutant variant hinders MT1-MMP internalization and trafficking, and with limited endocytic removal, MT1-MMP remains on the cell surface longer, leading to enhanced ECM degradation.

On the other hand, MT1-MMP-L-FFSS-C574A, a Cys^{574}/Ala substitution mutant, demonstrated weaker degradative properties than "L-LLY" ($p < 0.0001$), but still stronger than did the positive ($p < 0.001$) and negative control cells ($p < 0.0001$). Previous research has shown that Cys^{574} residue of the enzyme's cytoplasmic tail is part of a disulfide bridge that covalently links MT1-MMP monomers into oligomers at the cell surface, and that mutation of this residue abrogates the ability of MT1-MMP-C574A monomers to form this disulfide bridge (Rozanov et al., 2001). Additionally, this site is also crucial for proper cell migration and invasion (Labrecque et al., 2004). Hence, we suppose that decreased degradative ability of MT1-MMP-L-FFSS-C574A might be due to abolished MT1-MMP multimerization at the surface of cells.

As to MT1-MMP-L-FFSS-dCP, the MT1-MMP cytoplasmic domain deletion mutant, – it demonstrated higher degradative abilities than positive ($p < 0.01$) and negative control cells ($p < 0.0001$), but lower than those of "L-LLY" variant ($p < 0.0001$); compared to "L-WT", they were lower, but non-significantly ($p > 0.05$). Because the deletion of the cytoplasmic tail impairs MT1-MMP's localization and interaction with regulatory proteins, its limited degradative function aligns with existing literature, underscoring the critical role of cytoplasmic tail in MT1-MMP's function.

Finally, the general increase in MT1-MMP-L-FFSS constructs-transfected cells' gelatine degradation over that of positive and negative control cells may be explained by overall higher levels of MT1-MMP in cells transfected with it than in the non-transfected.

5.6. Desmoglein-2: an adhesion molecule in desmosomes

Desmoglein-2, a calcium-binding transmembrane glycoprotein, is a desmosomal cadherin functioning to structurally adhere adjacent cells together. Desmosomes are cell-cell junctions in epithelial, myocardial, and other tissues. The desmosome–intermediate filament complex (DIFC) comprises three components: intracellularly, desmosomal cadherins' cytoplasmic tails bind plakoglobin and plakophilins (forming the outer dense plaque), which then connect to desmoplakin; intercellularly, desmogleins and desmocollins interact through homophilic and heterophilic binding (Garrod & Chidgey, 2008).

5.6.1. The broad spectrum of desmoglein-2 roles

Desmoglein-2 (DSG2) interacts with several key proteins, including desmocollin-1 (Chitaev & Troyanovsky, 1997), plakophilin-3 (Bonné et al., 2003), plakoglobin (Bannon et al., 2001; Ozawa et al., 1995; Wahl et al., 2000), and $Na_V1.5$ (Rizzo et al., 2012). DSG2 also

plays critical roles in various diseases. It acts as an attachment receptor for human adenoviruses (Stasiak & Stehle, 2020) and is as an Alzheimer's disease risk factor (Kim et al., 2017). DSG2 is essential for intestinal epithelial barrier integrity in Crohn's disease (Gross et al., 2018) and is upregulated in pemphigus, where its interaction with DSG3 mitigates autoantibody-induced keratinocyte adhesion loss (Fuchs et al., 2022; Sigmund et al., 2020). Additionally, DSG2 induces vascular changes in Moyamoya disease (Wang et al., 2024) and its mutations are a major cause of arrhythmogenic cardiomyopathy (AC), as they weaken desmosomal adhesiveness due to the incorporation of uncleaved mutant proDSG2 under stress (Vite et al., 2020). DSG2 has been shown to interact with EGFR, whose inhibition enhances cardiomyocyte cohesion in AC by stabilizing desmosome integrity via ROCK (Shoykhet et al., 2023).

5.6.2. Desmoglein-2 in cancer

Desmoglein-2 (DSG2) plays a significant role in cancer progression and prognosis. In lung adenocarcinoma (LUAD), it is associated with poor prognosis, reduced survival (Jin et al., 2020; Lückstädt et al., 2024), tumour size, lymph node metastasis and TNM stage (Sun et al., 2020). DSG2 overexpression in LUAD promotes cell proliferation and migration via interaction with EGFR (Jin et al., 2020). In breast cancer, DSG2 interacts with FABP4, stimulating proliferation (Chen et al., 2023), while in cervical cancer, it is upregulated, correlating with poor prognosis and reduced immune infiltration (Zhang et al., 2024). In gastric cancer, abundant TROP2 expression reduces DSG2 levels, weakening desmosomal adhesion and increasing invasion, migration, and malignancy through EGFR/AKT and DSG2/PG/β-catenin pathways (Yang et al., 2022). DSG2-mediated adhesion in pancreatic cancer enhances circulating cell cluster size, promoting early liver metastases (Dietrich et al., 2024). Additionally, DSG2 upregulation is linked to early treatment failure in oral tongue squamous cell carcinoma (Thangaraj et al., 2021).

5.6.3. Other known interactions of desmoglein-2

DSG2 binds E-cadherin via Leu^{175}, facilitating desmosome assembly (Shafraz et al., 2018, 2020) and interacts with PI-3-kinase to regulate Claudin2 (Burkard et al., 2021). DSG2 also binds EGFR, modulating its adhesion function with Src (Ungewiß et al., 2018) , and is a substrate of S-acyltransferase DHHC5, essential for its plasma membrane localization and desmosomal patterning (Woodley & Collins, 2019). In addition, DSG2 interacts with PLAC1, influencing cell-to-cell communication (Wang et al., 2024).

5.7. Addressing the challenges of DSG2/MT1-MMP coimmunoprecipitation

5.7.1. Expected sizes of desmoglein-2 bands on Western blot

Desmoglein-2 is a 122.2 kDa protein composed of 1118 amino acids (*Cardiac Organellar Protein Atlas Knowledgebase (COPaKB) —— Protein Information*, 2016). According to the anti-DSG2 antibody's manufacturer (*Anti-Desmoglein 2/DSG2 antibody [EPR6768] (ab150372) | Abcam*, b.r.), DSG2 should be detected on Western blot as a single band of approximately 150 kDa (Figure 49, left). Nevertheless, in our experiments, detection with this DSG2 antibody always yielded four distinct and intensive bands of approximately 170 kDa, 110 kDa, 95 kDa and 64 kDa (Figure 49, right).

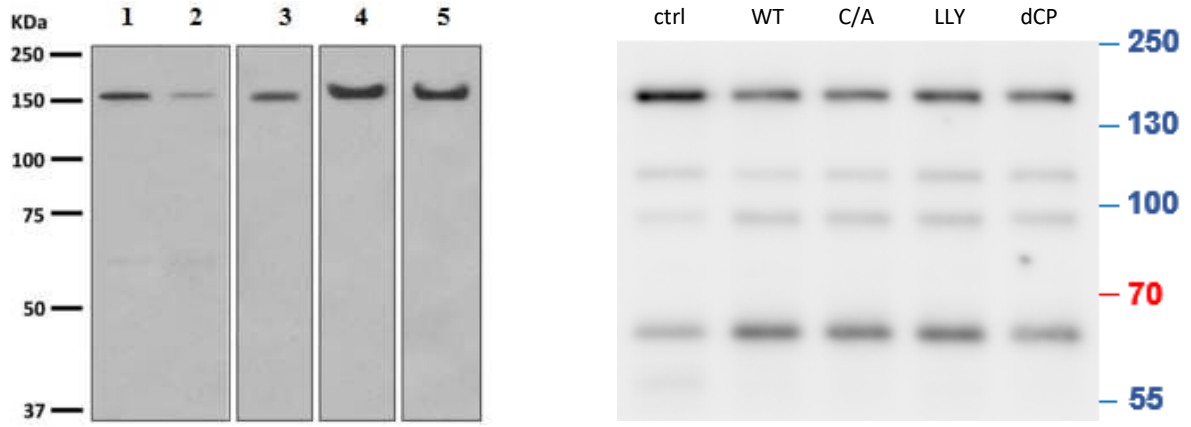

Figure 49. Western blot detection with DSG2 antibody (ab150372, Abcam): *(left)* an example provided by the manufacturer (*Anti-Desmoglein 2/DSG2 antibody [EPR6768] (ab150372) | Abcam*, b.r.) and *(right)* a typical membrane obtained during our experiments.

Studies using this DSG2 antibody (ab150372, Abcam) report detecting DSG2 as a band of as a band of 150 kDa (Liu et al., 2017), 160 kDa (Jin et al., 2020), or 170 kDa (Bortoli et al., 2023). Other publications show Western blots with multiple DSG2 bands of varying sizes, including 135 kDa, 100 kDa, 75 kDa, and 65 kDa (Vallverdú-Prats et al., 2023) or 130 kDa and 100 kDa (Butin-Israeli et al., 2016; Kamekura et al., 2015). The 130 kDa form is referred to as 'canonical DSG2' (Vallverdú-Prats et al., 2023), while the 100 kDa fragment is identified as a cleavage product of DSG2 (Butin-Israeli et al., 2016; Kamekura et al., 2015).

To conclude, although Desmoglein-2 (DSG2) is a 122.2 kDa protein based on its amino acid composition, in immunoblots DSG-2 is usually detected in range of 150-170 kDa, which could suggest post-translational modifications, such as glycosylation, increasing the apparent molecular weight. The detection of lower molecular weight bands (e.g., 100 kDa, 95 kDa, and

64 kDa) indicates that some DSG2 fragments might result from proteolytic cleavage, as supported by previous studies.

5.7.2. Non-specific DSG2 interaction with agarose beads

One significant challenge in our MT1-MMP/DSG2 coimmunoprecipitation experiments was non-specific DSG2 binding to the beads. All bead types we tested – Strep-Tactin® Superflow®, anti-FLAG® M2 magnetic beads, and nProtein A Sepharose™ 4 Fast Flow – utilize a 4% or 6% cross-linked agarose matrix, which forms a porous three-dimensional network. This agarose matrix has pores, whose size depends on the agarose concentration. Even at higher concentrations, such as 6%, the pores are still large enough to allow the diffusion of molecules with molecular weights up to 1–5 million Daltons into the beads, facilitating interactions with ligands immobilized on the bead surface.

5.7.3. Strategies of reducing DSG2 non-specific beads binding

To minimize non-specific DSG2 binding to these agarose-based beads, in our experiments we used several approaches. Firstly, we tried to optimize the lysis buffer composition. Based on the available publications that reported DSG2 immunoprecipitation (Gross et al., 2018; Hartlieb et al., 2014; Jiang et al., 2014; Nava et al., 2007; Wahl et al., 2000), we have come up with two alternative lysis buffers (see Table 2). After testing these two new buffers, we have not seen any improvement, hence, we have returned to the previously used 0.5% Triton X-100 lysis buffer (Table 2).

Secondly, we have decided to add EGTA (ethylene glycol bis(2-aminoethyl)tetraacetic acid), a chelating agent related to EDTA, to the lysis buffer. Compared to EDTA, it has a lower affinity for magnesium, making it more selective for calcium ions. EGTA is useful in buffer solutions that resemble the environment in living cells where calcium ions are usually at least a thousandfold less concentrated than magnesium (*ethylene glycol bis(2-aminoethyl)tetraacetic acid (CHEBI:30740)*, 2015).

Finally, we have established a lysates preclearing step (see 4.2.4.4.1. and Figure 41). After the lysates were prepared and before the immunoprecipitation, they were pre-incubated with the beads which were not functionalized with any specific groups, particularly with nProtein A Sepharose™ 4 Fast Flow beads. This allowed for reducing the overall amount of DSG2, and thus, its non-specific interacting with agarose-coated beads (see Figure 43).

Because some non-specific DSG2 binding still remained, additional strategies for removing non-specific binding of DSG2 may be required in further research. For example, pre-

incubation of the beads with blocking buffers (e.g., BSA or casein) can be employed. This step coats unoccupied binding sites on the beads, minimizing non-specific interactions. Other methods include optimizing buffer ionic strength and pH, as these parameters can modulate protein charge and matrix interactions, further reducing nonspecific binding.

5.7.4. DSG2–MT1-MMP coimmunoprecipitations

Eventually, this work included multiple attempts of DSG2/MT1-MMP coimmunoprecipitations. Numerous challenges were encountered involving non-specific DSG2 binding to the agarose-based beads, low DSG2 constructs expression levels, diversity in the observed DSG2 sizes. Additionally, it was discovered late in the experimental process that the DSG2-FLAG-EGFP construct's DNA used had been unintentionally mutagenized, likely during amplification by bacteria. This unexpected issue further compromised the ability to obtain reliable and reproducible results within the limited timeframe.

However, several experiments provided promising results applying different immunoprecipitation approaches: using anti-GFP-coupled sepharose beads (Figures 40 and 44), StrepTactin beads (Figure 42), and anti-FLAG® M2 magnetic beads (Figure 38). The initial methods were considerably improved throughout the investigation process, including establishing the proper lysis buffer composition, optimizing the time of incubation with the beads, implementation of the lysates preclearing step, usage of specific immunoprecipitation columns and more. These protocols' modifications should definitely be considered in further investigations of the potential MT1-MMP and desmoglein-2 interaction. Overall, we believe our work lays a significant groundwork for the future research of the potential MT1-MMP interaction partners.

6. Conclusion

Membrane Type 1 Matrix Metalloproteinase (MT1-MMP) is a critical enzyme involved in extracellular matrix (ECM) degradation and cancer cell invasiveness. The aim of this thesis was to explore the pool of MT1-MMP's interactions and to identify novel interaction partners of its cytoplasmic tail (CT), which would deepen our understanding of the MT1-MMP cytoplasmic domain's role in cellular processes. Using proximity-dependent biotinylation, affinity purification and mass spectrometry, we have identified a number of proteins potentially binding MT1-MMP's CT. These included some of the well-established interactors such as CD44, Eph receptor A2, and integrin β1, supporting the reliability of the findings. Other detected proteins included nectin-2, AHNAK, and AHNAK2, which have not been previously linked to MT1-MMP, introducing intriguing candidates for further investigations.

Among the newly identified potential interactors, desmoglein-2 (DSG2), a key desmosomal cadherin in cellular adhesion, emerged as a plausible candidate. Therefore, another goal of our research was to confirm the supposed interaction of MT1-MMP and DSG2 by coimmunoprecipitation. Substantial technical challenges were faced in the process, compromising our ability to obtain reliable and reproducible results within the limited timeframe. While the presence of the interaction could not be conclusively proven, this work provided valuable insights into the potential and limitations of current methodologies in studying protein-protein interactions. The immunoprecipitation protocols improved in this study should be considered in further exploration of the MT1-MMP–DSG2 interaction.

Additionally, the investigation offered noteworthy findings regarding different degradative capabilities of selected MT1-MMP mutant variants. We have also confirmed desmoglein-2 localisation to intercellular adhesions using fluorescence microscopy of living cells. The question of MT1-MMP and desmodlein-2 colocalization in cancer cells remained pending, yet the desmoglein-2 constructs employed in this work may be utilised to resolve it in future.

In summary, the interaction between MT1-MMP and DSG2 remains unproven, although *in silico* analysis has identified potential MT1-MMP cleavage sites within DSG2's extracellular domain, suggesting a plausible biochemical basis for their interplay. More studies should be conducted to clarify the functional interplay between MT1-MMP and DSG2 and its implications in oncological contexts. Future research is also needed to verify other presumed

interactions, since they may represent novel components of MT1-MMP's interactome, and thereby, could uncover promising therapeutic targets in cancer biology.

The groundwork established in this thesis will be further investigated by colleagues from the Laboratory of Cancer Cell Invasion, ensuring continuity in addressing the opened issues regarding MT1-MMP's interaction network, particularly its potential relationship with DSG2. This ongoing research is expected to contribute valuable insights into cellular adhesion and extracellular matrix remodelling interplay, advancing our understanding of these processes in the context of cancer cell invasion.

7. References

Anilkumar, N., Uekita, T., Couchman, J. R., Nagase, H., Seiki, M., & Itoh, Y. (2005). Palmitoylation at Cys574 is essential for MT1-MMP to promote cell migration. *FASEB Journal: Official Publication of the Federation of American Societies for Experimental Biology*, *19*(10), 1326–1328. https://doi.org/10.1096/fj.04-3651fje

Anti-Desmoglein 2/DSG2 antibody [EPR6768] (ab150372) | Abcam. (b.r.). Získáno 18. listopad 2024, z https://www.abcam.com/en-us/products/primary-antibodies/desmoglein-2-dsg2-antibody-epr6768-ab150372#lb

Augoff, K., Hryniewicz-Jankowska, A., & Tabola, R. (2020). Invadopodia: Clearing the way for cancer cell invasion. *Annals of Translational Medicine*, *8*(14), 902. https://doi.org/10.21037/atm.2020.02.157

Bannon, L. J., Cabrera, B. L., Green, K. J., & Stack, M. S. (2001). Isoform-Specific Differences in the Size of Desmosomal Cadherin/Catenin Complexes. *Journal of Investigative Dermatology*, *117*(5), 1302–1306. https://doi.org/10.1046/j.1523-1747.2001.01512.x

Beliën, A. T. J., Paganetti, P. A., & Schwab, M. E. (1999). Membrane-type 1 Matrix Metalloprotease (MT1-MMP) Enables Invasive Migration of Glioma Cells in Central Nervous System White Matter. *Journal of Cell Biology*, *144*(2), 373–384. https://doi.org/10.1083/jcb.144.2.373

Bonné, S., Gilbert, B., Hatzfeld, M., Chen, X., Green, K. J., & Roy, F. van. (2003). Defining desmosomal plakophilin-3 interactions. *The Journal of Cell Biology*, *161*(2), 403. https://doi.org/10.1083/jcb.200303036

Bork, B. (2020). Mass spectrometry identification of membrane-type 1 matrix metalloproteinase (MT1-MMP) binding partners following co-immunoprecipitation in MCF-7 cells. *Electronic Thesis and Dissertation Repository*. https://ir.lib.uwo.ca/etd/7144

Bortoli, M. D., Meraviglia, V., Mackova, K., Frommelt, L. S., König, E., Rainer, J., Volani, C., Benzoni, P., Schlittler, M., Cattelan, G., Motta, B. M., Volpato, C., Rauhe, W., Barbuti, A., Zacchigna, S., Pramstaller, P. P., & Rossini, A. (2023). Modeling incomplete penetrance in arrhythmogenic cardiomyopathy by human induced pluripotent stem cell derived cardiomyocytes. *Computational and Structural Biotechnology Journal*, *21*, 1759. https://doi.org/10.1016/j.csbj.2023.02.029

Brooks, P. C., Strömblad, S., Sanders, L. C., Schalscha, T. L. von, Aimes, R. T., Stetler-Stevenson, W. G., Quigley, J. P., & Cheresh, D. A. (1996). Localization of Matrix Metalloproteinase MMP-2 to the Surface of Invasive Cells by Interaction with Integrin αvβ3. *Cell*, *85*(5), 683–693. https://doi.org/10.1016/S0092-8674(00)81235-0

Burkard, N., Meir, M., Kannapin, F., Otto, C., Petzke, M., Germer, C.-T., Waschke, J., & Schlegel, N. (2021). Desmoglein2 Regulates Claudin2 Expression by Sequestering PI-3-Kinase in Intestinal Epithelial Cells. *Frontiers in Immunology*, *12*, 756321. https://doi.org/10.3389/fimmu.2021.756321

Butin-Israeli, V., Houser, M. C., Feng, M., Thorp, E. B., Nusrat, A., Parkos, C. A., & Sumagin, R. (2016). Deposition of microparticles by neutrophils onto inflamed epithelium: A new mechanism to disrupt epithelial intercellular adhesions and promote transepithelial migration. *The FASEB Journal*, *30*(12), 4007–4020. https://doi.org/10.1096/fj.201600734R

Butler, G. S., Dean, R. A., Tam, E. M., & Overall, C. M. (2008). Pharmacoproteomics of a Metalloproteinase Hydroxamate Inhibitor in Breast Cancer Cells: Dynamics of Membrane Type 1 Matrix Metalloproteinase-Mediated Membrane Protein Shedding. *Molecular and Cellular Biology*, *28*(15), 4896–4914. https://doi.org/10.1128/MCB.01775-07

Cardiac Organellar Protein Atlas Knowledgebase (COPaKB)——Protein Information. (2016, březen 4). https://web.archive.org/web/20160304094802/http://www.heartproteome.org/copa/ProteinInfo.aspx?QType=Protein%20ID&QValue=Q14126

Craene, B. D., & Berx, G. (2013). Regulatory networks defining EMT during cancer initiation and progression. *Nature Reviews Cancer*, *13*(2), Article 2. https://doi.org/10.1038/nrc3447

D'Alessio, S., Ferrari, G., Cinnante, K., Scheerer, W., Galloway, A. C., Roses, D. F., Rozanov, D. V., Remacle, A. G., Oh, E.-S., Shiryaev, S. A., Strongin, A. Y., Pintucci, G., & Mignatti, P. (2008). Tissue inhibitor of metalloproteinases-2 binding to membrane-type 1 matrix metalloproteinase induces MAPK activation and cell growth by a non-proteolytic mechanism. *The Journal of Biological Chemistry*, *283*(1), 87–99. https://doi.org/10.1074/jbc.M705492200

Datta, A., Deng, S., Gopal, V., Yap, K. C.-H., Halim, C. E., Lye, M. L., Ong, M. S., Tan, T. Z., Sethi, G., Hooi, S. C., Kumar, A. P., & Yap, C. T. (2021). Cytoskeletal Dynamics

in Epithelial-Mesenchymal Transition: Insights into Therapeutic Targets for Cancer Metastasis. *Cancers*, *13*(8), Article 8. https://doi.org/10.3390/cancers13081882

Dietrich, N., Castellanos-Martinez, R., Kemmling, J., Heuser, A., Schnoor, M., Schinner, C., & Spindler, V. (2024). Adhesion of pancreatic tumor cell clusters by desmosomal molecules enhances early liver metastases formation. *Scientific Reports*, *14*(1), 18189. https://doi.org/10.1038/s41598-024-68493-6

d'Ortho, M. P., Will, H., Atkinson, S., Butler, G., Messent, A., Gavrilovic, J., Smith, B., Timpl, R., Zardi, L., & Murphy, G. (1997). Membrane-type matrix metalloproteinases 1 and 2 exhibit broad-spectrum proteolytic capacities comparable to many matrix metalloproteinases. *European Journal of Biochemistry*, *250*(3), 751–757. https://doi.org/10.1111/j.1432-1033.1997.00751.x

Eberle, A., Stalder, L., Mathys, H., Orozco, R., & Mühlemann, O. (2008). Posttranscriptional Gene Regulation by Spatial Rearrangement of the 3′ Untranslated Region. *PLoS biology*, *6*, e92. https://doi.org/10.1371/journal.pbio.0060092

Eddy, R. J., Weidmann, M. D., Sharma, V. P., & Condeelis, J. S. (2017). Tumor Cell Invadopodia: Invasive Protrusions that Orchestrate Metastasis. *Trends in Cell Biology*, *27*(8), 595–607. https://doi.org/10.1016/j.tcb.2017.03.003

Eger, A., & Mikulits, W. (2005). Models of epithelial–mesenchymal transition. *Drug Discovery Today: Disease Models*, *2*(1), 57–63. https://doi.org/10.1016/j.ddmod.2005.04.001

Eisenach, P. A., de Sampaio, P. C., Murphy, G., & Roghi, C. (2012). Membrane Type 1 Matrix Metalloproteinase (MT1-MMP) Ubiquitination at Lys581 Increases Cellular Invasion through Type I Collagen. *The Journal of Biological Chemistry*, *287*(14), 11533–11545. https://doi.org/10.1074/jbc.M111.306340

Eisenach, P. A., Roghi, C., Fogarasi, M., Murphy, G., & English, W. R. (2010). MT1-MMP regulates VEGF-A expression through a complex with VEGFR-2 and Src. *Journal of Cell Science*, *123*(Pt 23), 4182–4193. https://doi.org/10.1242/jcs.062711

Esparza, J., Vilardell, C., Calvo, J., Juan, M., Vives, J., Urbano-Márquez, A., Yagüe, J., & Cid, M. C. (1999). Fibronectin Upregulates Gelatinase B (MMP-9) and Induces Coordinated Expression of Gelatinase A (MMP-2) and Its Activator MT1-MMP (MMP-14) by Human T Lymphocyte Cell Lines. A Process Repressed Through RAS/MAP Kinase Signaling Pathways. *Blood*, *94*(8), 2754–2766. https://doi.org/10.1182/blood.V94.8.2754.420k09_2754_2766

Ethylene glycol bis(2-aminoethyl)tetraacetic acid (CHEBI:30740). (2015). https://www.ebi.ac.uk/chebi/searchId.do;?chebiId=CHEBI:30740

Fairhead, M., & Howarth, M. (2015). Site-specific biotinylation of purified proteins using BirA. *Methods in molecular biology (Clifton, N.J.)*, *1266*, 171–184. https://doi.org/10.1007/978-1-4939-2272-7_12

Fehon, R. G., McClatchey, A. I., & Bretscher, A. (2010). Organizing the Cell Cortex: The role of ERM proteins. *Nature reviews. Molecular cell biology*, *11*(4), 276–287. https://doi.org/10.1038/nrm2866

Ferlay, J., Ervik, M., Lam, F., Colombet, M., Mery, L., Piñeros, M., & et al. (2020). Global Cancer Observatory: Cancer Today. *Lyon: International Agency for Research on Cancer*. https://gco.iarc.fr/today

Ferrari, R., Martin, G., Tagit, O., Guichard, A., Cambi, A., Voituriez, R., Vassilopoulos, S., & Chavrier, P. (2019). MT1-MMP directs force-producing proteolytic contacts that drive tumor cell invasion. *Nature Communications*, *10*, 4886. https://doi.org/10.1038/s41467-019-12930-y

Friedl, P., Borgmann, S., & Bröcker, E. B. (2001). Amoeboid leukocyte crawling through extracellular matrix: Lessons from the Dictyostelium paradigm of cell movement. *Journal of Leukocyte Biology*, *70*(4), 491–509.

Garrod, D., & Chidgey, M. (2008). Desmosome structure, composition and function. *Biochimica et Biophysica Acta (BBA) - Biomembranes*, *1778*(3), 572–587. https://doi.org/10.1016/j.bbamem.2007.07.014

Gifford, V., & Itoh, Y. (2019). MT1-MMP-dependent cell migration: Proteolytic and non-proteolytic mechanisms. *Biochemical Society Transactions*, *47*(3), 811–826. https://doi.org/10.1042/BST20180363

Gingras, D., Michaud, M., Di Tomasso, G., Béliveau, E., Nyalendo, C., & Béliveau, R. (2008). Sphingosine-1-phosphate induces the association of membrane-type 1 matrix metalloproteinase with p130Cas in endothelial cells. *FEBS Letters*, *582*(3), 399–404. https://doi.org/10.1016/j.febslet.2007.12.029

Gonzalo, P., Guadamillas, M. C., Hernández-Riquer, M. V., Pollán, Á., Grande-García, A., Bartolomé, R. A., Vasanji, A., Ambrogio, C., Chiarle, R., Teixidó, J., Risteli, J., Apte, S. S., del Pozo, M. A., & Arroyo, A. G. (2010). MT1-MMP Is Required for Myeloid Cell Fusion via Regulation of Rac1 Signaling. *Developmental Cell*, *18*, 77–89. https://doi.org/10.1016/j.devcel.2009.11.012

Grafinger, O. R., Gorshtein, G., Stirling, T., Brasher, M. I., & Coppolino, M. G. (2020). B1 integrin-mediated signaling regulates MT1-MMP phosphorylation to promote tumor cell invasion. *Journal of Cell Science*, *133*(9), jcs239152. https://doi.org/10.1242/jcs.239152

Gross, A., Pack, L. A. P., Schacht, G. M., Kant, S., Ungewiss, H., Meir, M., Schlegel, N., Preisinger, C., Boor, P., Guldiken, N., Krusche, C. A., Sellge, G., Trautwein, C., Waschke, J., Heuser, A., Leube, R. E., & Strnad, P. (2018). Desmoglein 2, but not desmocollin 2, protects intestinal epithelia from injury. *Mucosal Immunology*, *11*(6), 1630–1639. https://doi.org/10.1038/s41385-018-0062-z

Hartlieb, E., Rötzer, V., Radeva, M., Spindler, V., & Waschke, J. (2014). Desmoglein 2 Compensates for Desmoglein 3 but Does Not Control Cell Adhesion via Regulation of p38 Mitogen-activated Protein Kinase in Keratinocytes. *Journal of Biological Chemistry*, *289*(24), 17043–17053. https://doi.org/10.1074/jbc.M113.489336

Hay, E. D. (1995). An overview of epithelio-mesenchymal transformation. *Acta Anatomica*, *154*(1), 8–20. https://doi.org/10.1159/000147748

Hermanson, G. T. (2013). *Bioconjugate Techniques*. Academic Press.

Hernandez-Barrantes, S., Toth, M., Bernardo, M. M., Yurkova, M., Gervasi, D. C., Raz, Y., Sang, Q. A., & Fridman, R. (2000). Binding of Active (57 kDa) Membrane Type 1-Matrix Metalloproteinase (MT1-MMP) to Tissue Inhibitor of Metalloproteinase (TIMP)-2 Regulates MT1-MMP Processing and Pro-MMP-2 Activation*. *Journal of Biological Chemistry*, *275*(16), 12080–12089. https://doi.org/10.1074/jbc.275.16.12080

Hikita, A., Yana, I., Wakeyama, H., Nakamura, M., Kadono, Y., Oshima, Y., Nakamura, K., Seiki, M., & Tanaka, S. (2006). Negative Regulation of Osteoclastogenesis by Ectodomain Shedding of Receptor Activator of NF-κB Ligand *. *Journal of Biological Chemistry*, *281*(48), 36846–36855. https://doi.org/10.1074/jbc.M606656200

Hiraoka, N., Allen, E., Apel, I. J., Gyetko, M. R., & Weiss, S. J. (1998). Matrix Metalloproteinases Regulate Neovascularization by Acting as Pericellular Fibrinolysins. *Cell*, *95*(3), 365–377. https://doi.org/10.1016/S0092-8674(00)81768-7

Hotary, K., Allen, E., Punturieri, A., Yana, I., & Weiss, S. J. (2000). Regulation of Cell Invasion and Morphogenesis in a Three-Dimensional Type I Collagen Matrix by Membrane-Type Matrix Metalloproteinases 1, 2, and 3. *The Journal of Cell Biology*, *149*(6), 1309–1323.

Huxley-Jones, J., Clarke, T.-K., Beck, C., Toubaris, G., Robertson, D., & Boot-Handford, R. (2007). The evolution of the vertebrate metzincins; Insights from Ciona intestinalis and Danio rerio. *BMC evolutionary biology*, *7*, 63. https://doi.org/10.1186/1471-2148-7-63

Hwang, I. K., Park, S. M., Kim, S. Y., & Lee, S.-T. (2004). A proteomic approach to identify substrates of matrix metalloproteinase-14 in human plasma. *Biochimica et Biophysica Acta (BBA) - Proteins and Proteomics*, *1702*(1), 79–87. https://doi.org/10.1016/j.bbapap.2004.08.001

Chambers, A. F., & Matrisian, L. M. (1997). Changing Views of the Role of Matrix Metalloproteinases in Metastasis. *JNCI: Journal of the National Cancer Institute*, *89*(17), 1260–1270. https://doi.org/10.1093/jnci/89.17.1260

Chen, D., Wirth, K. M., Kizy, S., Muretta, J. M., Markowski, T. W., Yong, P., Sheka, A., Abdelwahab, H., Hertzel, A. V., Ikramuddin, S., Yamamoto, M., & Bernlohr, D. A. (2023). Desmoglein 2 Functions as a Receptor for Fatty Acid Binding Protein 4 in Breast Cancer Epithelial Cells. *Molecular Cancer Research: MCR*, *21*(8), 836–848. https://doi.org/10.1158/1541-7786.MCR-22-0763

Chitaev, N. A., & Troyanovsky, S. M. (1997). Direct Ca2+-dependent Heterophilic Interaction between Desmosomal Cadherins, Desmoglein and Desmocollin, Contributes to Cell–Cell Adhesion. *The Journal of Cell Biology*, *138*(1), 193. https://doi.org/10.1083/jcb.138.1.193

Cho, J.-A., Osenkowski, P., Zhao, H., Kim, S., Toth, M., Cole, K., Aboukameel, A., Saliganan, A., Schuger, L., Bonfil, R. D., & Fridman, R. (2008). The Inactive 44-kDa Processed Form of Membrane Type 1 Matrix Metalloproteinase (MT1-MMP) Enhances Proteolytic Activity via Regulation of Endocytosis of Active MT1-MMP. *The Journal of Biological Chemistry*, *283*(25), 17391–17405. https://doi.org/10.1074/jbc.M708943200

Chun, T.-H., Hotary, K. B., Sabeh, F., Saltiel, A. R., Allen, E. D., & Weiss, S. J. (2006). A Pericellular Collagenase Directs the 3-Dimensional Development of White Adipose Tissue. *Cell*, *125*(3), 577–591. https://doi.org/10.1016/j.cell.2006.02.050

Imai, K., Ohta, S., Matsumoto, T., Fujimoto, N., Sato, H., Seiki, M., & Okada, Y. (1997). Expression of membrane-type 1 matrix metalloproteinase and activation of progelatinase A in human osteoarthritic cartilage. *The American Journal of Pathology*, *151*(1), 245–256.

Itoh, Y. (2006). MT1-MMP: A key regulator of cell migration in tissue. *IUBMB Life*, *58*(10), 589–596. https://doi.org/10.1080/15216540600962818

Jacob, A., & Prekeris, R. (2015). The regulation of MMP targeting to invadopodia during cancer metastasis. *Frontiers in Cell and Developmental Biology*, *3*, 4. https://doi.org/10.3389/fcell.2015.00004

Janoštiak, R., Tolde, O., Brůhová, Z., Novotný, M., Hanks, S. K., Rösel, D., & Brábek, J. (2011). Tyrosine phosphorylation within the SH3 domain regulates CAS subcellular localization, cell migration, and invasiveness. *Molecular Biology of the Cell*, *22*(22), 4256–4267. https://doi.org/10.1091/mbc.E11-03-0207

Jiang, K., Rankin, C. R., Nava, P., Sumagin, R., Kamekura, R., Stowell, S. R., Feng, M., Parkos, C. A., & Nusrat, A. (2014). Galectin-3 Regulates Desmoglein-2 and Intestinal Epithelial Intercellular Adhesion. *The Journal of Biological Chemistry*, *289*(15), 10510–10517. https://doi.org/10.1074/jbc.M113.538538

Jin, G., Zhang, F., Chan, K. M., Xavier Wong, H. L., Liu, B., Cheah, K. S. E., Liu, X., Mauch, C., Liu, D., & Zhou, Z. (2011). MT1-MMP cleaves Dll1 to negatively regulate Notch signalling to maintain normal B-cell development. *The EMBO Journal*, *30*(11), 2281–2293. https://doi.org/10.1038/emboj.2011.136

Jin, R., Wang, X., Zang, R., Liu, C., Zheng, S., Li, H., Sun, N., & He, J. (2020). Desmoglein-2 modulates tumor progression and osimertinib drug resistance through the EGFR/Src/PAK1 pathway in lung adenocarcinoma. *Cancer Letters*, *483*, 46–58. https://doi.org/10.1016/j.canlet.2020.04.001

Kadono, Y., Shibahara, K., Namiki, M., Watanabe, Y., Seiki, M., & Sato, H. (1998). Membrane Type 1-Matrix Metalloproteinase Is Involved in the Formation of Hepatocyte Growth Factor/Scatter Factor-Induced Branching Tubules in Madin-Darby Canine Kidney Epithelial Cells. *Biochemical and Biophysical Research Communications*, *251*(3), 681–687. https://doi.org/10.1006/bbrc.1998.9531

Kajita, M., Itoh, Y., Chiba, T., Mori, H., Okada, A., Kinoh, H., & Seiki, M. (2001). Membrane-type 1 matrix metalloproteinase cleaves CD44 and promotes cell migration. *The Journal of Cell Biology*, *153*(5), 893–904. https://doi.org/10.1083/jcb.153.5.893

Kamekura, R., Nava, P., Feng, M., Quiros, M., Nishio, H., Weber, D. A., Parkos, C. A., & Nusrat, A. (2015). Inflammation-induced desmoglein-2 ectodomain shedding compromises the mucosal barrier. *Molecular Biology of the Cell*, *26*(18), 3165–3177. https://doi.org/10.1091/mbc.E15-03-0147

Kasurinen, A., Tervahartiala, T., Laitinen, A., Kokkola, A., Sorsa, T., Böckelman, C., & Haglund, C. (2018). *Data from: High serum MMP-14 predicts worse survival in gastric cancer* (Verze 1, s. 31115 bytes) [Dataset]. Dryad. https://doi.org/10.5061/DRYAD.HB62394

Kim, H., Yoo, J., Shin, J., Chang, Y., Jung, J., Jo, D.-G., Kim, J., Jang, W., Lengner, C. J., Kim, B.-S., & Kim, J. (2017). Modelling APOE ε3/4 allele-associated sporadic Alzheimer's disease in an induced neuron. *Brain: A Journal of Neurology*, *140*(8), 2193–2209. https://doi.org/10.1093/brain/awx144

Knäuper, V., Will, H., López-Otin, C., Smith, B., Atkinson, S. J., Stanton, H., Hembry, R. M., & Murphy, G. (1996). Cellular mechanisms for human procollagenase-3 (MMP-13) activation. Evidence that MT1-MMP (MMP-14) and gelatinase a (MMP-2) are able to generate active enzyme. *The Journal of Biological Chemistry*, *271*(29), 17124–17131. https://doi.org/10.1074/jbc.271.29.17124

Labrecque, L., Nyalendo, C., Langlois, S., Durocher, Y., Roghi, C., Murphy, G., Gingras, D., & Béliveau, R. (2004). Src-mediated tyrosine phosphorylation of caveolin-1 induces its association with membrane type 1 matrix metalloproteinase. *The Journal of Biological Chemistry*, *279*(50), 52132–52140. https://doi.org/10.1074/jbc.M409617200

Lagoutte, E., Villeneuve, C., Lafanechère, L., Wells, C. M., Jones, G. E., Chavrier, P., & Rossé, C. (2016). LIMK Regulates Tumor-Cell Invasion and Matrix Degradation Through Tyrosine Phosphorylation of MT1-MMP. *Scientific Reports*, *6*, 24925. https://doi.org/10.1038/srep24925

Li, A., Dawson, J. C., Forero-Vargas, M., Spence, H. J., Yu, X., König, I., Anderson, K., & Machesky, L. M. (2010). The actin bundling protein fascin stabilizes actin in invadopodia and potentiates protrusive invasion. *Current biology : CB*, *20*(4), 339–345. https://doi.org/10.1016/j.cub.2009.12.035

Liu, Y., Chidgey, M., Yang, V. W., & Bialkowska, A. B. (2017). Krüppel-like factor 5 is essential for maintenance of barrier function in mouse colon. *American Journal of Physiology - Gastrointestinal and Liver Physiology*, *313*(5), G478–G491. https://doi.org/10.1152/ajpgi.00172.2017

Lodish, H., Berk, A., Kaiser, C. A., Krieger, M., Bretscher, A., Ploegh, H., Amon, A., & Martin, K. C. (2016). *Molecular Cell Biology* (8. vyd.). W. H. Freeman and Company.

Lückstädt, W., Rathod, M., Möbus, L., Bub, S., Lucius, R., Elsner, F., Spindler, V., & Arnold, P. (2024). CD109 drives pro-tumorigenic cell properties in human non-small cell lung cancer through interaction with desmoglein-2. *Research Square*, rs.3.rs-4102385. https://doi.org/10.21203/rs.3.rs-4102385/v1

Ludwig, T., Theissen, S. M., Morton, M. J., & Caplan, M. J. (2008). The Cytoplasmic Tail Dileucine Motif LL572 Determines the Glycosylation Pattern of Membrane-type 1 Matrix Metalloproteinase. *The Journal of Biological Chemistry*, *283*(51), 35410–35418. https://doi.org/10.1074/jbc.M801816200

Mandeville, J. T., Lawson, M. A., & Maxfield, F. R. (1997). Dynamic imaging of neutrophil migration in three dimensions: Mechanical interactions between cells and matrix. *Journal of Leukocyte Biology*, *61*(2), 188–200. https://doi.org/10.1002/jlb.61.2.188

Miki, H., Suetsugu, S., & Takenawa, T. (1998). WAVE, a novel WASP-family protein involved in actin reorganization induced by Rac. *The EMBO Journal*, *17*(23), 6932–6941. https://doi.org/10.1093/emboj/17.23.6932

Mori, H., Tomari, T., Koshikawa, N., Kajita, M., Itoh, Y., Sato, H., Tojo, H., Yana, I., & Seiki, M. (2002). CD44 directs membrane-type 1 matrix metalloproteinase to lamellipodia by associating with its hemopexin-like domain. *The EMBO Journal*, *21*(15), 3949–3959. https://doi.org/10.1093/emboj/cdf411

Mori, T., Kitano, K., Terawaki, S., Maesaki, R., Fukami, Y., & Hakoshima, T. (2008). Structural Basis for CD44 Recognition by ERM Proteins. *The Journal of Biological Chemistry*, *283*(43), 29602–29612. https://doi.org/10.1074/jbc.M803606200

Moss, N. M., Liu, Y., Johnson, J. J., Debiase, P., Jones, J., Hudson, L. G., Munshi, H. G., & Stack, M. S. (2009). Epidermal Growth Factor Receptor-Mediated Membrane Type 1 Matrix Metalloproteinase Endocytosis Regulates the Transition Between Invasive Versus Expansive Growth of Ovarian Carcinoma Cells in Three-Dimensional Collagen. *Molecular cancer research : MCR*, *7*(6), 809–820. https://doi.org/10.1158/1541-7786.MCR-08-0571

Murphy, D. A., & Courtneidge, S. A. (2011). The „ins" and „outs" of podosomes and invadopodia: Characteristics, formation and function. *Nature Reviews. Molecular Cell Biology*, *12*(7), 413–426. https://doi.org/10.1038/nrm3141

Nagase, H., Visse, R., & Murphy, G. (2006). Structure and function of matrix metalloproteinases and TIMPs. *Cardiovascular Research*, *69*(3), 562–573. https://doi.org/10.1016/j.cardiores.2005.12.002

Nagase, H., & Woessner, J. F. (1999). Matrix metalloproteinases. *The Journal of Biological Chemistry*, *274*(31), 21491–21494. https://doi.org/10.1074/jbc.274.31.21491

Nava, P., Laukoetter, M. G., Hopkins, A. M., Laur, O., Gerner-Smidt, K., Green, K. J., Parkos, C. A., & Nusrat, A. (2007). Desmoglein-2: A Novel Regulator of Apoptosis in the Intestinal Epithelium. *Molecular Biology of the Cell*, *18*(11), 4565–4578. https://doi.org/10.1091/mbc.e07-05-0426

Niiya, D., Egawa, N., Sakamoto, T., Kikkawa, Y., Shinkawa, T., Isobe, T., Koshikawa, N., & Seiki, M. (2009). Identification and Characterization of Lutheran Blood Group Glycoprotein as a New Substrate of Membrane-type 1 Matrix Metalloproteinase 1 (MT1-MMP): A SYSTEMIC WHOLE CELL ANALYSIS OF MT1-MMP-ASSOCIATING PROTEINS IN A431 CELLS *. *Journal of Biological Chemistry*, *284*(40), 27360–27369. https://doi.org/10.1074/jbc.M109.029124

Nobes, C. D., & Hall, A. (1995). Rho, rac, and cdc42 GTPases regulate the assembly of multimolecular focal complexes associated with actin stress fibers, lamellipodia, and filopodia. *Cell*, *81*(1), 53–62. https://doi.org/10.1016/0092-8674(95)90370-4

Nyalendo, C., Michaud, M., Beaulieu, E., Roghi, C., Murphy, G., Gingras, D., & Béliveau, R. (2007). Src-dependent phosphorylation of membrane type I matrix metalloproteinase on cytoplasmic tyrosine 573: Role in endothelial and tumor cell migration. *The Journal of Biological Chemistry*, *282*(21), 15690–15699. https://doi.org/10.1074/jbc.M608045200

Ohuchi, E., Imai, K., Fujii, Y., Sato, H., Seiki, M., & Okada, Y. (1997). Membrane type 1 matrix metalloproteinase digests interstitial collagens and other extracellular matrix macromolecules. *The Journal of Biological Chemistry*, *272*(4), 2446–2451. https://doi.org/10.1074/jbc.272.4.2446

Ozawa, M., Terada, H., & Pedraza, C. (1995). The fourth armadillo repeat of plakoglobin (gamma-catenin) is required for its high affinity binding to the cytoplasmic domains of E-cadherin and desmosomal cadherin Dsg2, and the tumor suppressor APC protein. *Journal of Biochemistry*, *118*(5), 1077–1082. https://doi.org/10.1093/jb/118.5.1077

Page-McCaw, A., Ewald, A. J., & Werb, Z. (2007). Matrix metalloproteinases and the regulation of tissue remodelling. *Nature reviews. Molecular cell biology*, *8*(3), 221–233. https://doi.org/10.1038/nrm2125

Pothukuchi, P., Agliarulo, I., Pirozzi, M., Rizzo, R., Russo, D., Turacchio, G., Nüchel, J., Yang, J., Gehin, C., Capolupo, L., Hernandez-Corbacho, M. J., Biswas, A., Vanacore, G., Dathan, N., Nitta, T., Henklein, P., Thattai, M., Inokuchi, J., Hsu, V. W., …

Parashuraman, S. (2021). GRASP55 regulates intra-Golgi localization of glycosylation enzymes to control glycosphingolipid biosynthesis. *The EMBO Journal*, *40*(20), e107766. https://doi.org/10.15252/embj.2021107766

Provenzano, P. P., Inman, D. R., Eliceiri, K. W., Trier, S. M., & Keely, P. J. (2008). Contact Guidance Mediated Three-Dimensional Cell Migration is Regulated by Rho/ROCK-Dependent Matrix Reorganization. *Biophysical Journal*, *95*(11), 5374–5384. https://doi.org/10.1529/biophysj.108.133116

Qiang, L., Cao, H., Chen, J., Weller, S. G., Krueger, E. W., Zhang, L., Razidlo, G. L., & McNiven, M. A. (2019). Pancreatic tumor cell metastasis is restricted by MT1-MMP binding protein MTCBP-1. *The Journal of Cell Biology*, *218*(1), 317–332. https://doi.org/10.1083/jcb.201802032

Remacle, A. G., Chekanov, A. V., Golubkov, V. S., Savinov, A. Y., Rozanov, D. V., & Strongin, A. Y. (2006). O-glycosylation regulates autolysis of cellular membrane type-1 matrix metalloproteinase (MT1-MMP). *The Journal of Biological Chemistry*, *281*(25), 16897–16905. https://doi.org/10.1074/jbc.M600295200

Ries, C., Egea, V., Karow, M., Kolb, H., Jochum, M., & Neth, P. (2007). MMP-2, MT1-MMP, and TIMP-2 are essential for the invasive capacity of human mesenchymal stem cells: Differential regulation by inflammatory cytokines. *Blood*, *109*(9), 4055–4063. https://doi.org/10.1182/blood-2006-10-051060

Rizzo, S., Lodder, E. M., Verkerk, A. O., Wolswinkel, R., Beekman, L., Pilichou, K., Basso, C., Remme, C. A., Thiene, G., & Bezzina, C. R. (2012). Intercalated disc abnormalities, reduced Na+ current density, and conduction slowing in desmoglein-2 mutant mice prior to cardiomyopathic changes. *Cardiovascular Research*, *95*(4), 409–418. https://doi.org/10.1093/cvr/cvs219

Roghi, C., Jones, L., Gratian, M., English, W. R., & Murphy, G. (2010). Golgi reassembly stacking protein 55 interacts with membrane-type (MT) 1-matrix metalloprotease (MMP) and furin and plays a role in the activation of the MT1-MMP zymogen. *The FEBS Journal*, *277*(15), 3158–3175. https://doi.org/10.1111/j.1742-4658.2010.07723.x

Rohatgi, R., Ma, L., Miki, H., Lopez, M., Kirchhausen, T., Takenawa, T., & Kirschner, M. W. (1999). The interaction between N-WASP and the Arp2/3 complex links Cdc42-dependent signals to actin assembly. *Cell*, *97*(2), 221–231. https://doi.org/10.1016/s0092-8674(00)80732-1

Roche, J. (2018). The Epithelial-to-Mesenchymal Transition in Cancer. *Cancers*, *10*(2), 52. https://doi.org/10.3390/cancers10020052

Rösel, D., Brábek, J., Tolde, O., Mierke, C. T., Zitterbart, D. P., Raupach, C., Bicanová, K., Kollmannsberger, P., Panková, D., Vesely, P., Folk, P., & Fabry, B. (2008). Up-regulation of Rho/ROCK signaling in sarcoma cells drives invasion and increased generation of protrusive forces. *Molecular Cancer Research: MCR*, *6*(9), 1410–1420. https://doi.org/10.1158/1541-7786.MCR-07-2174

Rozanov, D. V., Deryugina, E. I., Ratnikov, B. I., Monosov, E. Z., Marchenko, G. N., Quigley, J. P., & Strongin, A. Y. (2001). Mutation analysis of membrane type-1 matrix metalloproteinase (MT1-MMP). The role of the cytoplasmic tail Cys(574), the active site Glu(240), and furin cleavage motifs in oligomerization, processing, and self-proteolysis of MT1-MMP expressed in breast carcinoma cells. *The Journal of Biological Chemistry*, *276*(28), 25705–25714. https://doi.org/10.1074/jbc.M007921200

Sakamoto, T., Niiya, D., & Seiki, M. (2011). Targeting the Warburg Effect That Arises in Tumor Cells Expressing Membrane Type-1 Matrix Metalloproteinase. *The Journal of Biological Chemistry*, *286*(16), 14691–14704. https://doi.org/10.1074/jbc.M110.188714

Samavarchi-Tehrani, P., Samson, R., & Gingras, A.-C. (2020). Proximity Dependent Biotinylation: Key Enzymes and Adaptation to Proteomics Approaches. *Molecular & Cellular Proteomics : MCP*, *19*(5), 757–773. https://doi.org/10.1074/mcp.R120.001941

Sato, H., Takino, T., Okada, Y., Cao, J., Shinagawa, A., Yamamoto, E., & Seiki, M. (1994). A matrix metalloproteinase expressed on the surface of invasive tumour cells. *Nature*, *370*(6484), 61–65. https://doi.org/10.1038/370061a0

Sato, T., Ovejero, M. del C., Hou, P., Heegaard, A.-M., Kumegawa, M., Tækker Foged, N., & Delaissé, J.-M. (1997). Identification of the membrane-type matrix metalloproteinase MT1-MMP in osteoclasts. *Journal of Cell Science*, *110*(5), 589–596. https://doi.org/10.1242/jcs.110.5.589

Seaman, M. N. J. (2021). The Retromer Complex: From Genesis to Revelations. *Trends in Biochemical Sciences*, *46*(7), 608–620. https://doi.org/10.1016/j.tibs.2020.12.009

Seiki, M. (2002). The cell surface: The stage for matrix metalloproteinase regulation of migration. *Current Opinion in Cell Biology*, *14*(5), 624–632. https://doi.org/10.1016/s0955-0674(02)00363-0

Shafraz, O., Rübsam, M., Stahley, S. N., Caldara, A. L., Kowalczyk, A. P., Niessen, C. M., & Sivasankar, S. (2018). E-cadherin binds to desmoglein to facilitate desmosome assembly. *eLife*, *7*, e37629. https://doi.org/10.7554/eLife.37629

Sharma, P., Parveen, S., Shah, L. V., Mukherjee, M., Kalaidzidis, Y., Kozielski, A. J., Rosato, R., Chang, J. C., & Datta, S. (2019). SNX27–retromer assembly recycles MT1-MMP to invadopodia and promotes breast cancer metastasis. *The Journal of Cell Biology*, *219*(1), e201812098. https://doi.org/10.1083/jcb.201812098

Sheetz, M. P., Felsenfeld, D. P., & Galbraith, C. G. (1998). Cell migration: Regulation of force on extracellular-matrix-integrin complexes. *Trends in Cell Biology*, *8*(2), 51–54. https://doi.org/10.1016/s0962-8924(98)80005-6

Shoykhet, M., Dervishi, O., Menauer, P., Hiermaier, M., Moztarzadeh, S., Osterloh, C., Ludwig, R. J., Williams, T., Gerull, B., Kääb, S., Clauss, S., Schüttler, D., Waschke, J., & Yeruva, S. (2023). EGFR inhibition leads to enhanced desmosome assembly and cardiomyocyte cohesion via ROCK activation. *JCI Insight*, *8*(6), e163763. https://doi.org/10.1172/jci.insight.163763

Schoumacher, M., Goldman, R. D., Louvard, D., & Vignjevic, D. M. (2010). Actin, microtubules, and vimentin intermediate filaments cooperate for elongation of invadopodia. *The Journal of Cell Biology*, *189*(3), 541–556. https://doi.org/10.1083/jcb.200909113

Schröder, H. M., Hoffmann, S. C., Hecker, M., Korff, T., & Ludwig, T. (2013). The tetraspanin network modulates MT1-MMP cell surface trafficking. *The International Journal of Biochemistry & Cell Biology*, *45*(6), 1133–1144. https://doi.org/10.1016/j.biocel.2013.02.020

Sigmund, A. M., Steinert, L. S., Egu, D. T., Bayerbach, F. C., Waschke, J., & Vielmuth, F. (2020). Dsg2 Upregulation as a Rescue Mechanism in Pemphigus. *Frontiers in Immunology*, *11*, 581370. https://doi.org/10.3389/fimmu.2020.581370

Sleeman, J., & Steeg, P. S. (2010). Cancer metastasis as a therapeutic target. *European Journal of Cancer*, *46*(7), 1177–1180. https://doi.org/10.1016/j.ejca.2010.02.039

Song, I.-W., Li, W.-R., Chen, L.-Y., Shen, L.-F., Liu, K.-M., Yen, J. J. Y., Chen, Y.-J., Chen, Y.-J., Kraus, V. B., Wu, J.-Y., Lee, M. T. M., & Chen, Y.-T. (2014). Palmitoyl Acyltransferase, Zdhhc13, Facilitates Bone Mass Acquisition by Regulating Postnatal Epiphyseal Development and Endochondral Ossification: A Mouse Model. *PLoS ONE*, *9*(3), e92194. https://doi.org/10.1371/journal.pone.0092194

Sounni, N. E., Roghi, C., Chabottaux, V., Janssen, M., Munaut, C., Maquoi, E., Galvez, B. G., Gilles, C., Frankenne, F., Murphy, G., Foidart, J.-M., & Noel, A. (2004). Up-regulation of vascular endothelial growth factor-A by active membrane-type 1 matrix metalloproteinase through activation of Src-tyrosine kinases. *The Journal of Biological Chemistry*, *279*(14), 13564–13574. https://doi.org/10.1074/jbc.M307688200

Stasiak, A. C., & Stehle, T. (2020). Human adenovirus binding to host cell receptors: A structural view. *Medical Microbiology and Immunology*, *209*(3), 325–333. https://doi.org/10.1007/s00430-019-00645-2

Stegemann, C., Didangelos, A., Barallobre-Barreiro, J., Langley, S. R., Mandal, K., Jahangiri, M., & Mayr, M. (2013). Proteomic Identification of Matrix Metalloproteinase Substrates in the Human Vasculature. *Circulation: Cardiovascular Genetics*, *6*(1), 106–117. https://doi.org/10.1161/CIRCGENETICS.112.964452

Strouhalova, K., Tolde, O., Rosel, D., & Brábek, J. (2023). Cytoplasmic Tail of MT1-MMP: A Hub of MT1-MMP Regulation and Function. *International Journal of Molecular Sciences*, *24*(6), 5068. https://doi.org/10.3390/ijms24065068

Suárez, H., López-Martín, S., Toribio, V., Zamai, M., Hernández-Riquer, M. V., Genís, L., Arroyo, A. G., & Yáñez-Mó, M. (2020). Regulation of MT1-MMP Activity through Its Association with ERMs. *Cells*, *9*(2), 348. https://doi.org/10.3390/cells9020348

Suetsugu, S., Miki, H., Yamaguchi, H., Obinata, T., & Takenawa, T. (2001). Enhancement of branching efficiency by the actin filament-binding activity of N-WASP/WAVE2. *Journal of Cell Science*, *114*(Pt 24), 4533–4542.

Sugiyama, N., Gucciardo, E., Tatti, O., Varjosalo, M., Hyytiäinen, M., Gstaiger, M., & Lehti, K. (2013). EphA2 cleavage by MT1-MMP triggers single cancer cell invasion via homotypic cell repulsion. *The Journal of Cell Biology*, *201*(3), 467–484. https://doi.org/10.1083/jcb.201205176

Sun, R., Ma, C., Wang, W., & Yang, S. (2020). Upregulation of desmoglein 2 and its clinical value in lung adenocarcinoma: A comprehensive analysis by multiple bioinformatics methods. *PeerJ*, *8*, e8420. https://doi.org/10.7717/peerj.8420

Takino, T., Tsuge, H., Ozawa, T., & Sato, H. (2010). MT1-MMP promotes cell growth and ERK activation through c-Src and paxillin in three-dimensional collagen matrix. *Biochemical and Biophysical Research Communications*, *396*(4), 1042–1047. https://doi.org/10.1016/j.bbrc.2010.05.059

Tam, E. M., Morrison, C. J., Wu, Y. I., Stack, M. S., & Overall, C. M. (2004). Membrane protease proteomics: Isotope-coded affinity tag MS identification of undescribed MT1–matrix metalloproteinase substrates. *Proceedings of the National Academy of Sciences*, *101*(18), 6917–6922. https://doi.org/10.1073/pnas.0305862101

Terawaki, S.-I., Kitano, K., Aoyama, M., Mori, T., & Hakoshima, T. (2015). MT1-MMP recognition by ERM proteins and its implication in CD44 shedding. *Genes to Cells: Devoted to Molecular & Cellular Mechanisms*, *20*(10), 847–859. https://doi.org/10.1111/gtc.12276

Thangaraj, S. V., Shyamsundar, V., Krishnamurthy, A., & Ramshankar, V. (2021). Deregulation of extracellular matrix modeling with molecular prognostic markers revealed by transcriptome sequencing and validations in Oral Tongue squamous cell carcinoma. *Scientific Reports*, *11*(1), 250. https://doi.org/10.1038/s41598-020-78624-4

Tochowicz, A., Goettig, P., Evans, R., Visse, R., Shitomi, Y., Palmisano, R., Ito, N., Richter, K., Maskos, K., Franke, D., Svergun, D., Nagase, H., Bode, W., & Itoh, Y. (2010). The Dimer Interface of the Membrane Type 1 Matrix Metalloproteinase Hemopexin Domain. *Journal of Biological Chemistry*, *286*(9), 7587–7600. https://doi.org/10.1074/jbc.M110.178434

Tomari, T., Koshikawa, N., Uematsu, T., Shinkawa, T., Hoshino, D., Egawa, N., Isobe, T., & Seiki, M. (2009). High throughput analysis of proteins associating with a proinvasive MT1-MMP in human malignant melanoma A375 cells. *Cancer Science*, *100*(7), 1284–1290. https://doi.org/10.1111/j.1349-7006.2009.01173.x

Uekita, T., Gotoh, I., Kinoshita, T., Itoh, Y., Sato, H., Shiomi, T., Okada, Y., & Seiki, M. (2004). Membrane-type 1 matrix metalloproteinase cytoplasmic tail-binding protein-1 is a new member of the Cupin superfamily. A possible multifunctional protein acting as an invasion suppressor down-regulated in tumors. *The Journal of Biological Chemistry*, *279*(13), 12734–12743. https://doi.org/10.1074/jbc.M309957200

Uekita, T., Itoh, Y., Yana, I., Ohno, H., & Seiki, M. (2001). Cytoplasmic tail–dependent internalization of membrane-type 1 matrix metalloproteinase is important for its invasion-promoting activity. *The Journal of Cell Biology*, *155*(7), 1345–1356. https://doi.org/10.1083/jcb.200108112

Ungewiß, H., Rötzer, V., Meir, M., Fey, C., Diefenbacher, M., Schlegel, N., & Waschke, J. (2018). Dsg2 via Src-mediated transactivation shapes EGFR signaling towards cell

adhesion. *Cellular and Molecular Life Sciences: CMLS*, *75*(22), 4251–4268. https://doi.org/10.1007/s00018-018-2869-x

Vallverdú-Prats, M., Carreras, D., Pérez, G. J., Campuzano, O., Brugada, R., & Alcalde, M. (2023). Alterations in Calcium Handling Are a Common Feature in an Arrhythmogenic Cardiomyopathy Cell Model Triggered by Desmosome Genes Loss. *International Journal of Molecular Sciences*, *24*(3), 2109. https://doi.org/10.3390/ijms24032109

Van Lint, P., & Libert, C. (2007). Chemokine and cytokine processing by matrix metalloproteinases and its effect on leukocyte migration and inflammation. *Journal of Leukocyte Biology*, *82*(6), 1375–1381. https://doi.org/10.1189/jlb.0607338

Vite, A., Gandjbakhch, E., Hery, T., Fressart, V., Gary, F., Simon, F., Varnous, S., Hidden Lucet, F., Charron, P., & Villard, E. (2020). Desmoglein-2 mutations in propeptide cleavage-site causes arrhythmogenic right ventricular cardiomyopathy/dysplasia by impairing extracellular 1-dependent desmosomal interactions upon cellular stress. *Europace: European Pacing, Arrhythmias, and Cardiac Electrophysiology: Journal of the Working Groups on Cardiac Pacing, Arrhythmias, and Cardiac Cellular Electrophysiology of the European Society of Cardiology*, *22*(2), 320–329. https://doi.org/10.1093/europace/euz329

Wahl, J. K., Nieset, J. E., Sacco-Bubulya, P. A., Sadler, T. M., Johnson, K. R., & Wheelock, M. J. (2000). The amino- and carboxyl-terminal tails of β-catenin reduce its affinity for desmoglein 2. *Journal of Cell Science*, *113*(10), 1737–1745. https://doi.org/10.1242/jcs.113.10.1737

Wang, A., Li, N., Zhang, N., Liu, J., Yang, T., Li, D., Li, C., Li, R., Jiang, T., & Xia, C. (2024a). Desmoglein-2 Affects Vascular Function in Moyamoya Disease by Interacting with MMP-9 and Influencing PI3K Signaling. *Molecular Neurobiology*, *61*(9), 6539–6552. https://doi.org/10.1007/s12035-024-04010-0

Wang, A., Li, N., Zhang, N., Liu, J., Yang, T., Li, D., Li, C., Li, R., Jiang, T., & Xia, C. (2024b). Desmoglein-2 Affects Vascular Function in Moyamoya Disease by Interacting with MMP-9 and Influencing PI3K Signaling. *Molecular Neurobiology*, *61*(9), 6539–6552. https://doi.org/10.1007/s12035-024-04010-0

Wang, S., & Chang, R. (2014). An emerging treatment option for glaucoma: Rho kinase inhibitors. *Clinical ophthalmology (Auckland, N.Z.)*, *8*, 883–890. https://doi.org/10.2147/OPTH.S41000

Wang, Y., & McNiven, M. A. (2012). Invasive matrix degradation at focal adhesions occurs via protease recruitment by a FAK–p130Cas complex. *The Journal of Cell Biology*, *196*(3), 375–385. https://doi.org/10.1083/jcb.201105153

Wei, Y., Lukashev, M., Simon, D. I., Bodary, S. C., Rosenberg, S., Doyle, M. V., & Chapman, H. A. (1996). Regulation of Integrin Function by the Urokinase Receptor. *Science*. https://doi.org/10.1126/science.273.5281.1551

Williams, K. C., & Coppolino, M. G. (2011). Phosphorylation of Membrane Type 1-Matrix Metalloproteinase (MT1-MMP) and Its Vesicle-associated Membrane Protein 7 (VAMP7)-dependent Trafficking Facilitate Cell Invasion and Migration. *The Journal of Biological Chemistry*, *286*(50), 43405–43416. https://doi.org/10.1074/jbc.M111.297069

Wolf, K., Mazo, I., Leung, H., Engelke, K., von Andrian, U. H., Deryugina, E. I., Strongin, A. Y., Bröcker, E.-B., & Friedl, P. (2003). Compensation mechanism in tumor cell migration. *The Journal of Cell Biology*, *160*(2), 267–277. https://doi.org/10.1083/jcb.200209006

Woodley, K. T., & Collins, M. O. (2019). S-acylated Golga7b stabilises DHHC5 at the plasma membrane to regulate cell adhesion. *EMBO Reports*, *20*(10), e47472. https://doi.org/10.15252/embr.201847472

Wu, Y. I., Munshi, H. G., Sen, R., Snipas, S. J., Salvesen, G. S., Fridman, R., & Stack, M. S. (2004). Glycosylation Broadens the Substrate Profile of Membrane Type 1 Matrix Metalloproteinase *. *Journal of Biological Chemistry*, *279*(9), 8278–8289. https://doi.org/10.1074/jbc.M311870200

Wyckoff, J. B., Pinner, S. E., Gschmeissner, S., Condeelis, J. S., & Sahai, E. (2006). ROCK- and myosin-dependent matrix deformation enables protease-independent tumor-cell invasion in vivo. *Current Biology: CB*, *16*(15), 1515–1523. https://doi.org/10.1016/j.cub.2006.05.065

Xiang, Y., Zhang, X., Nix, D. B., Katoh, T., Aoki, K., Tiemeyer, M., & Wang, Y. (2013). Regulation of protein glycosylation and sorting by the Golgi matrix proteins GRASP55/65. *Nature communications*, *4*, 1659. https://doi.org/10.1038/ncomms2669

Yana, I., & Seiki, M. (2002). MT-MMPs play pivotal roles in cancer dissemination. *Clinical & Experimental Metastasis*, *19*(3), 209–215. https://doi.org/10.1023/A:1015527220537

Yang, J., Kasberg, W. C., Celo, A., Liang, Z., Quispe, K., & Stack, M. S. (2017). Post-translational modification of the membrane type 1 matrix metalloproteinase (MT1-

MMP) cytoplasmic tail impacts ovarian cancer multicellular aggregate dynamics. *The Journal of Biological Chemistry*, *292*(32), 13111–13121. https://doi.org/10.1074/jbc.M117.800904

Yang, T., Jia, L., Bian, S., Chang, X., Zhang, Q., Tang, Q., Zhu, J., Yang, Z., & Feng, Z. (2022). TROP2 Down-regulated DSG2 to Promote Gastric Cancer Cell Invasion and Migration by EGFR/AKT and DSG2/PG/β-Catenin Pathways. *Current Cancer Drug Targets*, *22*(8), 691–702. https://doi.org/10.2174/1568009622666220407111013

Yu, X., Zech, T., McDonald, L., Gonzalez, E. G., Li, A., Macpherson, I., Schwarz, J. P., Spence, H., Futó, K., Timpson, P., Nixon, C., Ma, Y., Anton, I. M., Visegrády, B., Insall, R. H., Oien, K., Blyth, K., Norman, J. C., & Machesky, L. M. (2012). N-WASP coordinates the delivery and F-actin–mediated capture of MT1-MMP at invasive pseudopods. *The Journal of Cell Biology*, *199*(3), 527–544. https://doi.org/10.1083/jcb.201203025

Yumura, S., Mori, H., & Fukui, Y. (1984). Localization of actin and myosin for the study of ameboid movement in Dictyostelium using improved immunofluorescence. *The Journal of Cell Biology*, *99*(3), 894–899.

Zhang, G., Chen, Z., Wang, Y., Huang, A., Nie, F., Gao, L., Wang, Y., & Ren, F. (2024). Up-regulated DSG2 promotes tumor growth and reduces immune infiltration in cervical cancer. *Pathology, Research and Practice*, *262*, 155554. https://doi.org/10.1016/j.prp.2024.155554

Zhang, X. A., Bontrager, A. L., & Hemler, M. E. (2001). Transmembrane-4 superfamily proteins associate with activated protein kinase C (PKC) and link PKC to specific beta(1) integrins. *The Journal of Biological Chemistry*, *276*(27), 25005–25013. https://doi.org/10.1074/jbc.M102156200

8. Attachments

Attachment 1. Amino acid sequence of MT1-MMP.

```
  1 MSPAPRPPRC LLLPLLTLGT ALASLGSAQS SSFSPEAWLQ QYGYLPPGDL RTHTQRSPQS
 61 LSAAIAAMQK FYGLQVTGKA DADTMKAMRR PRCGVPDKFG AEIKANVRRK RYAIQGLKWQ
121 HNEITFCIQN YTPKVGEYAT YEAIRKAFRV WESATPLRFR EVPYAYIREG HEKQADIMIF
181 FAEGFHGDST PFDGEGGFLA HAYFPGPNIG GDTHFDSAEP WTVRNEDLNG NDIFLVAVHE
241 LGHALGLEHS SDPSAIMAPF YQWMDTENFV LPDDDRRGIQ QLYGGESGFP TKMPPQPRTT
301 SRPSVPDKPK NPTYGPNICD GNFDTVAMLR GEMFVFKERW FWRVRNNQVM DGYPMPIGQF
361 WRGLPASINT AYERKDGKFV FFKGDKHWVF DEASLEPGYP KHIKELGRGL PTDKIDAALF
421 WMPNGKTYFF RGNKYYRFNE ELRAVDSEYP KNIKVWEGIP ESPRGSFMGS DEVFTYFYKG
481 NKYWKFNNQK LKVEPGYPKS ALRDWMGCPS GGRPDEGTEE ETEVIIIEVD EEGGGAVSAA
541 AVVLPVLLLL LVLAVGLAVF FFRRHGTPRR LLYCQRSLLD KV
```

Attachment 2. Primers sequences.

Name	Purpose	Sequence
Avi_f	AviTag insertion between Ser^{577} and Leu^{578} of MT1-MMP	5‘ ATCTTTGAAGCGCAGAAAATTG AATGGCATGAACTGCTGGACAAG GTTTGACCGGTCGCC 3‘
Avi_r	AviTag insertion; Asp^{582}→Val mutation reversion; stop codon insertion	5‘ AATTTTCTGCGCTTCAAAGATA TCGTTCAGGCCGGAACGCTGGCA GTAGAGCA 3‘
BirA_IRES_f	PCR of insert (BirA) for cloning into IRES vector	5‘ CGGAATTCATGAAGGATAACA C 3‘
BirA_IRES_r		5‘ CGGGATCCTCAGTGGTGGTGGT GGTGGTGCTCG 3‘
FFSS-L_fwd (46)	inserting FFSS into MT1-MMP’s Linker region	5‘AGGTGGACGAGGAGGGCGGCG ACTACAAGGACGACGATG 3‘
FFSS_rev (47)	inserting FFSS into any MT1-MMP’s region	5‘ TCCTTTCTCGAACTGCGGGTGG CTCCAGCTTC 3‘
pcDNA3-MT1-LC_fwd (48)	inserting MT1-MMP’s C-terminal region after FFSS in Linker	5‘ACCCGCAGTTCGAGAAAGGAGG GGCGGTGAGCGCGGCTGC 3‘
pcDNA3-MT1-LC_rev (49)	inserting MT1-MMP’s C-terminal region after FFSS in Linker	5‘ GATCTAGAGTCGCGGCCGCTTC AGACCTTGTCCAGCAGGGAACGC TG 3‘
FFSS-H_fwd (50)	inserting FFSS into MT1-MMP’s Hinge region	5‘ AACCCAGGACTACCTCCCG GGACTACAAGGACGACGATG 3‘
pcDNA3-MT1-HC_fwd (52)	inserting MT1-MMP’s C-terminal region after FFSS in Hinge	5‘ ACCCGCAGTTCGAGAAAGG ACCTTCTGTTCCTGATAAACC 3‘
pcDNA3-MT1-HC_rev (53)	inserting MT1-MMP’s C-terminal region after FFSS in Hinge	5‘ GATCTAGAGTCGCGGCCGCTTC AGACCTTGTCCAGCAGGGAAC 3‘
pcDNA3-MT1-LC-dCP_fwd (54)	inserting MT1-MMP’s C-terminal region with dCP mutation after FFSS in Linker	5‘ ACCCGCAGTTCGAGAAAGGAG GGGCGGTGAGCGCGGCTG 3‘
pcDNA3-MT1-LC-dCP_rev (55)	inserting MT1-MMP’s C-terminal region with dCP mutation after FFSS in Linker	5‘ GATCTAGAGTCGCGGCCGCTTC AGAAGAAGAAGACTGCAAGGCCC ACCGC 3‘
pcDNA3-MT1-HC-dCP_fwd (56)	inserting MT1-MMP’s C-terminal region with dCP mutation after FFSS in Hinge	5‘ ACCCGCAGTTCGAGAAAGGAC CTTCTGTTCCTGATAAAC 3‘
pcDNA3-MT1-HC-dCP_rev (57)	inserting MT1-MMP’s C-terminal region with dCP mutation after FFSS in Hinge	5‘ GATCTAGAGTCGCGGCCGCTTC AGAAGAAGAAGACTGC 3‘
Sequencing primers		
tightseq5	pN1_MT1-MMP-Avi, pIRESpuro3_BirA	5‘ GTAGGCGTGTACGGTGGGA 3‘
MMP14r	pN1_MT1-MMP-Avi	5‘ ACCCAATGCTTGTCTCCTTTG 3‘
EGFPup	pN1_MT1-MMP-Avi, DSG2-FLAG-EGFP	5‘ GGACACGCTGAACTTGTGG 3‘
IP3seqR	pIRESpuro3_BirA	5‘ AGTACTCACCCCAACAGCT 3‘
DSG-2_fw1	DSG2-FLAG-EGFP, DSG2-mCherry	5‘ GTCTGTTGAAGAGTTGAGTGC 3‘
DSG-2_rv	DSG2-FLAG-EGFP, DSG2-mCherry	5‘ ATAAGCAGGCTCCAGAGATACG 3‘
DSG-2_fw2	DSG2-FLAG-EGFP, DSG2-mCherry	5‘ TTTGATGAGGACACTGGACTAC 3‘
DSG-2_fw3	DSG2-FLAG-EGFP, DSG2-mCherry	5‘ TCCGTCATTGACAAACCACC 3‘

DSG-2_fw4	DSG2-FLAG-EGFP, DSG2-mCherry	5‘ ACCACTGAAACCACGAAGAC 3‘
EGFP-C	DSG2-FLAG-EGFP	5‘ GTCCTGCTGGAGTTCGTG 3‘
EGFP-rev	DSG2-FLAG-EGFP	5‘ CTACAAATGTGGTATGGCTG 3‘
mCherry_fw1	DSG2-mCherry	5‘ ACCAGAGTCACCAAGCATAG 3‘
mCherry-UP	DSG2-mCherry	5‘ TCTCGAACTCGTGGCCGTT 3‘
mCherry-C	DSG2-mCherry	5‘ CACCATCGTGGAACAGTACG 3‘

Attachment 3. Gelatine degradation assays outcomes. The degraded gelatine area was measured per each particular cell and compared with the area occupied by that cell using ImageJ software. 32 cells were measured per each variant (*wild* type HT1080 cells, which served as a positive control; HT1080 MMP-14 KO cells (clone F3) as a negative control; and 4 variants of HT1080 MMP-14 KO (F3) cells, each transfected with a corresponding MT1-MMP-FFSS construct), the experiment was repeated thrice. The table represents data combined from three independent biological replicates, where each value is a calculated fraction of degraded area versus the area occupied by a cell in %. Each column contains data from one cell variant, each row represents one particular measurement (measurement of one cell).

	HT1080 (posit. ctrl)	HT1080 F3 (MMP KO, neg. ctrl)	HT1080 F3 L-WT	HT1080 F3 L-C/A	HT1080 F3 L-LLY	HT1080 F3 L-dCP
1st replicate	0,6	0,108	8,866	1,197	4,616	0,486
	0,263	0,017	3,554	0,714	6,857	1,1
	0,565	0,098	2,278	1,341	7,207	0,226
	0,64	0,007	0,525	1,044	0,565	0,618
	0,762	0,178	1,104	1,336	1,873	7,894
	0,504	0,08	4,236	3,289	1,532	0,734
	0,89	0,174	4,365	4,885	3,884	0,229
	0,19	0,519	11,369	1,968	0,467	3,485
	0,433	0,564	1,888	2,053	0,079	0,162
	0,943	1,418	1,372	1,769	3,97	7,785
	0,459	0,033	0,587	2,456	4,73	0,174
	0,313	0,017	3,254	4,23	7,348	5,167
	1,639	0,094	6,493	0,633	3,545	3,199
	0,479	1,113	1,734	1,783	4,311	3,161
	0,288	0,159	0,911	2,766	3,346	6,487
	0,293	0,16	3,848	2,516	5,099	0,361
	0,151	0,008	1,095	3,774	1,392	2,249
	1,548	0,118	1,032	2,3	4,896	0,982
	1,606	0,643	9,808	0,671	0,968	0,185
	1,463	0,304	6,506	7,39	3,582	6,736
	2,185	0,043	4,741	3,565	1,461	1,178
	4,552	0,061	1,816	0,161	1,559	0,34
	4,186	0,1	10,48	1,89	8,869	3,836
	0,567	0,044	1,099	0,405	2,882	1,222
	0,576	1,409	1,037	9,748	4,651	1,214
	0,48	0,344	1,775	1,411	1,189	3,959
	6,26	0,115	5,863	3,315	3,396	3,406
	0,701	0,025	2,649	6,117	2,442	0,881
	0,43	0,199	4,377	0,411	2,328	0,183
	0,577	0,204	2,177	1,625	2,942	0,578
	1,227	0,177	0,828	1,428	3,599	1,201
	0,355	0,693	1,515	0,979	3,344	0,178
2nd replicate	0,728	0,856	0,325	4,614	0,914	1,072
	0,41	0,905	3,482	1,59	4,13	0,707
	1,622	0,557	4,833	0,213	0,88	4,632
	0,719	0,653	0,799	2,098	1,119	1,621
	0,686	2,517	0,204	0,57	2,73	0,475
	0,819	0,916	6,163	4,13	3,033	1,126
	0,563	1,336	0,884	1,448	5,715	0,323
	0,796	0,648	1,08	1,603	0,181	6,337
	1,07	1,541	1,749	0,364	3,741	3,178
	0,853	1,829	3,811	1,206	3,132	0,918

	0,497	0,2	1,106	1,959	0,513	0,607
	0,739	0,638	0,462	2,676	5,253	0,344
	1,574	0,499	0,763	0,676	0,263	0,209
	1,61	0,267	3,257	0,926	4,799	0,733
	0,529	0,884	2,549	0,365	0,23	0,139
	0,239	0,59	0,507	4,107	0,873	2,986
	0,937	3,894	0,749	4,96	6,926	1,494
	0,67	0,601	0,517	2,716	0,427	0,434
	1,668	2,6	0,342	1,432	0,347	0,209
	0,221	0,818	0,879	1,498	4,513	0,36
	0,966	2,166	12,809	0,274	8,938	24,726
	1,449	0,35	0,455	0,239	2,295	10,732
	1,159	0,775	1,647	21,381	0,197	9,927
	2,102	0,771	0,7	3,355	0,076	0,23
	2,11	0,28	0,662	2,982	0,795	0,911
	2,57	0,337	0,561	1,495	2,709	0,499
	2,435	0,266	0,681	0,756	0,153	3,105
	1,337	0,65	1,478	0,672	0,193	0,854
	0,665	0,982	2,601	0,636	1,179	1,598
	0,176	1,381	0,811	0,225	1,433	3,405
	0,308	0,389	2,895	1,058	2,88	0,145
	0,362	0,209	0,937	0,846	0,082	0,769
3rd replicate	3,054	0,81	1,218	1,532	0,628	2,814
	2,008	0,277	2,578	0,533	1,506	1,439
	0,669	0,698	0,737	1,387	0,545	1,124
	0,276	0,267	2,763	0,866	1,814	1,163
	1,689	0,277	8,431	1,719	0,394	2,156
	0,664	0,44	4,709	4,183	0,512	7,508
	3,755	0,195	1,199	2,19	8,787	7,042
	0,408	0,088	1,854	0,912	2,391	0,61
	0,533	0,245	1,079	1,433	7,402	2,176
	2,119	0,499	0,16	0,266	0,481	0,972
	3,138	0,231	0,038	0,979	1,896	4,681
	2,18	0,347	2,235	0,991	4,356	2,337
	1,11	0,877	0,361	0,538	2,276	2,43
	0,678	0,731	0,379	1,531	0,528	4,746
	1,041	0,274	1,562	1,382	4,735	2,176
	1,474	0,259	1,714	0,791	3,877	0,086
	0,644	0,315	0,388	0,564	5,183	3,06
	1,183	0,634	0,371	10,561	0,216	1,191
	1,44	0,098	1,233	0,194	1,702	1,634
	0,467	0,267	3,782	1,088	0,254	0,306
	1,341	0,132	0,644	0,344	2,482	5,904
	3,757	0,099	0,359	0,156	4,366	2,527
	2,352	0,376	2,263	0,333	2,901	0,788
	4,127	0,507	0,081	0,386	0,425	4,478
	1,53	0,394	0,226	0,224	0,178	0,862
	0,787	0,311	1,713	0,603	0,58	0,823
	0,846	0,624	0,651	3,801	0,287	0,519
	0,503	0,25	6,575	0,56	10,052	6,46
	0,468	0,252	1,567	0,321	0,047	0,345
	0,528	0,108	7,264	1,926	3,674	0,416
	0,602	0,261	1,662	0,871	2,802	1,997
	0,611	0,14	0,305	0,599	0,349	2,022

Attachment 4. Amino acid sequence of DSG2.

```
   1 MARSPGRAYA LLLLLICFNV GSGLHLQVLS TRNENKLLPK HPHLVRQKRA WITAPVALRE
  61 GEDLSKKNPI AKIHSDLAEE RGLKITYKYT GKGITEPPFG IFVFNKDTGE LNVTSILDRE
 121 ETPFFLLTGY ALDARGNNVE KPLELRIKVL DINDNEPVFT QDVFVGSVEE LSAAHTLVMK
 181 INATDADEPN TLNSKISYRI VSLEPAYPPV FYLNKDTGEI YTTSVTLDRE EHSSYTLTVE
 241 ARDGNGEVTD KPVKQAQVQI RILDVNDNIP VVENKVLEGM VEENQVNVEV TRIKVFDADE
 301 IGSDNWLANF TFASGNEGGY FHIETDAQTN EGIVTLIKEV DYEEMKNLDF SVIVANKAAF
 361 HKSIRSKYKP TPIPIKVKVK NVKEGIHFKS SVISIYVSES MDRSSKGQII GNFQAFDEDT
 421 GLPAHARYVK LEDRDNWISV DSVTSEIKLA KLPDFESRYV QNGTYTVKIV AISEDYPRKT
 481 ITGTVLINVE DINDNCPTLI EPVQTICHDA EYVNVTAEDL DGHPNSGPFS FSVIDKPPGM
 541 AEKWKIARQE STSVLLQQSE KKLGRSEIQF LISDNQGFSC PEKQVLTLTV CECLHGSGCR
 601 EAQHDSYVGL GPAAIALMIL AFLLLLLVPL LLLMCHCGKG AKGFTPIPGT IEMLHPWNNE
 661 GAPPEDKVVP SFLPVDQGGS LVGRNGVGGM AKEATMKGSS SASIVKGQHE MSEMDGRWEE
 721 HRSLLSGRAT QFTGATGAIM TTETTKTARA TGASRDMAGA QAAAVALNEE FLRNYFTDKA
 781 ASYTEEDENH TAKDCLLVYS QEETESLNAS IGCCSFIEGE LDDRFLDDLG LKFKTLAEVC
 841 LGQKIDINKE IEQRQKPATE TSMNTASHSL CEQTMVNSEN TYSSGSSFPV PKSLQEANAE
 901 KVTQEIVTER SVSSRQAQKV ATPLPDPMAS RNVIATETSY VTGSTMPPTT VILGPSQPQS
 961 LIVTERVYAP ASTLVDQPYA NEGTVVVTER VIQPHGGGSN PLEGTQHLQD VPYVMVRERE
1021 SFLAPSSGVQ PTLAMPNIAV GQNVTVTERV LAPASTLQSS YQIPTENSMT ARNTTVSGAG
1081 VPGPLPDFGL EESGHSNSTI TTSSTRVTKH STVQHSYS
```

Attachment 5. In silico identification of MT1-MMP protease-specific substrate cleavage sites in DSG2 sequence. The table was generated by Procleave software. "Position" states the exact amino acid position where the cleavage may occur; "N-" and "C-fragment" are the potential fragments resulting from such cleavage; "Score" represents the probability of cleavage in this exact site. Because catalytic domain of MT1-MMP is localized in the extracellular space, only residues 50-609, which comprise the extracellular part of DSG2, are considered. Those extracellular residues of DSG2 with probability of cleavage higher than 50% are highlighted in bright yellow, while those of probability 20-50% are in light yellow. Only scores > 0.4 are shown.

Rank	Position	P4-P4' Site	N-fragment	C-fragment	Score	Family
1	961	QPQS†LIVT	112.67 kDa	18.10 kDa	0,679	M10.014
2	615	GPAA†IALM	72.54 kDa	58.24 kDa	0,607	M10.014
3	171	SVEE†LSAA	20.44 kDa	110.34 kDa	0,567	M10.014
4	375	TPIP†IKVK	44.25 kDa	86.52 kDa	0,549	M10.014
5	192	EPNT†LNSK	22.63 kDa	108.14 kDa	0,547	M10.014
6	831	DDLG†LKFK	98.16 kDa	32.61 kDa	0,544	M10.014
7	29	HLQV†LSTR	3.34 kDa	127.44 kDa	0,529	M10.014
8	58	APVA†LREG	6.69 kDa	124.08 kDa	0,514	M10.014
9	894	VPKS†LQEA	105.34 kDa	25.44 kDa	0,512	M10.014
10	177	AAHT†LVMK	21.02 kDa	109.75 kDa	0,511	M10.014
11	280	VLEG†MVEE	32.97 kDa	97.81 kDa	0,503	M10.014
12	126	TPFF†LLTG	15.08 kDa	115.69 kDa	0,492	M10.014
13	143	VEKP†LELR	17.12 kDa	113.65 kDa	0,492	M10.014
14	353	DFSV†IVAN	41.80 kDa	88.97 kDa	0,481	M10.014
15	101	PPFG†IFVF	12.05 kDa	118.72 kDa	0,481	M10.014
16	1090	PDFG†LEES	127.52 kDa	3.25 kDa	0,479	M10.014
17	158	DNEP†VFTQ	18.89 kDa	111.89 kDa	0,467	M10.014
18	145	KPLE†LRIK	17.37 kDa	113.41 kDa	0,459	M10.014
19	870	ASHS†LCEQ	102.65 kDa	28.13 kDa	0,454	M10.014
20	333	TNEG†IVTL	39.44 kDa	91.34 kDa	0,453	M10.014
21	271	DNIP†VVEN	31.88 kDa	98.89 kDa	0,444	M10.014
22	377	IPIK†VKVK	44.49 kDa	86.28 kDa	0,442	M10.014
23	906	VTQE†IVTE	106.68 kDa	24.10 kDa	0,441	M10.014
24	24	VGSG†LHLQ	2.75 kDa	128.03 kDa	0,439	M10.014
25	1015	VPYV†MVRE	119.05 kDa	11.73 kDa	0,435	M10.014
26	1057	PAST†LQSS	123.68 kDa	7.09 kDa	0,432	M10.014
27	928	LPDP†MASR	109.04 kDa	21.74 kDa	0,427	M10.014
28	422	EDTG†LPAH	49.91 kDa	80.86 kDa	0,427	M10.014
29	213	PVFY†LNKD	25.07 kDa	105.70 kDa	0,425	M10.014
30	237	SSYT†LTVE	27.93 kDa	102.85 kDa	0,424	M10.014
31	673	VPSF†LPVD	79.38 kDa	51.40 kDa	0,421	M10.014
32	775	FLRN†YFTD	91.53 kDa	39.24 kDa	0,419	M10.014
33	654	TIEM†LHPW	77.15 kDa	53.63 kDa	0,418	M10.014
34	44	KHPH†LVRQ	5.10 kDa	125.67 kDa	0,416	M10.014
35	1085	VPGP†LPDF	126.88 kDa	3.90 kDa	0,411	M10.014
36	211	YPPV†FYLN	24.76 kDa	106.01 kDa	0,406	M10.014
37	442	ISVD†SVTS	52.29 kDa	78.49 kDa	0,402	M10.014
38	503	LIEP†VQTI	59.31 kDa	71.46 kDa	0,402	M10.014

Attachment 6. In silico identification of MMP-2 protease-specific substrate cleavage sites in DSG2 sequence. The table was generated by Procleave software. "Position" states the exact amino acid position where the cleavage may occur; "N-" and "C-fragment" are the potential fragments resulting from such cleavage; "Score" represents the probability of cleavage in this exact site. Because catalytic domain of MT1-MMP is localized in the extracellular space, only residues 50-609, which comprise the extracellular part of DSG2, are considered. Those extracellular residues of DSG2 with probability of cleavage higher than 50% are highlighted in bright yellow, while those of probability 20-50% are in light yellow. Only scores > 0.4 are shown.

Rank	Position	P4-P4' Site	N-fragment	C-fragment	Score	Family
1	961	QPQS†LIVT	112.67 kDa	18.10 kDa	0,995	M10.003
2	101	PPFG†IFVF	12.05 kDa	118.72 kDa	0,99	M10.003
3	894	VPKS†LQEA	105.34 kDa	25.44 kDa	0,984	M10.003
4	126	TPFF†LLTG	15.08 kDa	115.69 kDa	0,981	M10.003
5	192	EPNT†LNSK	22.63 kDa	108.14 kDa	0,961	M10.003
6	73	PIAK†IHSD	8.49 kDa	122.29 kDa	0,953	M10.003
7	571	EIQF†LISD	67.34 kDa	63.43 kDa	0,948	M10.003
8	615	GPAA†IALM	72.54 kDa	58.24 kDa	0,939	M10.003
9	52	KRAW†ITAP	6.14 kDa	124.64 kDa	0,927	M10.003
10	58	APVA†LREG	6.69 kDa	124.08 kDa	0,923	M10.003
11	724	EHRS†LLSG	85.77 kDa	45.00 kDa	0,916	M10.003
12	619	IALM†ILAF	72.97 kDa	57.81 kDa	0,912	M10.003
13	1057	PAST†LQSS	123.68 kDa	7.09 kDa	0,907	M10.003
14	974	PAST†LVDQ	114.07 kDa	16.70 kDa	0,907	M10.003
15	673	VPSF†LPVD	79.38 kDa	51.40 kDa	0,903	M10.003
16	413	IIGN†FQAF	48.78 kDa	81.99 kDa	0,898	M10.003
17	531	GPFS†FSVI	62.54 kDa	68.23 kDa	0,891	M10.003
18	375	TPIP†IKVK	44.25 kDa	86.52 kDa	0,86	M10.003
19	111	DTGE†LNVT	13.32 kDa	117.46 kDa	0,86	M10.003
20	171	SVEE†LSAA	20.44 kDa	110.34 kDa	0,834	M10.003
21	973	APAS†TLVD	113.97 kDa	16.80 kDa	0,831	M10.003
22	409	SKGQ†IIGN	48.27 kDa	82.50 kDa	0,801	M10.003
23	651	IPGT†IEML	76.77 kDa	54.00 kDa	0,793	M10.003
24	77	IHSD†LAEE	8.94 kDa	121.84 kDa	0,792	M10.003
25	681	QGGS†LVGR	80.36 kDa	50.41 kDa	0,788	M10.003
26	310	WLAN†FTFA	36.50 kDa	94.28 kDa	0,784	M10.003
27	1085	VPGP†LPDF	126.88 kDa	3.90 kDa	0,758	M10.003
28	704	SSAS†IVKG	83.12 kDa	47.66 kDa	0,744	M10.003
29	775	FLRN†YFTD	91.53 kDa	39.24 kDa	0,741	M10.003
30	594	VCEC†LHGS	69.97 kDa	60.81 kDa	0,73	M10.003
31	11	RAYA†LLLL	1.17 kDa	129.60 kDa	0,725	M10.003
32	353	DFSV†IVAN	41.80 kDa	88.97 kDa	0,71	M10.003
33	1008	GTQH†LQDV	118.23 kDa	12.54 kDa	0,694	M10.003
34	8	SPGR†AYAL	0.87 kDa	129.91 kDa	0,692	M10.003
35	1002	GSNP†LEGT	117.45 kDa	13.32 kDa	0,665	M10.003
36	623	ILAF†LLLL	73.41 kDa	57.36 kDa	0,634	M10.003

37	951	PPTT†VILG	111.55 kDa	19.23 kDa	0,585	M10.003
38	452	KLAK†LPDF	53.35 kDa	77.43 kDa	0,58	M10.003
39	588	QVLT†LTVC	69.32 kDa	61.46 kDa	0,568	M10.003
40	212	PPVF†YLNK	24.91 kDa	105.87 kDa	0,568	M10.003
41	181	LVMK†INAT	21.49 kDa	109.28 kDa	0,563	M10.003
42	1087	GPLP†DFGL	127.09 kDa	3.69 kDa	0,548	M10.003
43	906	VTQE†IVTE	106.68 kDa	24.10 kDa	0,533	M10.003
44	807	ETES†LNAS	95.23 kDa	35.54 kDa	0,531	M10.003
45	767	AAVA†LNEE	90.52 kDa	40.26 kDa	0,528	M10.003
46	761	MAGA†QAAA	90.01 kDa	40.77 kDa	0,522	M10.003
47	617	AAIA†LMIL	72.72 kDa	58.05 kDa	0,522	M10.003
48	632	VPLL†LLMC	74.40 kDa	56.38 kDa	0,516	M10.003
49	1056	APAS†TLQS	123.58 kDa	7.19 kDa	0,515	M10.003
50	667	PPED†KVVP	78.72 kDa	52.06 kDa	0,51	M10.003
51	392	FKSS†VISI	46.29 kDa	84.49 kDa	0,507	M10.003
52	1026	FLAP†SSGV	120.36 kDa	10.41 kDa	0,502	M10.003
53	213	PVFY†LNKD	25.07 kDa	105.70 kDa	0,482	M10.003
54	659	HPWN†NEGA	77.79 kDa	52.98 kDa	0,481	M10.003
55	293	EVTR†IKVF	34.50 kDa	96.28 kDa	0,478	M10.003
56	690	GVGG†MAKE	81.64 kDa	49.14 kDa	0,466	M10.003
57	933	ASRN†VIAT	109.60 kDa	21.18 kDa	0,453	M10.003
58	480	YPRK†TITG	56.73 kDa	74.04 kDa	0,449	M10.003
59	1028	APSS†GVQP	120.54 kDa	10.24 kDa	0,444	M10.003
60	177	AAHT†LVMK	21.02 kDa	109.75 kDa	0,442	M10.003
61	705	SASI†VKGQ	83.23 kDa	47.54 kDa	0,437	M10.003
62	860	KPAT†ETSM	101.60 kDa	29.17 kDa	0,432	M10.003
63	817	CCSF†IEGE	96.34 kDa	34.43 kDa	0,411	M10.003
64	1061	LQSS†YQIP	124.10 kDa	6.68 kDa	0,409	M10.003
65	24	VGSG†LHLQ	2.75 kDa	128.03 kDa	0,406	M10.003
66	26	SGLH†LQVL	3.00 kDa	127.78 kDa	0,405	M10.003